POLITECNICO
MILANO 1863

SCUOLA DI INGEGNERIA INDUSTRIALE
E DELL'INFORMAZIONE

Near-Earth Objects deflection strategies: a multicriteria comparison for the target asteroid 2023 PDC

Tesi di Laurea Magistrale in
Space Engineering - Ingegneria Spaziale

Author: **Samuele Alberti**

Student ID: 103492
Advisor: Prof. Camilla Colombo
Academic Year: 2022-23

When referring to this work, full bibliographic details must be given, i.e. Samuele Alberti, "Near-Earth Objects deflection strategies: a multicriteria comparison for the target asteroid 2023 PDC". 2023, Politecnico di Milano, Faculty of Industrial Engineering, Department of Aerospace Science and Technologies, Master in Space Engineering, Supervisor: Camilla Colombo. Printed in Italy

Abstract

Our Solar System is populated by many asteroids and comets which orbit around the Sun. Some of these objects trajectories can cross Earth's orbit, causing a collision. The bodies which have a trajectory close to the Earth's one and in addition have a diametre ranging from metres to tens of kilometres are called Near Earth Objects (NEO).
Historically, asteroids and comets have been sources of huge devastation, and they are thought to have caused at least one mass extinction. In recent years many other minor events happened, as the Chelyabinsk event, in 2013. This has motivated space agencies to start Planetary protection programs, planning different strategies for the deflection of potentially lethal asteroids and protect Earth from the resulting impact, which in some cases can be catastrophic.
In this thesis all the strategies found in literature are described and compared, considering asteroid 2023 PDC as a target, a fictitious asteroid presented by NASA as an exercise in the Planetary Defence Conference (PDC).
NASA considered only two strategies, kinetic impactor and nuclear standoff explosion, and concluded that only the second one is useful for the deflection.
The aim of this work of thesis is to determine which strategies can be used to deflect the asteroid and avoid a collision with Earth. A genetic algorithm multiobjective optimisation process is performed on four selected technologies in order to compute the maximum deflection that can be obtained and also which strategies guarantee the minimum Probability of Collision. The results are shown in terms of Pareto fronts, using the deviation at Minimum Orbital Interception Distance (MOID), the initial spacecraft mass and the warning time as variables for the optimisation.
The conclusion of this process is that, in addition to Nuclear Explosion, also Multiple Kinetic Impactor, Multiple Gravity Tractor and Laser Ablation can be used to completely deviate the trajectory of asteroid 2023 PDC and avoid collision with Earth.

Keywords: Near Earth Objects, Deflection strategies, Planetary protection, multiobjective optimisation

Sommario

Il nostro Sistema Solare è costellato da molti asteroidi e comete che orbitano attorno al Sole.
Alcuni di questi oggetti potrebbero avere delle traiettorie tali da incrociare l'orbita terrestre, causando una collisione. Gli oggetti che hanno una traiettoria vicina all'orbita terrestre ed hanno diametro compreso tra centinaia di metri e kilometri sono chiamati Near Earth Objects (NEO).
Nel corso della storia del nostro pianeta, asteroidi e comete sono stati la causa di enormi distruzioni e si pensa che abbiano causato almeno un'estinzione di massa. Negli anni più recenti molti altri eventi minori sono accaduti, come ad esempio la meteora di Chelyabinsk, nel 2013. Per questo motivo le agenzie spaziali hanno iniziato programmi di protezione planetaria, pianificando molte strategie per deviare asteroidi potenzialmente pericolosi e quindi proteggere la Terra da un impatto, che in alcuni casi potrebbe essere catastrofico.
In questa tesi tutte le strategie trovate in letteratura vengono descritte e paragonate, considerando l'asteroide 2023 PDC come obbiettivo. 2023 PDC è stato presentato dalla NASA come un esercizio nella Planetary Defence Conference.
La NASA ha considerato solo due strategie, Impatto Cinetico (KI) ed esplosione nucleare, concludendo che solo la seconda opzione è efficace per la deflessione.
Lo scopo di questa tesi è quello di determinare quali strategie possono essere usate per deviare l'asteroide ed evitare la collisione. Quindi viene usato un processo di ottimizzazione multioggetto tramite algoritmo genetico su quattro strategie, con lo scopo di calcolare la massima deviazione possibile e anche quale strategia permette di ottenere la minima probabilità di collisione. I risultati sono mostrati tramite i fronti di Pareto, ottenuti usando come variabili di ottimizzazione la deviazione alla minima distanza orbitale, la massa iniziale del satellite e l'intervallo di tempo tra il lancio e l'istante di minima distanza orbitale.
Oltre all'esplosione nucleare, anche l'utilizzo di più satelliti disposti su un'orbita Halo (tecnologia Gravity Tractor) o utilizzare il processo di sublimazione tramite laser (Laser Ablation) sono strategie vincenti che possono essere usate per deviare completamente la traiettoria dell'asteroide 2023 PDC ed evitare la collisione con la Terra.

Parole chiave: Asteroidi, strategie di deviazione, Protezione Planetaria, Ottimizzazione multioggetto

Acknowledgements

First of all, I would like to thanks my professor and supervisor Camilla Colombo for all her professional teachings, suggestions and for having always encourage and support me in these last months.
Five years ago, when I start my university studies at Politecnico di Milano, a big challenge was ahead of me and I've never doubt whether it's worth it or not, but it has been a path full of obstacles.
Fortunately several people helped me, starting from my family, which has always support me, especially in the tough moments.
A special "Thank you" to my father and my mother, and in particular to my sister Emma, always with a great patience in helping me in the difficulties (and in particular with my English grammar errors!).
Last but not least, I would like to spend a few words about my closest friends. With them I share a great part of my life and now it has become normal having you by my side, since the funny period at the high school, but this acknowledgements occasion allows me to remember how lucky I am to have met you many years ago. Now that we have grow up it's time to show to the world how much valuable we are!
A special mention for Andrea, with him I have shared also this troubled journey at PoliMi, in addition to countless train travels.
An important period of my life has now come to an end, and I don't know how the future as a Space Engineer will be, but I certainly know that the university taught me a lot, not only from an academic point of view, but also how to face with problems in my life, to always believe in yourself and to never stop in front of difficulties.

Contents

List of Figures

List of Tables

List of Symbols

Variable	Description	SI unit
$\boldsymbol{A}$	Area	m^2
$\boldsymbol{\vec{a}}$	Acceleration imparted to the asteroid	m/s^2
$\boldsymbol{b^*}$	Impact parameter	m
$\boldsymbol{B_0}$	Magnetic field	T
$\boldsymbol{c}$	Heat capacity	J/kgK
$\boldsymbol{c3}$	Launch energy	km^2/s^2K
$\boldsymbol{d}$	Standoff distance	m
$\boldsymbol{d_{spot}}$	Spot diametre	m
$\boldsymbol{E_g}$	Gravitational binding energy	J
$\boldsymbol{E_t}$	Total energy	J
$\boldsymbol{E_v}$	Vaporization enthalpy	J
$\boldsymbol{f_r}$	Fragmentation ratio	-
$\boldsymbol{G}$	Gravitational constant	Nm^2/kg^2
$\boldsymbol{g_0}$	Gravity acceleration at sea level	m/s^2
$\boldsymbol{H}$	Absolute magnitude	-
$\boldsymbol{k}$	Thermal conductivity	W/mK
$\boldsymbol{k_p}$	Jet constant	-
$\boldsymbol{I_0}$	Incident radiation energy	J/m^2
$\boldsymbol{I_s}$	Specific impulse	s
$\boldsymbol{I_{TOT}}$	Total impulse	s
$\boldsymbol{L}$	Length of the tether	m
$\boldsymbol{M_{ast}}$	Asteroid mass	kg
$\boldsymbol{M_m}$	Molar mass	g/mol
$\boldsymbol{\dot{m}}$	Mass flow rate	kg/s

Variable	Description	SI unit
$\boldsymbol{m_{dry}}$	Dry mass	kg
$\boldsymbol{m_{fuel}}$	Fuel mass	kg
$\boldsymbol{m_{LS}}$	Laser system mass	kg
$\boldsymbol{m_{m,sc}}$	Spacecraft magnetic moment	Am^2
$\boldsymbol{m_{m,ast}}$	Asteroid magnetic moment	Am^2
$\boldsymbol{m_b}$	Mass of the ballast	kg
$\boldsymbol{m_{mat}}$	Mass of the ejected material	kg
$\boldsymbol{m_{nuc}}$	Nuclear system mass	kg
$\boldsymbol{m_{pp}}$	Mass of the power plant	kg
$\boldsymbol{m_{sc}}$	Spacecraft mass	kg
$\boldsymbol{m_{wh}}$	Nuclear warhead mass	kg
$\boldsymbol{N_{rev}}$	Number of revolutions	$-$
$\boldsymbol{n}$	Orbital angular velocity	rad/s
$\boldsymbol{P_L}$	Laser input power	W
$\boldsymbol{P_{e,LT}}$	Power for LT trajectory	W
$\boldsymbol{P_{hov}}$	Power for hovering	W
$\boldsymbol{P_{s/s}}$	Power for spacecraft subsystems	W
$\boldsymbol{Q^*}$	Critical specific energy	J/kg
$\boldsymbol{Q_{cond}}$	Conductive heat	W
$\boldsymbol{Q_{rad}}$	Radiation heat	W
$\boldsymbol{R}$	Gas constant	$J/Kmol$
$\boldsymbol{R_c}$	Capture radius	m
$\boldsymbol{R_E}$	Earth radius	m
$\boldsymbol{R_{ast}}$	Asteroid radius	m
$\boldsymbol{S_{flux}}$	Solar flux	W/m^2
$\boldsymbol{S_{sc}}$	Scattering factor	-
$\boldsymbol{T_a}$	LT trajectory acceleration	m/s^2
$\boldsymbol{T_{rot}}$	Rotational period	s
$\boldsymbol{T_e}$	Electron temperature	K
$\boldsymbol{T_{sub}}$	Sublimation temperature	K
$\boldsymbol{T_{amb}}$	Space ambient temperature	K
$\boldsymbol{t_0}$	Launch time	s
$\boldsymbol{t_{1/2}}$	Half life time	s

Variable	Description	SI unit
t_{DSM}	DSM date	s
t_{MOID}	MOID date	s
t_w	Warning time	s
$\bar{v}$	Average velocity	m/s
v_e	Ejection velocity	m/s
v_{rot}	Rotational velocity	m/s
v_∞	Excess velocity	m/s
α	Asteroid albedo	-
α_P	Mass per unit power	kg/kW
α_L	Specific mass of the laser	kg/kW
β	Momentum Enhancement Factor	-
γ	Spin axis obliquity	rad
Δv	Velocity variation	m/s
Δv_{sc}	Relative velocity s/c-asteroid	m/s
δr_{MOID}	Deviation at MOID	m
$\delta t_{shooting}$	Shooting time interval	s
δ	Plasma sheat thickness	m
μ	Planetary constant	m^3/s^2
μ_0	Material opacity	m^2/kg
μ_{en}	Mass-absorption coefficient	m^2/kg
ϵ_0	Dielectric constant in vacuum	C^2/Nm^2
ϵ_{bb}	Black body emissivity	-
ϵ_r	Radiator emissivity	-
η	Absorbance	$1/m$
η_L	Laser efficiency	-
$\eta_{thruster}$	Thruster efficiency	-
η_{PPU}	PPU efficiency	-
θ_{MOID}	True anomaly at MOID	rad
θ^*	Argument of latitude	rad
λ	Debye length	m
$\tilde{\lambda}$	Effective shielding length	m
ρ	Density	kg/m^3

Variable	Description	SI unit
$\boldsymbol{\rho_{\xi\zeta}}$	Statistical correlation	m^2
$\boldsymbol{\sigma}$	Stefan-Boltzmann constant	W/m^2K^4
$\boldsymbol{\sigma_\xi}$	Covariance in position	m
$\boldsymbol{\phi}$	Plume half-angle	rad
$\boldsymbol{\phi_0}$	Surface potential	V
$\boldsymbol{\phi_i}$	Shaping functions (LT trajectory)	V
$\boldsymbol{\tau}$	Mass-to-power ratio	kg/W
$\boldsymbol{\tau_g}$	Absorption of the laser beam	-
$\boldsymbol{\xi}$	Specific thrust	N/W
$\boldsymbol{\psi_{vf}}$	View angle	rad

Acronyms

Acronym	Description
AT	Asteroid Tugboat
DSM	Deep Space Manoeuvre
EGT	Enhanced Gravity Tractor
EUV	Extreme UltraViolet
GT	Gravity Tractor
MOID	Minimum Orbital Intersection Distance
KI	Kinetic Impactor
KRUSTY	Kilopower Reactor Using Stirling TechnologY
IBS	Ion Beam Shepherd
MKI	Multiple Kinetic Impactor
NEO	Near-Earth Object
NEA	Near-Earth Asteroid
PDC	Planetary Defence Conference
YTW	Yield-To-Weight
YORP	Yarkovsky-O'Keefe-Radzievskii-Paddack
PPU	Power Processing Unit
SKE	Specific Kinetic Energy
RTG	Radioisotope Thermal Generator
TRL	Technology Readiness Level
TOF	Time Of Flight

1 | Introduction

1.1. Asteroid classification and population

The asteroids are classified as Small Solar System Bodies and form a large and scattered group of Sun-orbiting objects [20]. Asteroids were formed simultaneously with the major planets. The primeval asteroids were large chunks, most of them orbiting between Mars and Jupiter. Because of mutual collisions and fragmentation, the present asteroids are debris of those primordial bodies which were never able to form a large planet. The current (2023/11/20) known asteroid count is: 1,308,871 [62]. The diametre of asteroids vary from hundreds of meters to hundreds of kilometers while the structure and the composition range from comet-like icy and loose clumps of material to iron-nickel or stony hard and solid bodies. The number of catalogued asteroids is always increasing by thousands every month. It has been estimated that more than half a million asteroids larger than 1 km exist in the Solar System [45]. Most of the asteroids orbit the Sun in the asteroid belt between Mars and Jupiter.
The smaller objects are more numerous with respect to the bigger ones because of the large number of fragmentation, so that the number density distribution follows the law [36]:

$$N(m) \sim m^{\frac{-11}{6}} \tag{1.1}$$

where m is the mass of the asteroid. The size of an asteroid, but more in general of a celestial body, is measured through the absolute magnitude (H), which is a measure of how bright the object is to an observer at a distance of 1 AU and at a zero phase angle. Larger values of H mean dimmer objects in a logarithmic scale. The diametre of the asteroid can be computed as [2]:

$$D = 10^{0.5(6.259 - log_{10}(\alpha) - 0.4H)} \tag{1.2}$$

where α is the albedo (percentage of light reflected by the object), which depends on the

physical and chemical properties of the asteroid, and D is the diametre of the body in km.

1.1.1. Asteroid classification: composition

Asteroids are classified on the base of their chemical composition [6]:

- C-type (chondrite) asteroids: are most common. They consist of clay and silicate rocks, the color is dark in appearance. It is the most common type of asteroids and they are also the most ancient objects in the solar system.
- S-types ("stony"): are made up of silicate materials and nickel-iron.
- M-types: are metallic (made of nickel-iron).

The different composition depends on how far from the Sun they formed because the high temperature caused the melting of some material and only the iron nucleus survived. The composition is very important for the mission of asteroid deflection. In the case of the kinetic impactor strategy the momentum enhancement factor β, used to determine the Δv given to the asteroid, depends on the composition. It is also very important to determine the attachment system between the spacecraft and the asteroid in the case of the tugboat strategy or to determine the best place to land the spacecraft for mission like the mass driver strategy.

So for some types of missions an early reconnaissance mission is needed to determine well the chemical composition. This mission is very time critical and so simplifying the spacecraft design at this stage is crucial to minimize the development time, we have to use well known technologies (high TRL) [82]. There are two types of early reconnaissance mission: flyby mission or rendezvous mission. With a flyby it is possible to reach the asteroid in a very short time but the arrival velocity has to be limited to ensure that the scientific instruments dedicated to characterizing the asteroid operate within usual data acquisition and slew rates and it is needed to ensure that Sun phase angle at arrival shall be less than 90 degrees to guarantee that the asteroid is illuminated from the spacecraft point of view. While performing a rendezvouz mission requires longer time of flight because it is needed to match the velocity of the asteroid, but the resolution and volume of the data collected by the spacecraft are increased and so the characterization of the asteroid is more accurate. In addition if the spacecraft remains in proximity of the asteroid in the course of the deflection mission it can determine if the deflection succeeds or fails.

1.2. The importance of asteroid deflection

Throughout the history of our planet Earth there have been a lot of asteroid impact events and in many other cases they melt because of ablation in the atmosphere. The impacts of asteroids modify the composition of the planets, infact as soon as the planet were formed an intense bombardement of metorite generated a huge amount of heat which cause the melting of terrestrial planets and this is the origin of the planetary differentiation process (heaviest element like iron fell into the centre forming a dense core) [45]. Nowadays the vast majority of these impacts are from very small objects, but there have been some remarkable exceptions. One of the most important event was the the Chelyabinsk one in 2013: an asteroid of about 20 meters in diametre entered Earth's atmosphere above the city of Chelyabinsk, in Russia. It exploded 30 km above the ground and so the damage was very little, even if it created a strong shockwave.

Another important event happened in Tunguska in 1908, the asteroid was 30 meters of diametre and the explosion had been estimated 1000 times more powerful than the one of the atomic bomb at Hiroshima. Luckily it happens in a remote zone in Siberia and so nobody was injured.
The most known asteroid impact event is the one that happened 65 billions years ago which killed 70% of all species on Earth, including the dinosaurs. In that case an asteroid of 10-15 kilometers hit the Earth in the Yucatan penisula, Mexico (Chicxulub crater). The impact caused devasting effects, like megatsunami and millions of shooting stars which then hit the surface of Earth.

An event like this is very rare but nowadays it would cause the extinction of humanity. The Torino scale has been defined by the International Astronomical Union IAU in 1999 in order to study the potential danger of an asteroid. The scale goes from 0 to 10 and a color is associated to each number, from white to red, to facilitate the comprehension of the event gravity [95].

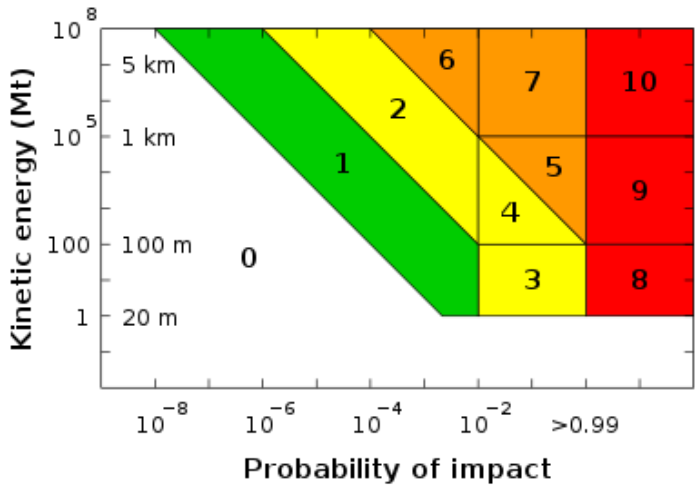

Figure 1.1: Torino scale in a graph, reporting the impact energy and the probability of impact. The scale in metres is the asteroid diametre. [95]

Even if the probability of large events is very small, it is necessary to study and continue monitoring the trajectory of the asteroids and that's why planetary protection programs have been started. So, to protect our planet and the humanity we have to accurately define and study all the strategies possible to deviate the trajectory of these asteroids.

1.3. Past and future missions to asteroids

The first mission to an asteroid was the Galileo mission in 1991 which flew around the 12-km Gaspra, but it was just a mission to study the characteristics of the asteroid. Considering asteroid defelction missions, the European Space Agency in 2005 started to study the mission Don Quijote, which would investigate the effects of the kinetic impactor strategy to deflect the orbit of an asteroid. This mission did not proceed beyond the initial phase and was later substituted by AIDA [61].

NASA in 2013 announced a mission called ARM (Asteroid Redirect Mission), but then it was cancelled in June 2017. The mission consisted in a rendezvous with a large NEA and then the use of a robotic arm to collect mass from the asteroid and so change the trajectory exploiting the mass driver strategy. The mission was cancelled because of budget problems. Before ARM the Orion Asteroid Mission had been proposed by NASA, but then was cancelled in 2011. In this mission a spacecraft would have landed on an asteroid to study the impact [61].

The most important asteroid deflection missions were proposed by NASA and ESA in a

joint program called AIDA (Asteroid Impact and Deflection Assessment) in 2015. This program consists in two separate missions: DART (which has already been launched with success) and the following mission is Hera. The DART mission exploits the kinetic impactor strategy to hit Dimorphos (a minor-planet moon of the asteroid Didymos) to change its orbit. On 26 September 2022 the spacecraft reached the moon and shortened its orbital period of 32 minutes. The mission was declared a success by NASA.
The mission Hera will be launched in October 2024 (to be confirmed) and will study the evolution of the Didymos binary asteroid system that was impacted by DART and will definitely validate the kinetic impactor strategy for asteroid deflection.

In addition a lot of missions were performed to study the physical and chemical characteristics of the asteroid (sample-return mission), like for example the Japanese mission Hayabusa (2005) or the mission Dawn by NASA (2007).

In order to identify possible potentially dangerous asteroids for Earth NASA proposed the mission NEOSM, NEO Surveillance Mission. This mission is necessary because the biggest asteroids (with diametre higher than 1 km) are almost discovered, but also smallest ones can create a lot of damage if they impact on Earth. It is estimated that there are around 25000 NEOs between 140 meters and 1 km of size and nowadays only 35% of these have been discovered [3].

The second mission that NASA will develop, not officially, but following the purpose of Brent W. Barbee (NASA, Goddard Space Flight Center) [3] will probably be a reconnaissance mission with a small but capable spacecraft that could be rapidly developed and launched. As explained in the previous section, a reconnaissance mission is very important for a correct deflection mission, so it is plausible that NASA will build this type of mission in the future. DART mission demonstrates the possibility of using kinetic impactor strategy to deflect an asteroid, but for sure we can't rely only on this technology, so other missions are needed to validate other important technologies, like the nuclear standoff explosion.

But NASA and ESA are not the only ones interested in this type of mission, China recently announced its intention to launch a mission in 2026 that will also hit an asteroid. the target is 2020 PN1, a potentially dangerous NEA of the Apollo family, about 40 meters in diametre. The main difference between the Chinese project and DART is that the two vehicles (the impactor and the descent module) will be sent to the asteroid simultaneously. The last one will have to make a soft landing on 2020 PN1 to examine it and evaluate the consequences of the impact.

1.4. Multicriteria comparison: state of the art

The multicriteria comparison of asteroid deflection strategies consists in the comparison between the effectiveness of different methods in order to deviate the trajectory of an asteroid and to develop a mathematical model for each strategy discussed.

The first multicriteria comparison was presented by NASA in 2006 [64] because in 2005 the U.S. Congress decided to build an analysis of alternatives that could be employed to divert an object in collision course with Earth. In this document for the first time the strategies are divided into impulsive, if they act instantaneously, or slow push if the action is continuous. Only one year later NASA released another paper [70] which compares a lot of strategies and it is a continuation of the previous work. The papers published by NASA are qualitative, without mathematical models which describe the strategies in detail.

One of the first paper in which it is possible to find also mathematical models, so a system engineering approach, is the one by Sanchez et Al. [21] published in 2007. The concept of one Pareto set dominance over another is used to compare the effectiveness of each strategy. In 2009 Sanchez et Al. published another article, probably the most complete one until now, concerning multicriteria analysis [84].

More recently, in 2015, Michael C.F. Bazzocchi and M. Reza Emami [5] developed a comparative analysis of asteroid redirection method, but instead of using Pareto optimization, in order to compare each strategy they used a Monte Carlo analysis to find the average Δv and the standard deviation for each redirection method.

In 2017 Thiry and Vasile [92] performed a statistical multicriteria evaluation of non-nuclear asteroid deflection methods, using a global optimisation strategy based on a multi-population adaptive inflationary differential evolution algorithm (MP-AIDEA).

1.5. Aim of the thesis

As first the scope of the thesis is to describe each asteroid deflection strategy found in literature qualitatively and then show a mathematical model to compute the variation of velocity Δv imparted to the asteroid. The strategies proposed in the past years are numerous, but the scope is to retrieve all of them to give the most complete possible overview. In appendix A the results of the models are validated through the ones found literature.

Once the strategies are described, the objective is to find the most useful and effective

technologies through a qualitative comparison.
Four selected alternatives are used to evaluate if they are able to deflect the target asteroid 2023 PDC. This object was proposed by NASA [68] as a fictitious asteroid in order to simulate an emergency response.

The selected strategies are optimised through a genetic algorithm multiobjective process (function *gamultiobj* in matlab) in order to determine the mission which will lead to the maximum deflection of the asteroid and also the one which will minimise the collision probability.
So the final objective of the thesis is to determine which of the strategies selected can be used to completely deviate the asteroid, in addition to the one selected by NASA, which is the Nuclear Standoff Explosion [68].
Asteroid 2023 PDC is used as a target also because uncertainties about its physical properties are still present, so the strategies are applied to different masses and dimensions.
The conclusion of the optimisation process is that, in addition to Nuclear Explosion, also Multiple Kinetic Impactor, Multiple Gravity Tractor and Laser Ablation can be used to completely deviate the trajectory of asteroid 2023 PDC and avoid collision with the Earth.

1.6. Thesis outline

In the second chapter all the asteroid deflection strategies are described, dividing them in two big sectors: impulsive deflection strategies and slow push deflection strategies, following the method done by NASA [64].

Then a qualitative comparison of the alternatives is explained (see section 2.4), based on various parameters, as for example the TRL level, the complexity of the mission and the dependence on asteroid composition and size. Just few technologies have been chosen for the optimisation process. The reasons are explained in section 2.4.2.

The formulas for the impulsive deviation and the low thrust deviation are described in chapter 3 together with the asteroid deviation problem, that is to say how to compute the deviation at MOID in both cases (impulsive and slow push strategies).
The target asteroid is a fictitious asteroid called 2023 PDC that NASA created as an exercise for the IAA Planetary Defence Conference 2023 [68]. The description of the asteroid and a preliminary risk assessment is shown in section 3.7 .

Finally in chapter 4 the performance of the optimisation process is described and the Pareto fronts obtained for each strategies and for the two types of missions (maximum deflection and minimum collision probability mission) are reported. In addition for each

type of strategy a first preliminary mission design is performed, in order to evaluate the feasibility of the mission.

2 | Asteroid deflection strategies

2.1. Asteroid fragmentation

Before entering in the details of the strategies for the deflection, it is important to focus on asteroid fragmentation.
This condition can be seen both as a problem and as a solution. It is a problem because in the case of impulsive deviation strategies like kinetic impactor or nuclear explosives it is needed to avoid fragmentation, because the asteroid will divide in a lot of small or big pieces which can create a lot of debris or in the worst case can become dangerous reaching the surface of Earth. But on the other side it can be a solution in the extreme case when the warning time is too small. The asteroid is completely destroyed and the impact on Earth is avoided. Anyway for both this cases it is important to understand when fragmentation happen and which are the effect of this event.

Following the definition given in [83] the critical specific energy Q^* is defined as the energy per unit of mass necessary to *barely catastrophically disrupt* an asteroid. This happens when the biggest fragment is half the mass of the initial asteroid. So it is possible to define the fragmentation ratio, defined as [83]:

$$f_r = \frac{m_{max}}{M_a} \tag{2.1}$$

Where m_{max} is the mass of the biggest fragment and M_a the initial mass of the asteroid. A fragmentation is defined catastrophic when $f_r < 0.5$. It is very difficult to quantify exactly the value of Q^*, because it depends on a lot of factors, such as the chemical composition and the structure of the asteroid but also the velocity and the size of the impactor. Using the scaling laws explained in the work of Ryan and Melosh [83], Housen and Holsapple [39] and Holsapple [38], it is possible to retrieve the value of the critical energy depending on the size of the asteroid (fig. 2.1).

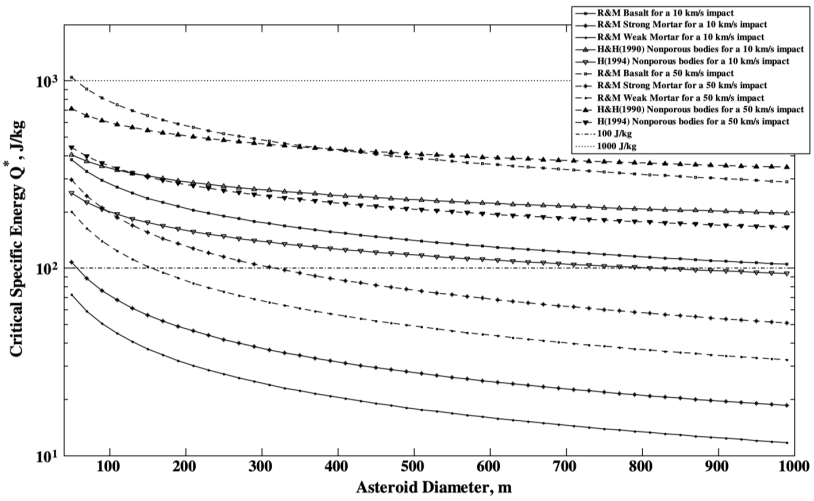

Figure 2.1: Values of Q^* for asteroid with diametre between 40 m and 1 Km [90]

So if the energy delivered by the impact is higher then the fragmentation limit Q^*, the asteroid is considered disrupted. For example, for the kinetic impactor strategy, the energy that the asteroid absorbs is the Specific Kinetic Energy SKE, and it is defined as [83]:

$$SKE = \frac{1}{2}\frac{(M_a + m_{s/c})^2}{\beta^2 M_a m_{s/c}}\Delta v^2 \tag{2.2}$$

So this is an important value to be controlled during the design of an asteroid deflection mission using kinetic impactor. The shape of the fragments cloud will evolve as a pulsing ellipsoid with the semimajor axis which grows in time [35]. Concerning the distribution in size of the fragments, a simple model is the one explained in [90]. The number of fragments N with mass higher than m can be modelled as [90]:

$$N(> m) = Cm^{-b} \tag{2.3}$$

Where

$$C = m_{max}^b \tag{2.4}$$

$$b = \left(1 + \frac{m_{max}}{M_a}\right)^{-1} = (1 + f_r)^{-1} \tag{2.5}$$

As can be seen in the plot in fig. 2.2, the larger number of fragments have the smaller mass. It can be noticed also that the higher is the value of the fragmentation ratio the higher is the mass of the fragments.

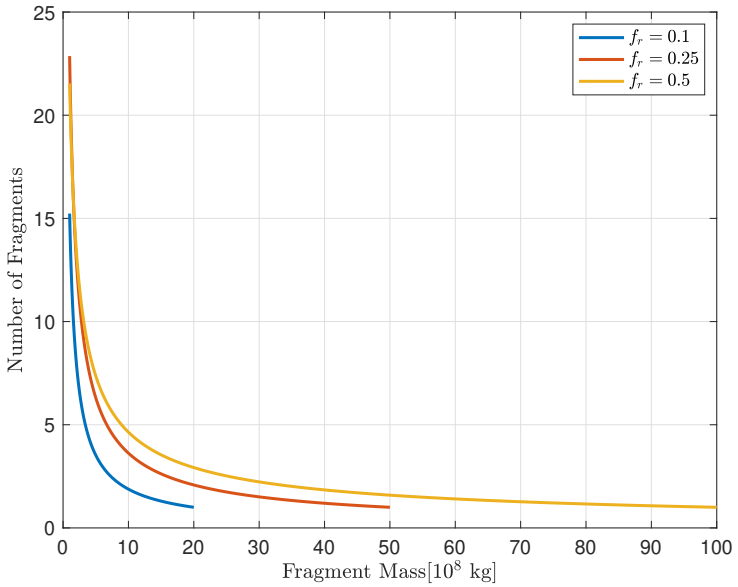

Figure 2.2: Number of fragments estimated after the fragmentation of an asteroid with mass equal to $2 \cdot 10^{10}$ kg with different values of f_r

2.2. Impulsive deflection

Impulsive deflection means that the deflection action is instantaneous. The impulsve defelction technologies are mainly two: the Kinetic Impactor and the version with Multiple Kinetic Impactors, and Nuclear Explosion (which can be standoff explosion or subsurface explosion). Also conventional chemical explosives can be used, but their efficacy is very limited with respect to nuclear explosion.

2.2.1. Kinetic impactor

The idea behind the concept of the Kinetic Impactor strategy is quite simple: to impact the target asteroid with a massive projectile at a high relative speed. The total impulse given to the asteroid will be the sum of the pure kinetic impulse of the interceptor, plus the impulse due to the thrust of material ejected from the impact crater. The variation of velocity given by the spacecraft to the asteroid can be computed from the momentum conservation equation [84]:

$$\Delta v = \beta \frac{m_{sc}}{M_a + m_{sc}} \Delta v_{sc} \tag{2.6}$$

where m_{sc} is the mass of the spacecraft at the time of the impact and Δv_{sc} is the relative velocity of the spacecraft with respect to the asteroid at the impact point. β is the momentum enhancement factor and it is introduced because in reality the collision is not

inelastic. When $\beta = 1$ the collision is inelastic and so the asteroid produces no ejecta (ideal case), while when $\beta = 2$ the momentum of the ejecta is the same of the momentum of the impactor in the opposite direction [111] (fully elastic collision). If $\beta > 2$ the collision is hyperelastic. In a very rare case β can be less than 1, and this could be a problem, because it counteracts the action of the impactor [81].

$$\beta = \frac{Momentum\ gained\ by\ the\ asteroid}{Momentum\ of\ the\ impactor} \tag{2.7}$$

Its correct value can be exactly estimated only through cratering analysis, following the work of Holsapplel [42] or more in detail the thesis of Chignoli [16], and hypervelocity experiments, like the one of Hoerth [37].
The Kinetic Impactor is a useful technique because of the high TRL and the simplicity of the mission design, but it can be inefficient for large asteroid and in addition an impact with high velocity can cause the fragmentation of the object (section 2.1). That's why the Multiple Kinetic Impactor technique has been introduced. The idea, proposed by Wie [109], is to use several small impactors to hit the asteroid with small impact velocity so that the risk of fragmentation is reduced and the overall deviation achieved is larger than the single kinetic impactor.

2.2.2. Standoff Nuclear Explosion

The first asteroid deviation strategy ever proposed suggested to use a nuclear bomb to change the trajectory of the asteroid (Icarus project, MIT, 1979). Even nowadays it is still the strategy which carries the highest energy density with respect to all the other alternatives. However all the political and security issues have to be considered because a nuclear warhead has to be launched into space and the consequences of a failure would be catastrophic. Standoff explosion means that the nuclear bomb explodes at a certain distance H with respect to the asteroid surface. In this way the method is less sensitive to the physical and chemical characteristics of the asteroid material.
The deviation is obtained through X-rays, neutrons, gamma radiations and debris which hit the surface. The fraction of energy carried by all this elements depends on the type of nuclear explosion, so fusion or fission. Fusion means that two light nuclei, as two isotopes of Hydrogen, deuterium and Tritium, combine to form an heavier nucleus (Helium, $H_1^2 + H_1^3 \rightarrow He_2^4 + \text{n}$) and release a huge quantity of energy (17.6 MeV). While fission explosion exploits the classical reactions of a nuclear reactor, so an heavy nucleus (Uranium) is splitted (hit by a neutron) to form lighter nuclei (fission products).

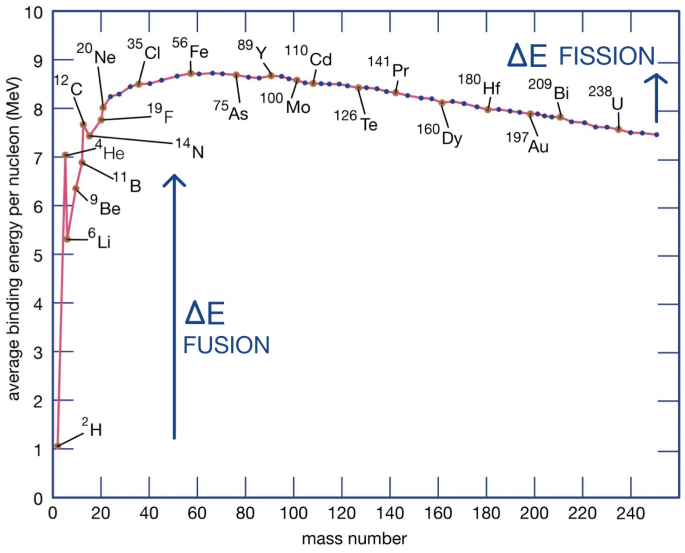

Figure 2.3: Binding energy per nucleon as a function of the mass number [80]

As can be seen in fig. 2.3 the energy jump in the case of fusion is much higher then the one obtained with fission, so in the end a bomb based on fusion reaction (H bomb) produces an higher deviation effect to the asteroid with respect to a bomb based on fission.

The two types of reaction are completely different and also the fraction of energy generated by the different elements changes, as can be seen in table 2.1, data taken from Hammerling [34].

Source	X-rays	Neutrons	γ rays	Debris	Others
Fission	70%	1%	2%	20%	7%
Fusion	55%	20%	1%	20%	4%

Table 2.1: Energy distribution [84]

The procedure to compute the total Δv is the one explained in [34],[84] and [99].
The effect due to the debris is the first one to be considered. The debris are part of the spacecraft structure or of the bomb which are ejected and impact the asteroid. Assuming that the explosion generates a spherical distribution of the fragments, the mass of the debris which hits the surface is

$$m_{debris} = S m_{sc,i} \tag{2.8}$$

Where $m_{sc,i}$ is the initial mass of the spacecraft and the factor $S = 0.5(1 - sin(\lambda_{max}))$ (refer to fig. 2.4 for the definitions) represents the fact that the asteroid covers just a part of the spherical distribution.

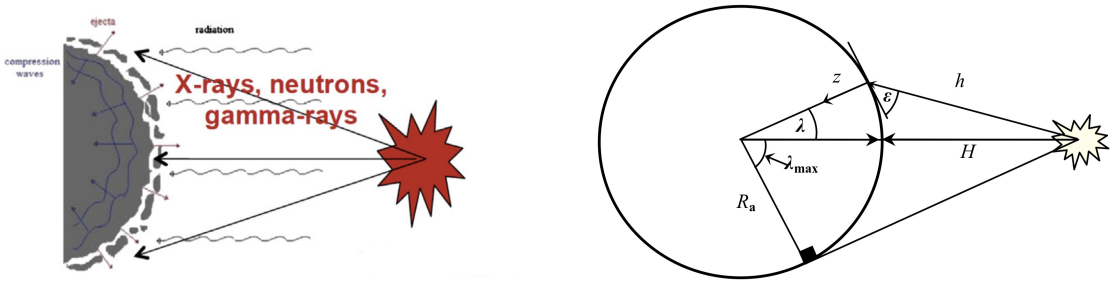

(a) Illustration of the Nuclear Standoff explosion [79]

(b) Geometrical diagram of the Nuclear Standoff explosion [84]

Figure 2.4: Nuclear standoff explosion

The total energy released by the nuclear explosion is $E_t = YTWm_{wh}$, where YTW is the yield-to-weight-ratio (which varies from 0.6 $ktons/kg$ to 2.2 $ktons/kg$) and m_{wh} is the mass of the nuclear warhead, considered equal to $0.3m_{sc}$ [84]. Once the total yield released is defined the velocity of the debris can be computed:

$$v_{debris} = \sqrt{\frac{2f_{debris}E_t}{m_{debris}}} \tag{2.9}$$

The asteroid variation of velocity caused by them is:

$$\Delta v_{debris} = \beta S_{sc}\frac{m_{debris}v_{debris}}{M_{ast}} \tag{2.10}$$

Where $S_{sc} = 2/\pi$ is the scattering factor and β is the momentum enhancement factor (see section 2.2.1).
The effect due to radiations is derived from the Beer-Lambert law of absorption, which in the general form is:

$$I(z) = I_0 e^{-\rho_{ast}\mu_0 z} \tag{2.11}$$

Where I_0 is the incident radiation energy per unit area, z is the depth and μ_0 is the opacity of the material (also called mass-attenuation coefficient). The opacity indicates how much the energy is attenuated as it passes through the asteroid, so low opacity means that the material is almost transparent to that particular radiation. The coefficient μ depends on the type of the radiation considered (indicated with a ν). In this case the radiation energy depends also on the angle λ and the incident angle ϵ has to be considered, so in the end:

$$I^{\nu}(\lambda, z) = \sin\epsilon(\lambda) I_0^{\nu}(\lambda) e^{-\rho_{ast}\mu_{\nu}\frac{z}{\sin\epsilon(\lambda)}} \tag{2.12}$$

Where the incident radiation depends on the energy fraction, on the total energy of the explosion and on the distance h:

$$I_0^\nu(\lambda) = \frac{f}{4\pi h^2(\lambda)} E_t \tag{2.13}$$

$$h = \sqrt{(H + (1 - \cos\lambda)R_{ast})^2 + R_{ast}^2 \sin^2\lambda} \tag{2.14}$$

$$\sin\epsilon = \frac{(R_{ast} + H)\cos\lambda - R_{ast}}{h(\lambda)} \tag{2.15}$$

The amount of energy absorbed is, by definition, the derivative of the radiation intensity, so, summing up for all the types of radiations:

$$E(\lambda, z) = \sum_\nu \mu_{en} I_0^\nu e^{-\rho_{ast}\mu_\nu \frac{z}{\sin\epsilon(\lambda)}} \tag{2.16}$$

Where μ_{en} is the mass-absorption coefficient, which theoretically differs from the mass-attenuation coefficient: μ_{en} gives an estimation of the statistical energy that is absorbed by a sample of matter, while μ_ν accounts for both scattering and absorption of energy [34][84]. Both the values of the coefficients are reported in table 2.2 and are computed using tables of radiations attenuation from the *National Institute of Standard and Technologies* [40][84]. More information about the computation of these coefficients can be found in Appendix appendix A.1.1.

	X-ray	Neutron	γ-ray
μ_0 $[m^2/kg]$	1.426	0.00496	0.00445
μ_{en} $[m^2/kg]$	1.370	0.00496	0.00234

Table 2.2: Opacity and mass-absorption coefficients for forsterite (Mg_2SiO_4)

Part of the energy is used to vaporize the material, so the average velocity of the gas particles is estimated considering the vaporization enthalpy E_v:

$$v(\lambda, z) = \sqrt{2(E(\lambda, z) - E_v)} \tag{2.17}$$

The linear momentum per unit area becomes:

$$P_A = \int_0^{z_{max}} dp_A dz = \int_0^{z_{max}} \rho_{ast} v dz = \int_0^{z_{max}} \rho_{ast} \sqrt{2\left(\mu_{en} I_0 e^{-\rho_{ast}\mu_\nu \frac{z}{\sin\epsilon}} - E_v\right)} dz \tag{2.18}$$

Where $z_{max}(\lambda)$ can be computed by setting the velocity to zero with (2.17), so:

$$z_{max} = \frac{\sin\epsilon}{\rho_{ast}\mu_\nu} \ln\left(\frac{\mu_{en} I_0^\nu}{E_v}\right) \tag{2.19}$$

The linear momentum has to be integrated over the radiated surface. So using the equation of a spherical cap:

$$S_{cap} = 2\pi R_{ast}^2 (1 - \cos\lambda) \tag{2.20}$$

and dividing by the total asteroid mass the velocity variation due to radiations is obtained through a double integral:

$$\Delta v_{rad} = \sqrt{8}\pi \frac{R_{ast}^2 \rho_{ast}}{M_{ast}} \int_0^{\lambda_{max}} \int_0^{z_{max}(\lambda)} \left(\mu_{en} I_0 e^{-\rho_{ast}\mu_\nu \frac{z}{\sin\epsilon}} - E_v\right)^{1/2} dz \sin\lambda \, d\lambda \tag{2.21}$$

The detail of the integration over a spherical cap can be found in [84]. So the total deviation obtained with Nuclear Standoff Explosion strategy is the sum of the one obtained with the debris and the one obtained with each radiation type, so:

$$\Delta v = \Delta v_{debris} + \Delta v_{X-rays} + \Delta v_{neutrons} + \Delta v_{\gamma-rays} \tag{2.22}$$

The deviation obtained with a fusion device is one order of magnitude higher with respect to fission (as can be seen also in fig. 2.5 and in [99]).

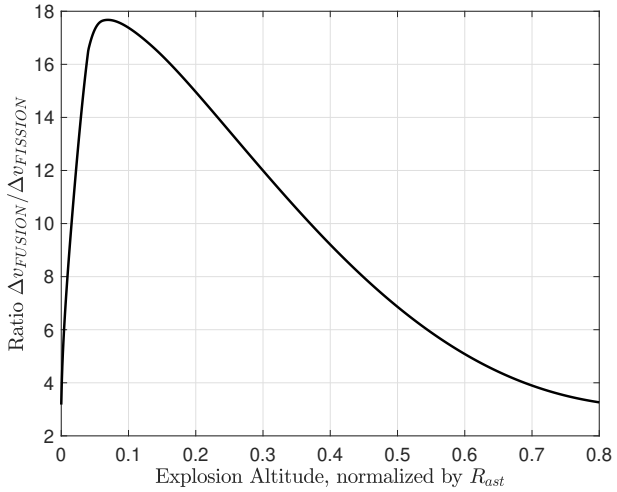

Figure 2.5: Ratio between the deviation obtained with a fusion and a fission device

As can be seen in fig. A.1, the neutrons give the highest contribution to the whole Δv, because, even if the mass absorption coefficient is lower than the one of X-rays, they are able to penetrate deeper into asteroid surface (higher z_{max}) and this translates in an

higher value of deviation.

An issue of this technology is the definition of the optimal standoff distance (which maximises the deviation). This value depends on the physical dimension of the asteroid and it is very important because the deviation decreases a lot (one order of magnitude) if the distance is non optimal. So in this work it will be computed precisely through the maximisation of the value in eq. (2.22), even if Hammerling [34] estimated the optimal distance with the formula: $H_{opt} = (\sqrt{2} - 1)R_{ast}$.

2.2.3. Subsurface nuclear explosion

The concept of subsurface nuclear explosion consists in the use of a nuclear bomb (based on fission or fusion) which penetrates some meters above the surface of the asteroid and then the explosion will completely destroy it. In 2012, Pitz, Kaplinger, Wie and Dearborn [79] proposed an hypervelocity nuclear interceptor, that will be able to provide very quickly the disruption of the asteroid. The idea is to have a leader spacecraft which acts as a kinetic energy impactor, so it creates the crater, and then a follower spacecraft which contains the nuclear explosives.

In astrophysics the gravitational binding energy E_g is defined as the energy required to completely destroy a celestial body, transforming it into dust and debris.

$$E_g = \frac{3GM^2}{5R} \tag{2.23}$$

Where $G = 6.67259 \cdot 10^{-11}\ Nm^2/kg^2$.
So in order to disrupt an asteroid of 1 km of diametre it is needed a 1 Mt (Megaton) nuclear subsurface explosion. If we consider to have Uranium as a fissile material (U-235) the available energy is 0.9 MeV (MegaelettronVolt) for nucleon, so the energy density is $8.6 \cdot 10^7\ MJ/kg$ [80]. If we want 1 Mt of energy (corresponding to $4.2 \cdot 10^9\ MJ$) the mass of Uranium needed is 48.6 kg, so a feasible mass value to be launched. If we consider fusion explosion the value will be even smaller.
The subsurface nuclear explosion can be used not only with the goal of destroying the asteroid, but as a deflection technique to provide a Δv to the asteroid. The problem is that the probability of disruption is very high. Anyway a simple model (presented by [55]) to estimate the velocity variation is:

$$\Delta v = 4592 Q^{7/6} G_{BN}(\bar{h}) \tag{2.24}$$

Where G_{BN} is a coefficient that depends on $\bar{h} = hQ^{-1/3}$ (h is the depth of the explosion,

Q is the power) and its tabulated values can be found in [56].

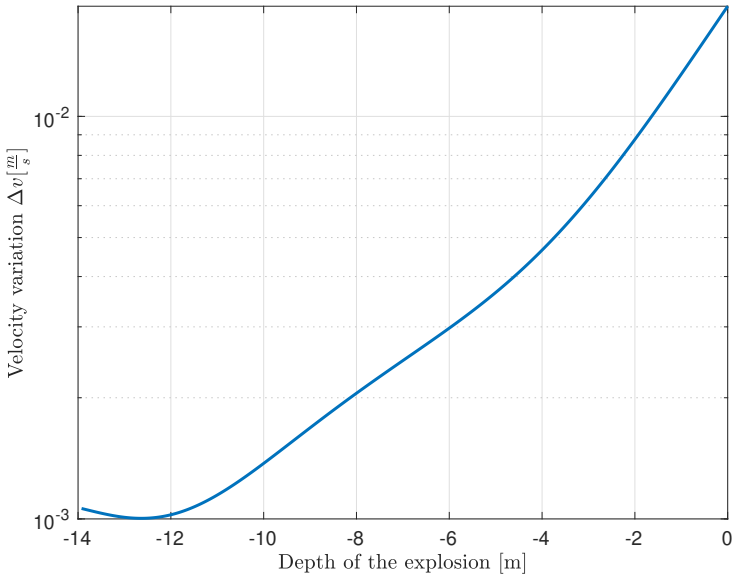

Figure 2.6: Velocity variation varying the depth of the explosion, fixing $Q = 100$ *ktons*

2.3. Slow push deflection

If the deflection action is continuous in time then the strategy is considered as a slow push deflection. In literature a huge number of these types of strategies can be found. In the following sections each one of the alternatives is listed and explained.

2.3.1. Gravity tractor

The concept of the gravity tractor technique for asteroid deflection was first proposed by Edward T. Lu and Stanley G. Love in the article titled *Gravitational tractor for towing asteroids* [47]. The idea is simple: to exploit the gravitational attraction between the mass of the spacecraft and the mass of the asteroid to tow the asteroid and in this way change its trajectory. The spacecraft hovers in proximity of the asteroid with the thrusters directed such that the exhaust does not impinge on the surface. So we define the exhaust-plume half-width angle ϕ, as can be seen in fig 2.7.

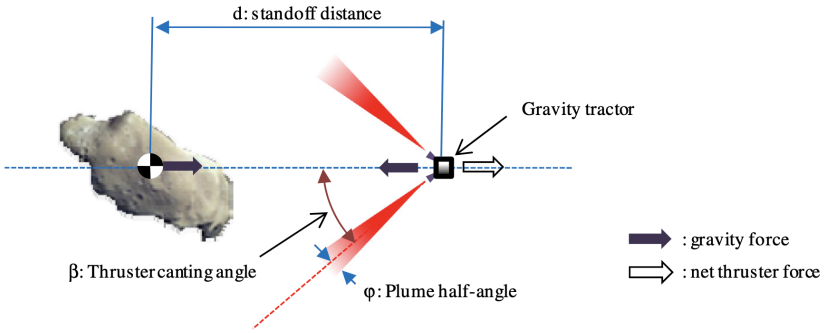

Figure 2.7: Geometric diagram of the gravity tractor configuration [84]

Since an hovering position has to be maintained, the mass of the spacecraft decreases in time and, assuming that the mass consumption is linearly proportional to the pulling force, it can be computed through the following formula:

$$m(t) = m_i e^{-\left(\frac{GM_a(t-t_0)}{d^2 cos\left(arcsin\left(\frac{R_a}{d}+\phi\right)\right) I_s g_0}\right)} \tag{2.25}$$

Where the parameters are defined as in fig. [47]. The acceleration acting on the asteroid is given by:

$$a_{GT}(t) = \frac{Gm(t)}{d^2} \tag{2.26}$$

Integrating the acceleration over the total time of the deviating action is possible to obtain the Δv given to the asteroid.

The hovering distance d is computed equalizing the hovering force (which is the net thrust force in fig. 2.7) and the gravitational force, so:

$$F_{hover} = T_n \cos\left(\arcsin\left(\frac{R_{ast}}{d}\right) + \phi\right) = F_g = \frac{GM_{ast}m_{sc,i}}{d^2} \tag{2.27}$$

Where the thrust T_n is computed as:

$$T_n = m_{power}\frac{\xi}{\tau} = \frac{m_{dry}}{2}\frac{\xi}{\tau} \tag{2.28}$$

Where m_{power} is the mass of the power subsystem and can be approximated as half the value of the spacecraft dry mass, $\tau = 25\ kg/kW$ is the mass-to-power ratio and $\xi = 34\ mN/kW$ is the specific thrust. The value represents on average the performances

of an electric thruster [106]. The dry mass of the spacecraft is computed through (2.25), so $m_{dry} = m(t = t_f)$ where t_f is the final instant of the deviation action $\Delta t = t_f - t_0$. So in the end the distance d is computed solving the equation:

$$\frac{1}{2}m_i e^{-\left(\frac{GM_a(t-t_0)}{d^2 cos\left(arcsin\left(\frac{R_a}{d}+\phi\right)\right)I_s g_0}\right)} \frac{\xi}{\tau} cos\left(\arcsin\left(\frac{R_{ast}}{d}\right)+\phi\right) - \frac{GM_{ast}m_{sc,i}}{d^2} = 0 \tag{2.29}$$

Since the propellant mass is consumed in order to maintain the hovering condition the whole spacecraft becomes lighter and the gravitational force decreases in time. So the rate of growth of Δv becomes smaller and smaller as the deviation action time increases. In the paper of McInnes [53] and Yamaguchi [110], and then revived by Vasile [98], it is proposed a variant of the gravity tractor technique which is based on the idea of placing the tractor on an halo orbit maintained artificially with a constant thrust (fig. 2.8). The advantage of the halo configuration is that only one engine is needed, instead of two.

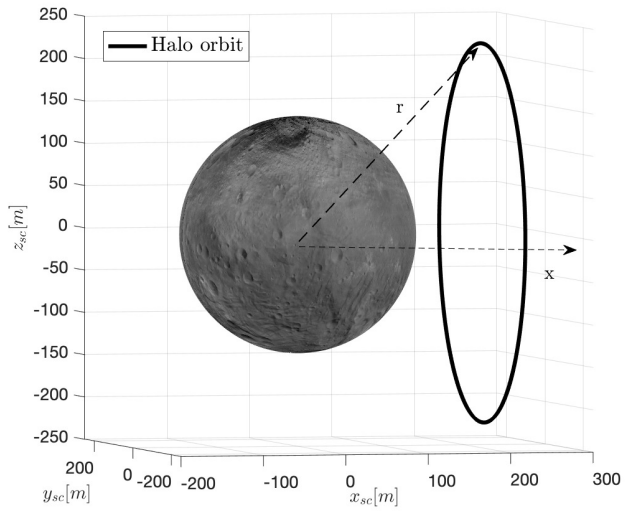

Figure 2.8: Halo orbit around an asteroid, obtained using the Clohessy-Wiltshire-Hill equations

The variation of mass and the acceleration produced in this configuration is:

$$m_H(t) = m_{H0} e^{\frac{GM_{ast}\tau}{R_a^2 I_s g_0} t} \tag{2.30}$$

$$a_{GT,halo}(t) = \frac{GM_H(t)}{R_a^2}\tau \tag{2.31}$$

Where $\tau = cos(\psi)sin(\psi - \phi)^2$ (ψ is the angle between the horizontal x-axis and the vector r, *phi* is the thrust divergence angle).

Enhanced gravity tractor

The idea of the Enhanced Gravity Tractor (EGT) was proposed because with the Gravity Tractor the deviation achieved is very small and the time required in order to significantly change the trajectory of the asteroid is high. The EGT exploits mass collected in situ in order to augment the mass of the spacecraft and so to increase the gravitational force between the objects. Depending on the mass collected the EGT technique can reduce the deflection time by a factor from 10 to 50 [52].

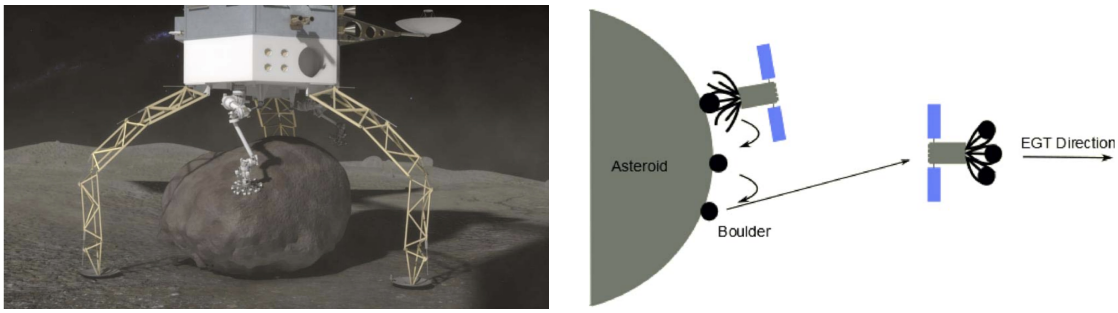

(a) Mass capture system (credit NASA/AMA, Inc.)

(b) Illustration of the EGT strategy (credit NASA/AMA, Inc.)

Figure 2.9: EGT strategy illustration

If we consider a mass collected of 50 tons, the deviation achieved is around one order of magnitude higher with respect to the classical gravity tractor (fig. 2.10a).

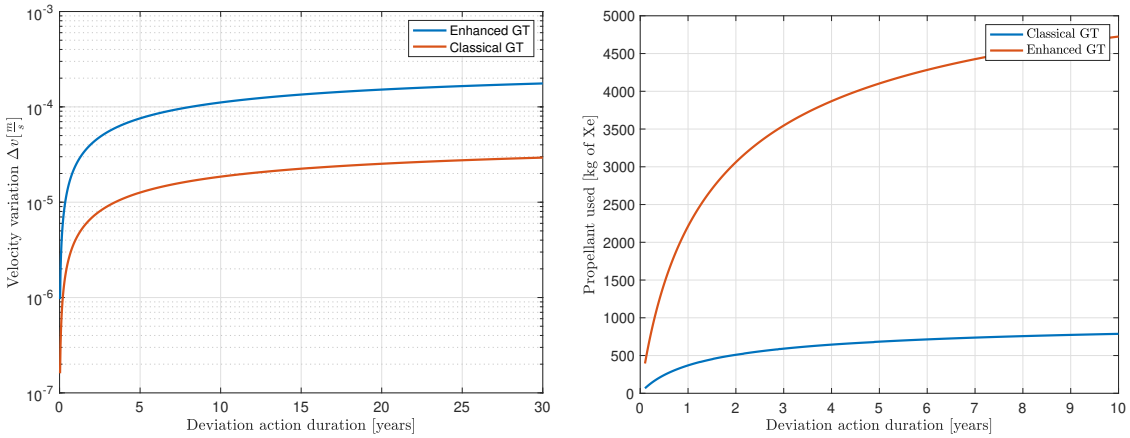

(a) Δv obtained with EGT and GT

(b) Mass of propellant (Xenon) consumed: comparison between EGT and GT

Figure 2.10: Comparison between EGT and GT

However the EGT brings to a much higher consumption of propellant, as can be seen in fig. 2.10b. This has to be taken into account in the mission design, because the initial mass at launch will be higher.

2.3.2. Electrostatic tractor

The idea of the electrostatic tractor was first introduced by Murdoch, Izzo, et Al. [58] in 2008. This technique exploits the mutual electrostatic interaction between two charged bodies. So the charged hovering spacecraft slowly accelerates the asteroid (which has to be charged) towards or away from it. The direction of the attraction depends on the sign of the charges.
Obviously also the action of the gravity has to be considered, so the overall deflection is the sum of the gravitational one and the electrostatic one.

In order to use this technology the spacecraft must be charged. The ambient space plasma and photoelectric effect given by the solar extreme ultraviolet EUV are the major sources of spacecraft charging currents [26]. The spacecraft will accumulate charge until equilibrium is reached (zero net current). But with the emission of ions or electrons this equilibrium can be broken and the charge can be controlled. Experiment on charge control has been performed in the SCATHA mission, but the objective was to obtain neutrally charged spacecraft, so the knowledge about satellite charged with high potential is low. In recent years some work has been performed in order to study the Coulomb formation flying, arguing that potentials up to 20 kV can be obtained [76].
The system is modelled as a spherical capacitor, as in [26] and [58], considering the

spacecraft as a charged sphere of radius R, so the capacitance is expressed as:

$$C = 4\pi\epsilon_0 \frac{R+\delta}{\delta} R \tag{2.32}$$

The distance between the two shells is equal to the plasma sheath thickness δ. The value can be modelled by the Child law (valid for $V < 40\ kV$):

$$\delta = \frac{\sqrt{2}}{3}\lambda \left(\frac{2V}{T_e}\right)^{\frac{3}{4}} \tag{2.33}$$

Where λ is the Debye length, V is the potential of the spacecraft and T_e is the electron temperature. Space plasma is a neutral plasma (number density of ions equal to the one of electrons), but departure from neutrality can happen on short spatial scale, quantified as the Debye length [4].

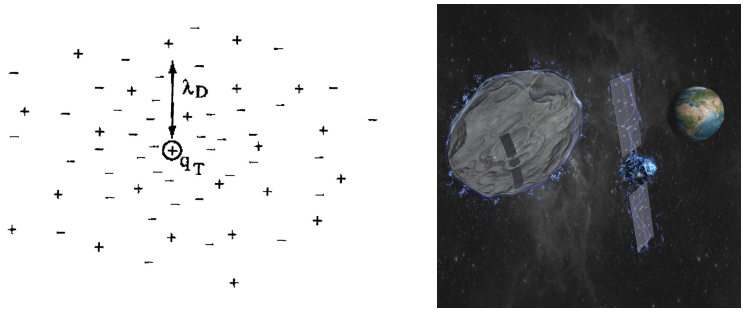

(a) Debye length, indicated as λ_D, used to quantify the electrostatic force in space plasma

(b) Artistic illustration of the Electrostatic Tractor. Credits: ESA

Figure 2.11: Electrostatic tractor

The charge to mass ratio can be expressed as:

$$\frac{q}{m} = 4\pi\epsilon_0 \frac{\frac{R+\delta}{\delta}R}{m_{sc} + 4\pi\rho_s s R^2} V \tag{2.34}$$

Where m is mass of the spacecraft and the charged sphere:

$$m = m_{sc} + 4\pi R^2 \rho_s \tag{2.35}$$

The real bottleneck of this technology is charging the asteroid. Also in this case the environment creates an electrostatic field on the surface through the solar radiation and

the solar wind (flow of ionised solar plasma). The solar wind tends to transport charged grains and so, as a consequence, to generate an electric field. But the asteroid is not a conductive body, so electric charges will not be able to move freely generating a complex charge diffusion.
A first approximation of the power required to maintain a certain voltage on the asteroid can be seen in fig. 2.12. It can be noted that negatively charged asteroids are a better option because the power consumption is lower.

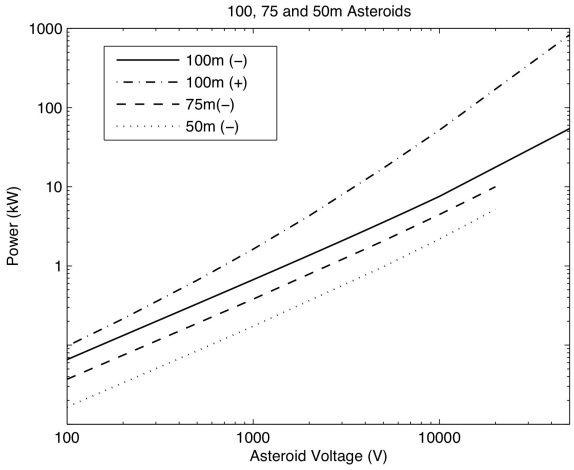

Figure 2.12: Power required to maintain different sized asteroids at a given voltage [58]

The procedure used to obtain the power needed to charge an asteroid, together with the methods proposed to generate such an high power, are explained in appendix A.4.1.

In the end in order to compute the electrostatic force and so the deviation obtained, the potential field around the asteroid has to be evaluated. Two models are presented, one considers the plasma interactions, which can shield the electric field created, and the other ignore the presence of plasma.
Considering the plasma environment the potential can be computed using the Debye-Hückel expression:

$$\frac{\phi}{\phi_0} = \frac{R_{ast}}{r} e^{-\frac{r-R_{ast}}{\lambda}} \tag{2.36}$$

Where ϕ_0 is the surface potential, λ is the Debye length and r is the hovering distance. Ignoring the presence of plasma the expression of the potential is given simply by the Laplace formula:

$$\frac{\phi}{\phi_0} = \frac{r}{R_{ast}} \tag{2.37}$$

So the correct value of the electrostatic potential around a spherical and conductive

charged asteroid immersed in a plasma lies between this two limits, given in (2.36) and (2.37) [58]. The solution is obtained following the turning point method proposed by Thiébault in [94]. The expression obtained to quantify the potential is:

$$\frac{\phi}{\phi_0} = \frac{R_{ast}}{r} e^{-\frac{r-R_{ast}}{\alpha\lambda}} \tag{2.38}$$

Where $\tilde{\lambda} = \alpha\lambda$ is the effective shielding length, which depends on the potential and on the radius of the asteroid (its values are tabulated [58]).
In the end the total force acting on the asteroid (F), considering also the force given by gravitational attraction, can be computed following the method in [58].

$$F = \frac{G m_{sc} M_{ast}}{r^2} - \frac{q\phi_0 R_{ast}}{r} e^{-\frac{r-R_{ast}}{\tilde{\lambda}}} \left(\frac{1}{r} + \frac{1}{\tilde{\lambda}}\right) \tag{2.39}$$

Where the charge of the spacecraft q can be computed from eq. 2.34.

2.3.3. Magnetic tractor

A novel technique presented by Brown in [12] exploits the magnetic attractive force to deviate the trajectory of the asteroid. In this case it is needed to place a magnet on the asteroid and on the spacecraft. Brown suggests to launch an array of small magnets with the same orientation from the spacecraft in the direction of the asteroid. The problem is the attachment system, because we need to know very well the surface composition of the asteroid.

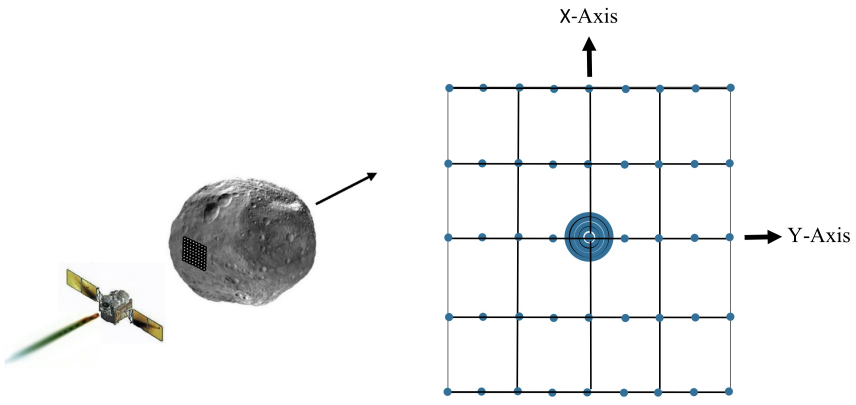

(a) Conceptual illustration of magnetic tractor (repulsive force)

(b) Coordinate system definition

Figure 2.13: Magnetic Tractor [12]

A large magnet has to be placed also on the satellite. A solution can be a superconductive magnet able to produce strong magnetic field, in the order of 30 T, through current flowing in the superconductive coils. So the magnetic moment is modelled as a solenoid:

$$m_{m,sc} = \frac{2\pi R^3}{\mu_0} B_0 \tag{2.40}$$

Where B is the magnetic field and $\mu_0 = 4\pi \cdot 10^{-7}\ H/m$ is the magnetic permeability in vacuum. The asteroid magnet can be modelled as [12]:

$$m_{m,ast} = \frac{B_0 \pi R^2 L}{\mu_0} \tag{2.41}$$

Where L and R are the dimension of the array of magnet. The reference system is defined as in fig 2.13b, so $m_{m,sc}$ is directed in +z direction, while $m_{m,ast}$ is directed in -z direction. The spacecraft magnet is located at the origin, so the magnetic force is:

$$\vec{F}_{(i)} = \frac{3\mu_0 m_{sc} m_{ast}}{4\pi} \left(\frac{(x_i^2 + y_i^2 - 4z^2)}{x_i^3 (x_i^2 + y_i^2 + z^2)^{3/2}}, \frac{(x_i^2 + y_i^2 - 4z^2)}{y_i^3 (x_i 2 + y_i^2 + z^2))^{3/2}}, \frac{3(x_i^2 + y_i^2) - 2z^2}{z^3 (x_i^2 + y_i^2 + z^2)^{3/2}} \right) \tag{2.42}$$

Where (x_i, y_i, z) is the position of one magnet of the array placed on the asteroids, so for an array of N magnets, the total force is:

$$\vec{F}_{mag} = \sum_{i=1}^{N} \vec{F}_{(i)} \tag{2.43}$$

The Δv is obtained multiplying the magnetic force by the time of the deviating action and dividing by the asteroid mass. The Δv obtained with the simple Gravity Tractor has to be summed up, so:

$$\Delta v_{tot} = \Delta v_{mag} + \Delta v_{GT} = \frac{F_{mag} \Delta t}{M_{ast}} + \Delta v_{GT} \tag{2.44}$$

2.3.4. Mass driver

The mass driver strategy is simply based on Newton's third law of dynamics, so for every action it corresponds an equal and opposite reaction. So in our case the idea is to remove in-situ material from the asteroid and eject it, in this way a force in the opposite

direction is generated on the asteroid: momentum is conserved. This idea was formally demonstrated by Gerard O'Neill in 1977, which was the first that proposed to use this technique to deviate an asteroid.
So the strategy is to land on the equator of the asteroid and then periodically launch some material in line with the redirection vector [5].
The most studied configuration in literature is to have small modular mass drivers landers, as can be seen in fig. 2.14. This idea was proposed in 2003 by the SpaceWorks Engineering, Inc. (SEI) and also developed by NASA [73] with the name of MADMEN (Modular Asteroid Deflection Mission Ejector Node).

Figure 2.14: Illustration of the MADMEN concept [73]

The power converted to kinetic energy depends on the mass of the power system, considered as 30% of the total mass [5], and on the mass to power ratio τ, as an average equal to 25 kg/kW [84]. Considering an efficiency of the rail gun system of 30%:

$$P_k = 0.3\frac{m_{power}}{\tau} \tag{2.45}$$

Then the mass of the ejected material with each shot is:

$$m_{mat} = \frac{2P_k\Delta t_{shooting}}{v_e^2} \tag{2.46}$$

Where v_e is the ejection velocity, considered equal to 200 m/s [72], and $\Delta t_{shooting}$ is the interval of time available to shoot. Considering that the mass ejector can fire in a + or -5° window of the desired direction, the time available can be computed as:

$$\Delta t_{shooting} = \frac{10°}{360°}T_{rot} \tag{2.47}$$

In the end the total Δv, considering the whole number of launches, is:

$$\Delta v = n_{launches} \frac{m_{mat}}{m_{ast}(t)} v_e \tag{2.48}$$

Note that the mass of the asteroid decreases in time, and this has to be considered in the computation of the the Δv. Looking at the previous formula it can be noted that mass driver can be considered also as an impulsive deflection strategy, because the action is not really continuous, but it is an instantaneous action repeated many times. Anyway also NASA in [64] and in [70] classified mass driver as a slow push deflection.

2.3.5. Ion Beam Shepherd

The Ion Beam Shepherd (IBS) concept was proposed by Bombardelli and Peláez in 2011 [9]. The idea is to point an high velocity ion beam, produce by an on board ion thruster of a shepherd spacecraft, towards the asteroid and in this way modify its orbit.

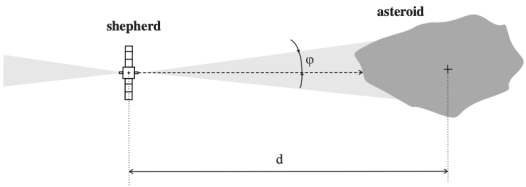

Figure 2.15: Scheme of asteroid deflection through IBS [9]

The ion thruster exploits the process of electron avalanche: electrons (generated by an ionization cathode) move towards the anode thanks to an electric field and collide with neutral particles of gas (Xenon) generating positive ions which are then accelerated through a grid. So high velocity ions of the quasi neutral plasma (see 2.3.2) are shot by the thruster on the spacecraft and penetrate into the asteroid surface until they stop, totally losing they energy. If the beam fully intercepts the surface the force generated on the asteroid is equal, and opposite, to the one on the spacecraft [10].
Obviously, as can be seen in fig. 2.15, the station keeping is maintained by another thruster opposite to the one used for the deflection.

The formulas to compute the asteroid velocity variation obtained with this strategy are presented without going in the details of the ion thruster design. The total mass of the IBS is computed as the sum of the fuel mass, the mass of the power plant needed to feed the ion thruster and the structural mass of the spacecraft: $m_{IBS} = m_{fuel} + m_{pp} + m_{structure}$.

In detail:

$$m_{fuel} = \frac{2F_{th}\Delta t}{v_e} \tag{2.49}$$

$$m_{pp} = \frac{2F_{th}\alpha v_e}{2\eta} \tag{2.50}$$

Where α is the inverse specific power, considered equal to 10 kg/W, $\eta = 60\%$ is the thruster efficiency (data taken from [5]) and $v_e = I_s g_0$ is the exit velocity of the ions, which depends on the specific impulse. Δt is the total thrust time.
The optimal exit velocity is the Irving-Stuhlinger characteristic velocity [88]:

$$v_{e,opt} = \sqrt{\frac{2\eta\Delta t}{\alpha}} \tag{2.51}$$

So the force of the thruster can be computed inverting the mass equation, and then the Δv of the ion beam method can be computed [5].

$$F_{th} = \frac{m_{IBS} - m_{structure}}{2\left(\frac{\Delta t}{v_e} + \frac{\alpha v_e}{2\eta}\right)} \tag{2.52}$$

$$\Delta v = \frac{3F_{th}\Delta t}{\rho_{ast} d_{ast}^3} \tag{2.53}$$

Where ρ_{ast} is the density and d_{ast} is the diametre of the asteroid.
The hovering distance has to be defined so that the whole plume impinges on the asteroid. As explained in [9] this distance can't overcome the value:

$$d_{max} = \frac{L}{2sin(\phi)} \tag{2.54}$$

Where L is the smallest dimension of the asteroid and ϕ is the angle defined in 2.15.

2.3.6. Tugboat

The concept of asteroid tugboat consists in deflecting the NEO by docking with it for a long period of time and push (or pull) with the thrusters in the correct direction to modify the trajectory and avoid the collision with Earth. It was first proposed by Schweickart, Lu, Hut and Chapman in 2003 [86].

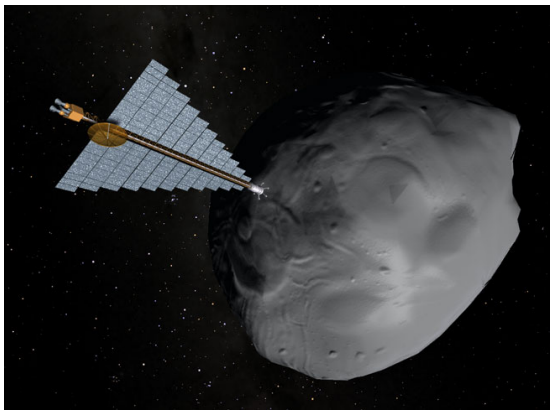

Figure 2.16: Illustration of the Asteroid Tugboat concept

The model proposed in [84] is followed for the computation of the total impulse . The thrust of the system can be expressed as:

$$T = m_{power}\frac{\xi}{\tau} \tag{2.55}$$

The parameters are the same defined for the GT strategy in section 2.3.1. Considering the duration of the pushing action Δt, from [84] the equation of the dry mass is:

$$m_d = \frac{m_i}{1 + \frac{\xi}{2\pi I_s g_0}\frac{\Delta t}{2}} \tag{2.56}$$

So the total impulse:

$$I_t = T\frac{\Delta t}{2} \tag{2.57}$$

It is possible to compute the velocity variation that can be obtained with the asteroid tugboat strategy from the total impulse, dividing by the mass of the asteroid. The acceleration is instead obtained dividing the thrust by the asteroid mass. Integrating step by step the Gauss equations the variation of the orbital elements can be obtained (assuming that the acceleration is only tangential) and so also the deviation can be computed.

2.3.7. Solar collector

The use of solar collectors for asteroid deflection was first proposed by Melosh and Nemchinov in 1993 [54]. The mission starts with a rendezvous with the asteroid, then the spacecraft will maintain a stable hovering position and a solar collector is deployed. The collector will focus sunlight on the surface of the asteroid to ablate the material. The escaping gas and particles produce a continuous thrust which changes the trajectory of

the asteroid [44].

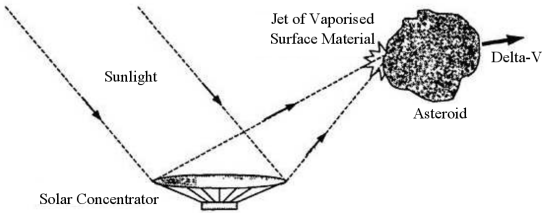

Figure 2.17: Principles of the Solar Concentrator [32]

The power density received by the concentrator is:

$$P_{solar} = \eta \frac{S_{flux}}{r^2} A_m (1 - \alpha) \tag{2.58}$$

Where η is the efficiency of the system, A_m is the surface of the mirror illuminated, r is the distance between spacecraft and Sun, $S_{flux} = 1367\ W/m^2$ is the solar flux at a distance of 1 AU from the Sun and α is the albedo of the asteroid. The value of the albedo depends on the composition of the asteroid, in a worst case it can be set equal to 0.2 [84]. The heat generated by the solar light produces sublimation, but the losses due to heat dissipated in conductive way and in radiative way have to be considered.

$$E_v \frac{dm(t)}{dt} = P_{solar} - Q_{loss} = P_{solar} - Q_{cond} - Q_{rad} \tag{2.59}$$

E_v is the enthalpy of sublimation, which can be set equal to $14.5 \cdot 10^6\ J/kg$ [1] and $\frac{dm(t)}{dt}$ is the mass flow rate (per unit surface, so measured in $[\frac{kg}{sm^2}]$). The radiation heat is defined following the black body radiation formula:

$$Q_{rad} = \sigma \epsilon_{bb} (T_{sub}^4 - T_{amb}^4) \tag{2.60}$$

Where σ is the Stefan-Boltzmann constant and $\epsilon_{bb} = 0.95$ is the black body emissivity [59]. T_{sub} is the sublimation temperature of the illuminated material and can vary from 3175 K to 3800 K [99], while $T_{amb} = 4\ K$ is the space ambient temperature. For the conductive heat it is here reported the formula obtained in [84]:

$$Q_{cond} = (T_{subl} - T_0) \sqrt{\frac{ck\rho_a}{\pi t}} \tag{2.61}$$

In this case T_0 is the temperature at the centre of the asteroid, assumed to be equal to 298 K [29], c is the heat capacity, considered equal to 1361 J/kgK [22], and k is the

thermal conductivity, which is function of the sublimation temperature [99]:

$$k = k_0 \left(\frac{298}{T_{sub}} \right)^{0.5} \tag{2.62}$$

Then the specific mass flow rate (per unit surface) has to be integrated over the illuminated area. Note that the mass flow rate can result a negative value, but in this case the power is not enough to start the sublimation and so its value has to be increased. The horizontal position x can be expressed in terms of time using the rotational velocity of the asteroid, so $x = v_{rot}t$, and so $dx = v_{rot}dt$. So the double integral is in terms of the direction y and in terms of the exposure time. So t_{in} and t_{out} are the time instants in which the asteroid moves inside and outside the illuminated area.

$$\dot{m} = 2v_{rot} \int_0^{y_{max}} \int_{t_{in}}^{t_{out}} \frac{1}{E_v} (P_{in} - Q_{rad} - Q_{conv}(t))\, dt\, dy \tag{2.63}$$

The average velocity of the ejecta gas particles is computed using the Maxwell's distribution of an ideal gas [84].

$$\overline{v} = \sqrt{\frac{8RT_{subl}}{\pi M_m}} \tag{2.64}$$

Where R is the gas constant and M_m is the mass of a molecule of the material considered, in this case forsterite [44], a magnesium-silicate material (Mg_2SiO_4). One of the possible reactions which can happen when forsterite is heated up and sublimated is:

$$2Mg_2SiO_4 \leftrightarrow 4MgO + 2SiO + 2O_2 \tag{2.65}$$

So the average molar mass is 40 g/mol. The value of velocity found is 552 m/s. So it is possible to compute the thrust produced by the evaporated material and the acceleration:

$$F = \lambda \overline{v} \dot{m} \tag{2.66}$$

$$a = \frac{F}{M_a(t)} \tag{2.67}$$

Where $M_a(t)$ is the mass of the asteroid, which decreases in time, and $\lambda = \frac{2}{\pi}$ is the scatter factor, used to take into account the uniform expansion of the ejecta flow over an half sphere [29].

Theoretically the lifetime of a solar collector is unlimited because the energy comes from the Sun. But there are some important problems such as the degradation of the collector caused by condensing vapour, focusing mismatch on a rugged surface and the strong

dependence on the asteroid rotational velocity. The work by Kahle [43] concludes that a maximum lifetime for a solar collector can be from 10 to 30 minutes. For these reasons the solar collector technique has been recently substituted with the laser ablation strategy, explained in the following chapter.

2.3.8. Laser ablation

The idea of exploiting a laser to ablate the surface of an asteroid and so change its trajectory is conceptually similar to the one of solar collectors explained in the previous section, but in this case a laser beam is used, powered by a nuclear reactor or by solar arrays. The thrust is produced in the same way as explained in the previous section: the ablated material generate a plume of gas which is expelled from the surface of the asteroid. As can be seen in fig. 2.18 also in this case an halo orbit can be exploited or a multi-satellite configuration, which augment the deviation obtained.

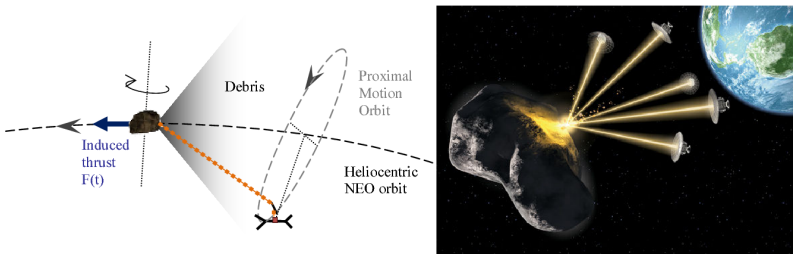

Figure 2.18: Illustration of laser ablation strategy for asteroid deflection (multi satellite-configuration) [27]

So the mathematical model is the same presented before, but in this case the power is not generated by a solar collector, but by a laser. The parameters are summed up in table 2.3.

Parameter	Value
Density of the material ρ	$3500 kg/m^3$
Sublimation enthalpy (olivine) E_v [1]	$14.5 \cdot 10^6 J/kg$
Black body emissivity ϵ_{bb} [59]	0.97
Temperature at the asteroid centre T_0	273 K
Solid heat capacity c [22]	1361 J/kgK
Thermal conductivity k_0 [99]	4.51 W/mK
Sublimation temperature T_{sub} [99]	3500 K
Space ambient temperature T_{amb}	4 K

Table 2.3: Parameters for laser ablation

The absorbed laser power per unit area can be expressed as [99]:

$$P_{in} = \frac{\tau \tau_g \alpha_M \eta_L P_L}{A_{spot}} \tag{2.68}$$

Where τ is the degradation factor, which accounts for the effects of the re-condensed deposited ejected material [99], τ_g is a coefficient which represents the absorption of the laser beam inside the plume of gas and ejecta. From experimental analysis it is expected to be equal to 0.1. η_L is the efficiency of the laser system, which for pure laser diode systems is around 60%. The coefficient $\alpha_m = (1 - \epsilon_a \alpha_s)$ is the absorption at the spot and depends on the albedo α_s and on the increment in reflectivity at the frequency of the laser beam ϵ_a. The albedo is expected to be around 0.1 and 0.3 for an asteroid of the S-type [29] and for a frequency between $750 - 800$ nm the reflectivity increment (with respect to a central frequency of 505 nm) is 20% [13].
The point now is to quantify the degradation factor. The model proposed in the work of Kahle [44] is followed. First of all the density of the gas plume is computed. It depends on the distance r from the spot and on the elevation angle θ from the normal to the surface (see fig. 2.19):

$$\rho_{plume}(r, \theta) = \rho^* k_p \frac{d_{spot}^2}{(2r + d_{spot})^2} \left[cos\left(\frac{\pi \theta}{2\theta_{max}} \right) \right]^{\frac{2}{k-1}} \tag{2.69}$$

Note that this equation is valid only for continuum flow regime. Considering diatomic molecules the jet constant k_p is equal to 0.345 and $k = 1.44$. The maximum expansion angle θ_{max} is set equal to 130.45°. The plume density at the spot ρ^* (density at the throat

of the nozzle) is:

$$\rho^* = \frac{\dot{m}}{A_{spot}\overline{v}} \tag{2.70}$$

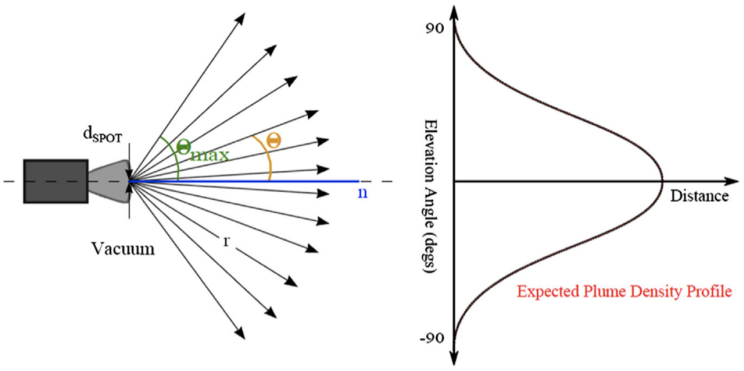

Figure 2.19: Laser spot and geometry of the ejecta plume [30]

The variation of the height of the layer is obtained through the layer growth rate, considering that $h_{layer} = v_{layer}t$:

$$v_{layer} = \frac{\overline{v}\rho_{plume}(r,\theta)}{\rho_{layer}} \tag{2.71}$$

$$\frac{dh_{layer}}{dt} = \frac{\overline{v}\rho_{plume}(r,\theta)}{\rho_{layer}} cos(\psi_{vf}) \tag{2.72}$$

Where ρ_{layer} is the density of the deposited material, which can be set equal to 250 kg/m^3 [99], while ψ_{vf} is the view angle. The degradation factor can be expressed through the Beer-Lambert-Bougier law, considering the absorbance per unit length of the accumulated ejecta $\eta = 5 \cdot 10^4$ $1/m$ [28]:

$$\tau = e^{-\eta h_{layer}} \tag{2.73}$$

The thrust generated is the same of the one obtained in the previous section, so $F = \lambda\overline{v}\dot{m}$. The velocity variation generated can be easily computed with an integral over the deflection time:

$$\Delta v = \int_{t_i}^{t_f} \frac{F(t)}{M_{ast}(t)}\, dt \tag{2.74}$$

Note that the mass of the asteroid M_{ast} varies in time because of the sublimation.

2.3.9. Yarkovsky effect

The Yarkovsky effect takes its name from a Russian engineer, which in 1901 published an article declaring that heating a rotating planet should generate an acceleration in its

motion. Since his work was not complete, he was only able to estimate the order of magnitude of the force, the idea of Yarkovsky was valid and other following studies were performed by Spitale in 2002 [87], by Scheeres in 2004 [85] and more recently (2014) by Basart [33].
The Yarkovsky effect is a non gravitational force caused by thermal radiation from a body which has non uniform surface temperatures. During daylight the asteroid absorbs the energy from the Sun which is then re-irradiated, so the thermal photons which leave the surface carry momentum and produce a force on the asteroid. The higher is the temperature the higher is the force generated.

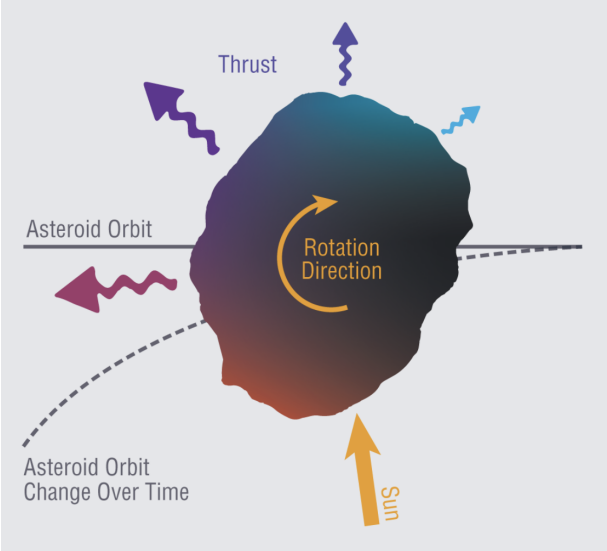

Figure 2.20: Illustration of the Yarkovsky effect [101]

Since there is a delay between the instant when the surface receives the maximum insolation and the time it reaches the highest temperature, an acceleration is generated which changes the semi-major axis of the asteroid orbit.
So the Yarkovsky effect is a natural effect, but can be augmented artificially to enhance its effect. There are two parameters that can be varied: the albedo and the thermal conductivity.
Assuming a linearization of the surface boundary conditions, a fixed rotation about the spin axis and a circular orbit of the asteroid the variation of the semi-major axis can be computed distinguishing two different effects, one diurnal and one seasonal [85]:

$$\left(\frac{da}{dt}\right)_{diurnal} = -\frac{8}{9}\frac{A\Phi}{n} f(R_{\nu_d}, \Theta_{\nu_d}) cos(\gamma) \tag{2.75}$$

$$\left(\frac{da}{dt}\right)_{seasonal} = \frac{4}{9}\frac{A\Phi}{n} f(R_{\nu_s}, \Theta_{\nu_s}) sin^2(\gamma) \tag{2.76}$$

Where $\Phi = \pi R^2 S/(mc)$ is a characteristic factor related to absorbed or scattered sunlight, with R which is the radius of the asteroid, S is the solar radiation flux (at the orbital distance), m is the mass of the body, $c = 3 \cdot 10^8\ m/s$ is the speed of light, n is the orbital mean motion and $A = 1 - \alpha$, where α is the albedo. The two effects have a different dependence on the spin axis obliquity γ, the seasonal part is always positive and so it always leads to a decrease of the semi-major axis, while the diurnal effect can be also negative so it increases the semi-major axis. The dependence on the thermal conductivity K is in the function $f(R_{\nu_d}, \Theta_{\nu_d})$, defined as:

$$f(R_\nu, \Theta_\nu) = \frac{f_1(R_\nu)\Theta_{nu}}{1 + 2f_2(R_\nu)\Theta_\nu + f_3(R_\nu)\Theta_\nu^2} \tag{2.77}$$

So this function is determined by the thermal parameters of the body at a frequency ν. For the diurnal case $\nu = \omega$ (rotation frequency), while for the seasonal case $\nu = n$. The functions f_1, f_2, f_3 depend on the non dimensional radius, defined as: $R_\nu = R/l_\nu$, where $l_\nu = \sqrt{K/(\rho C \nu)}$, C is the surface heat capacity. The term Θ_ν depends on the surface thermal inertia $\Gamma = \sqrt{K\rho C}$, so $\Theta_\nu = \Gamma\sqrt{\nu}/(\epsilon\sigma T_*^3)$, where ϵ is the emissivity of the surface, σ the Stefan-Boltzmann constant and T_* is the subsolar temperature: $T_*^4 = \alpha S/\epsilon\sigma$.
The results obtained, fixing the action time interval to 10 years, can be seen in fig. 2.21. The rotational velocity is set to 5 *cycles/day* and the target asteroid is 2023 PDC [68]. The coefficient f_1, f_2 and f_3 are extrapolated from the graph in the paper by D. Vokrouhlicky [100], since their calculation is very complex and comes from the solution of the thermodynamic differential equations.

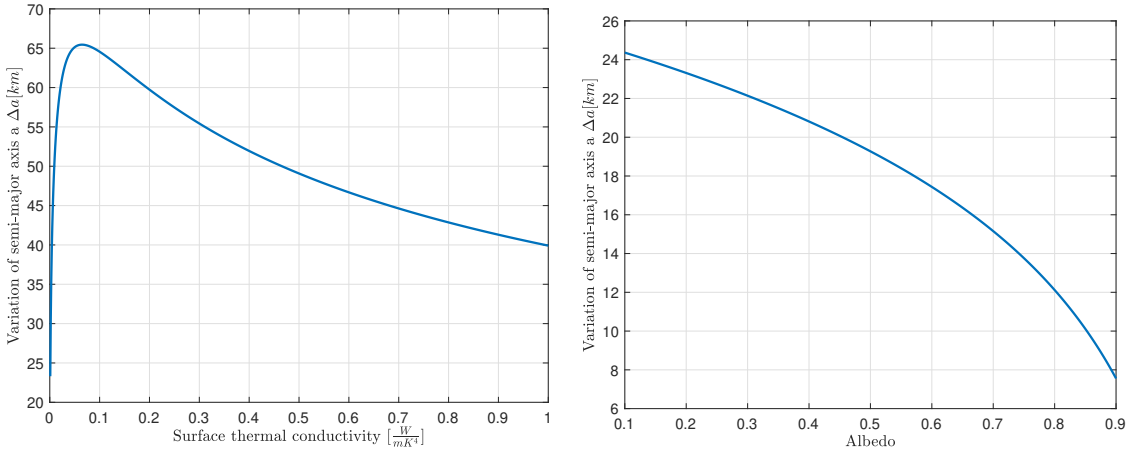

(a) Variation of semi-major axis varying the thermal conductivity

(b) Variation of semi-major axis varying the albedo

Figure 2.21: Results of the Yarkovsky effect mathematical model proposed

The thermal conductivity (k) of bare-rock (material of the asteroid) is around 1 W/mK^4 It can be noted that decreasing the value of k an higher variation of semi-major axis Δa is obtained, until it reaches a maximum at around 0.05 W/mK^4. This value means that the surface has to be transformed in porous regolith. How to do it is the real issue, the only solution proposed (by Spitale [87]) is to bombard the surface with explosives, but the results are not guaranteed and the complexity of the mission becomes very high. Another way to augment the variation Δa is to change the albedo of the surface. In order to reduce the albedo it is possible to cover the surface of the asteroid with dirt and dust. If asteroid 2023 PDC is considered spherical with a radius of 1 km and the thickness is $h = 1\ cm$ [87], the volume is $4\pi r^2 h = 1.25 \cdot 10^5\ m^3$, so the mass of dirt needed is: $m_{dirt} = Vol \cdot \rho_{dirt} = 153\ tons$. This value of mass can't be launched with the current technology, so the mission is unfeasible.

YORP effect

Half a century after Yarkovsky's work, the Yarkovsky-O'Keefe-Radzievskii-Paddack (YORP) effect was proposed. The YORP effect is the rotational counterpart of the Yarkovsky effect, infact the rotation of small asteroids can be affected on long timescales by a net torque that is caused by directly scattered sunlight and thermal radiation from the surface of the asteroids. This is the YORP effect, which can change the direction of the rotation axis and the rotation rates [11].

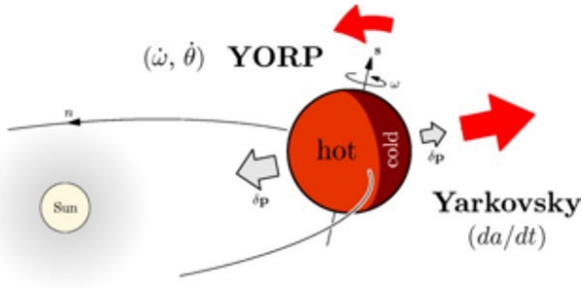

Figure 2.22: Illustration of the YORP effect. Credit: University of Arizona

The YORP effect generates a variation in the rotational rate ω and in the spin axis obliquity γ. So it doesn't affect directly the trajectory, but a change in the spin rate of the asteroid affects the deviation that can be achieved with the Yarkovsky effect or with the laser ablation technique, so it can be exploited to augment the effect of other strategies.

2.3.10. Tether-ballast system

The tether-ballast system was first proposed by French and Mazzoleni in 2009 [23]: it involves the use of a long tether and a ballast mass attached to the NEO. The trajectory is modified in two ways, first the center of mass is immediately changed after the attachment of the ballast mass, and so also the orbit change. Second the tether tension that adds a perturbing force which affects the trajectory has to be considered.

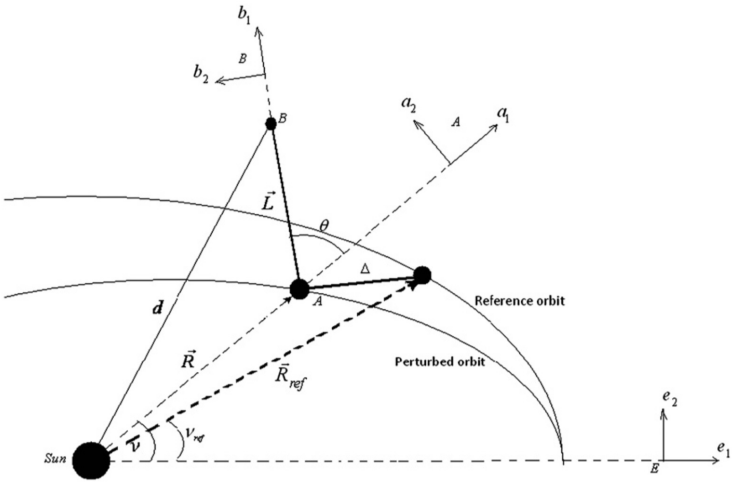

Figure 2.23: Dynamical illustration of the tether-ballast system [50]

The kinetic and potential energy of the system are:

$$K = \frac{m_A}{2}(\dot{R}^2 + R^2 * \dot{\nu}^2) + m_b L(\dot{\nu} + \dot{\theta}) \left(\frac{L}{2}(\dot{\nu} + \dot{\theta}) + R\dot{\nu}cos(R) - \dot{\theta}sin(\theta) \right) \tag{2.78}$$

$$V = -\mu \left(\frac{m_A}{R} + \frac{m_b}{d} \right) \tag{2.79}$$

The definitions of the variables can be seen in fig. 2.24, while m_A is the mass of the asteroid, m_b is the mass of the ballast and L is the length of the tether. Using the Lagrange equation it is possible to derive the equations of motions of the system, which are not reported here for simplicity, but can be found in literature ([50] [23]).

$$\frac{d}{dt}\left(\frac{\partial K}{\partial \dot{q}_i}\right) - \left(\frac{\partial K}{\partial q_i}\right) + \left(\frac{\partial V}{\partial q_i}\right) = Q_i \tag{2.80}$$

Where the generalized coordinates q_i are the distance Sun-asteroid (R), the true anomaly (ν) and the inclination of the tether θ.
In the work by Mashayekhi published in 2002 [50] it is proposed also to cut the tether at a certain time to enhance the diversion achieved. In fig. 2.24 it is reported the deviation achieved considering a mass ratio $m_r = m_b/m_A = 0.001$ and $L = 10000\ km$.

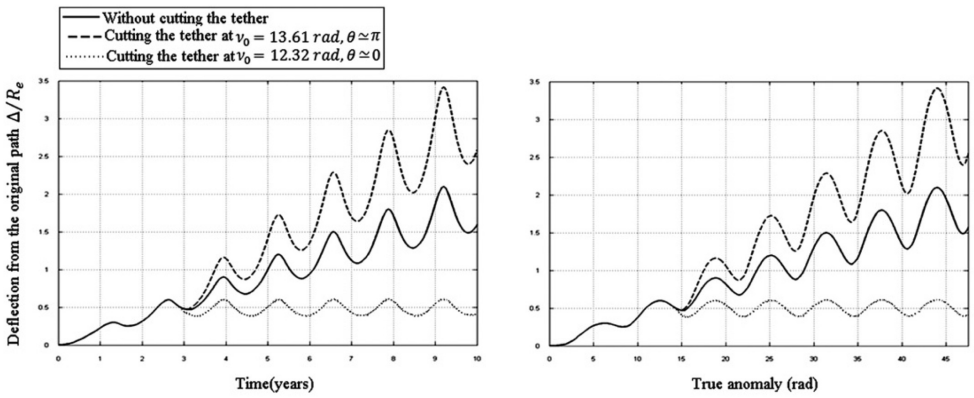

Figure 2.24: Deviation achieved with the tether-ballast system, taken from [50]

Note that considering the asteroid 2023 PDC, which has in the worst case a mass of $5 \cdot 10^{11}\ kg$, the mass of the ballast would be $m_b = 500000\ tons$, so the strategy becomes very difficult to be performed, even considering to collect the mass in loco.
In conclusion this strategy can be used for small asteroids, for which the ballast mass required is smaller, but it is necessary to consider other problems, like the slack tether phenomenon, which could affect the performance of the strategy. In addition cut the tether brings a big advantage in terms of deviation achieved, but, as French underlined in

[24], there is no more the possibility to adjust the trajectory of the system by increasing or decreasing the length of the tether.

2.4. Comparison between strategies

In this section a comparison between the asteroid deflection strategies presented is performed. In order to compare them the deviations are computed considering as a target asteroid 2023 PDC, a fictitious asteroid which has been prepared by NASA as an exercise for the 2023 Planetary Defense Conference [68] (see section 3.7 for details). The dimension and mass considered are the median values.

Starting from the impulsive strategies, the main problem of this kind of deflection is the possibility of destroying the asteroid, as explained in section 2.1. But in some extreme cases, when the warning time is very small, the fragmentation is also an opportunity to avoid the impact and it is also possible to study the atmospheric trajectory of a fragment through an aerothermodynamical analysis, assuring that the mass is completely ablated and performing a risk assessment analysis [74]. So the method of using a subsurface nuclear explosion has to be conisdered in particular for large asteroid and in case of extremely short warning time.

If instead the warning time is higher, it is possible to consider the other two impulsive deflection strategies: kinetic impactor (KI) and nuclear standoff explosion. Concerning the kinetic impactor strategy the main advantage is the maturity of the concept (proved by DART mission), so the high TRL (Technology Readiness Level). In addition it has been defined by Mazanek (senior space system engineer at NASA) the "simplest strategy" [51] and actually the mission is not complex, it does not require to land, to perform in situ operation or to keep an hovering position around the asteroid.
On the contrary the structural properties of the asteroid limit the impact velocity (because we have to avoid disruption), so it becomes very important to know well the physical and chemical characteristic of the asteroid surface and its composition. Uncertainties in the size, density, mass, and composition of the asteroid can bring to a wrong prediction of the deviation, in particular the factor β is strongly affected by this properties and an early reconnaissance mission is needed (section 1.1.1). To underline the effect of this uncertainties let's consider the case of the DART mission: the prediction was wrong because the objective was to reduce the orbital period of the asteroid Dimorphos by 10 minutes, but in reality the reduction was of 32 minutes. In particular the momentum enhancement factor β depends on the along-track component of the velocity change Δv,

the mass of the asteroid M and the net ejecta momentum direction $\vec{E}$ [15]:

$$\beta = 1 + \frac{\frac{M}{m_{sat}}\Delta v_T - U_T}{(\vec{E} \cdot \vec{U})E_T} \tag{2.81}$$

Where $\vec{U}$ is the satellite velocity with respect to the asteroid. The major unknowns are in the computation of β, Δv_T, M and $\vec{E}$. For example for DART mission: $\Delta v_T = -2.70 \pm 0.1(1\sigma)\ mm/s$ and the expected value of β ranges between 2.2 and 4.9 [15].
As mentioned before, KI can bring to fragmentation of the asteroid, that's why the Multiple Kinetic Impactors (MKI) strategy has been proposed. In addition we have to consider also that terminal targeting becomes more difficult as relative velocity (between asteroid and satellite) increases [51].

So, while the kinetic impactor technique can be very useful for small asteroids, a nuclear explosion is more effective for large ones. Standoff nuclear explosion carries the highest energy density among all the deviation methods [98] and it is less sensitive to possible uncertainties in the asteroid composition and surface morphology, since the explosion happens at a certain distance from the surface and so it is not necessary to land. It is useful when warning time is small [108]. In addition it is the most mass efficient technique [51], so for the same deflection obtained the mass required for nuclear explosion is smaller than all the other strategies.
On the other hand, since it is an impulsive technique it could generate fragments, as the KI strategy. As Olds underlines in [72], more critical studies are needed to verify the safety, more than in other missions because in case of a failure during the launch a huge quantity of radioactive materials (in particular Caesium-137) would be released in the atmosphere, as it happened with the atomic bomb test many years ago. In order to understand the problem, a study made in Germany [89] estimates that Caesium-137, which comes from atmospheric military tests, is still present in the boars and it creates much more damages (in particular from human health) than the ones created by Chernobyl disaster. As a consequence many issues related to international treaties and public acceptance have to be considered. Moreover the TRL is low because, for the reason explained before, only theoretical studies have been done.

As far as the slow push methods are concerned, the problem of accidentally destroying the asteroid is no more present, but other issues arise, specific for each strategy.
Starting from the Gravity Tractor, the main advantage of this technique is that it is a contactless deflection, so it doesn't require to land on the asteroid, but it just requires a rendezvous. So it is insensitive to structure, composition and rotation of the NEA [47] and this brings to low uncertainties in the final results. In addition it guarantees a finer

control of asteroid deflection with respect to impulsive strategies.
The main disadvantage of this technology is that it needs a very massive spacecraft and a very long warning time, otherwise the Δv provided is not enough to deflect the asteroid [10]. In addition the difficulty in controlling the proximity hovering position of the spacecraft has to be considered. So in the end it is a useful technique only when warning time is very high (>10 years) [108].
The Halo configuration provides an higher Δv with respect to the standard one if the warning time is higher than a certain value, so as underlined also in [98], the standard configuration of the gravity tractor can guarantee higher tractions in a smaller time interval. In the case of asteroid 2023 PDC, considered in this chapter as a target for the comparison, the action time for the deviation is very small, so probably the halo configuration is not useful. But an interesting configuration has been proposed by Wie and Bong in [107], where two different Halo orbits are used in which more than one satellite is placed. In this way the deviation action is augmented.
A variation of the gravity tractor is the Enhanced Gravity Tractor (EGT), which considers to collect mass in loco to augment the mass of the spacecraft. With this technique the deflection time is reduced by a factor of 10 to 50 with respect to normal GT because it increases the gravitational force between spacecraft and asteroid. But one of the main advantage of the GT is lost, because it is no more a contactless technology, but it is needed to land, so it becomes a very complex mission, in particular the collection of a large value of mass (tons) from the asteroid is something that has never been done before and requires more detailed studies. In addition there was a mission proposed by NASA, called ARM (see section 1.3), in which the collection of mass from an asteroid would have been demonstrated, but this mission was cancelled, so in the end the TRL is low. This is valid also for the mass driver strategy. It has to be considered also that with the EGT strategy more propellant mass is consumed in order to maintain the hovering position. In fig. 2.26 it is considered to collect a mass of 50 *tons*.

As far as the Electrostatic Tractor is concerned, it increases the net force between spacecraft and asteroid, because it is the sum of gravity and electrostatic force. It is possible to pull or push the asteroid, it depends on the sign of the charge, and so a finer control is obtained.
The problems in this case are a lot, first of all the spacecraft has to be charged, and this high potential could create problems with on board electronic components. Also the asteroid has to be charged, and again for this kind of mission the TRL is very low. Moreover plasma interactions have to be considered, because they tend to shield the electric field created [58].

Anyway the performances of this strategy are analysed and a comparison with all the "tractor" strategies can be seen in fig. 2.26. The value of $\tilde{\lambda}$ for an asteroid with diametre of 1539 m (as 2023 PDC worst case [68]) has been obtained considering a linear dependence starting from the values tabulated in Murdoch et al. [58]. Obviously the Δv obtained is higher then the one obtained with the GT.

The Magnetic Tractor strategy produces deflection forces two orders of magnitude higher than GT and so can be used for shorter warning time, but also in this case the complexity of the mission is very high and the main problem is to find a very strong superconductive magnet (i.e. neodynium) to generate a suitable magnetic field. The performances of the Magnetic Tractor are slightly lower than the one obtained with the Electrostatic Tractor, but higher than the one obtained with GT and EGT.

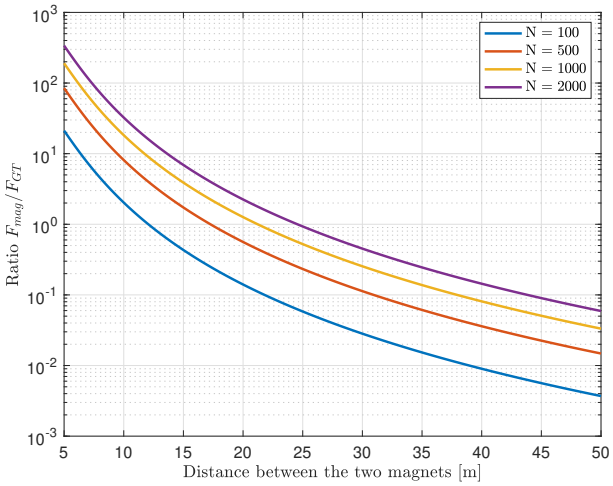

Figure 2.25: Ratio between magnetic force and gravity force varying the hovering distance and the number of magnets

It can be seen in fig. 2.25 that the magnetic force is strongly dependent on the number of magnets and on the hovering distance. Increasing the number of magnets brings to an higher mission complexity and also small distance from the surface of the asteroid can bring to problems considering the plume ejecta of the thrusters which interact with the surface.

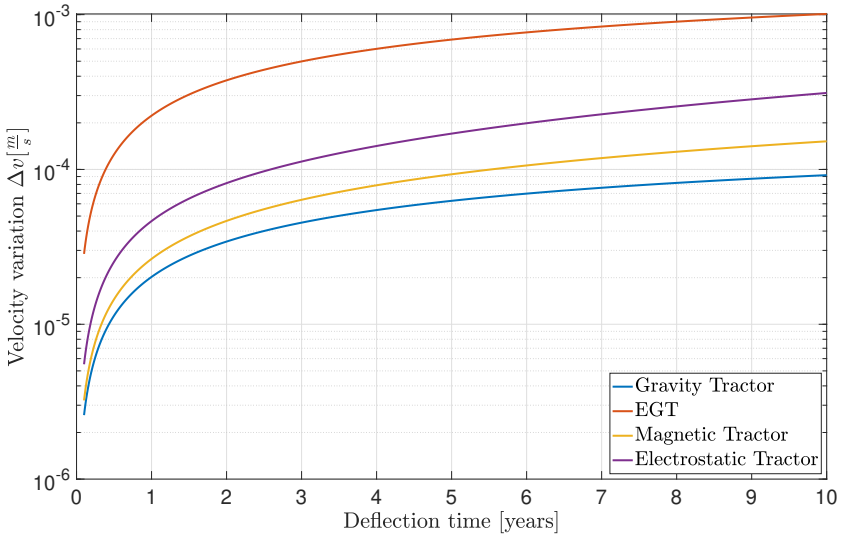

Figure 2.26: Comparison between the "tractor" strategies, $M_{ast} = 2.5 \cdot 10^{11}\ kg$, $d_{ast} = 620\ m$

The Mass Driver strategy is one of the first strategies proposed for asteroid deflection. In this case a controlled application of perturbing force is obtained and it provides more impulse with respect to the tractor strategies (gravity, electrostatic and magnetic) [72], as it can be noted from the comparison in fig. 2.28, where it is considered a frequency of one launch per day. On the other hand, as explained before for the Enhanced Gravity Tractor, the TRL is low. In addition high power requirements are needed and uncertainties in impact location and composition of the asteroid are a problem for the design of the mass collector.

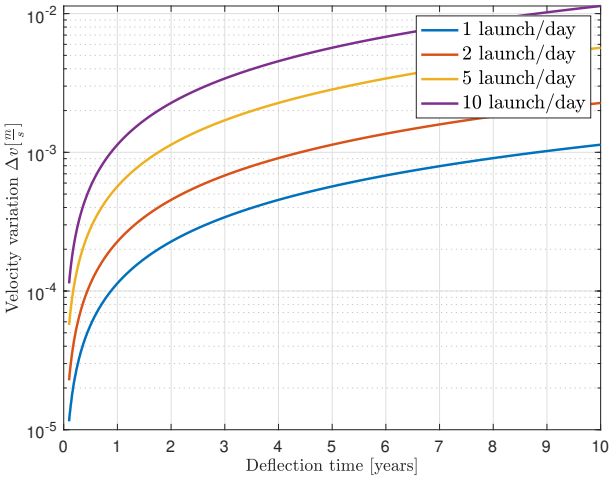

Figure 2.27: Variation of Δv of mass driver strategy increasing the launch frequency

In conclusion the Mass Driver strategy could be a good alternative to impulsive deflection techniques, because, if the frequency of the launches is high enough, as can be seen in fig. 2.27 the Δv is strongly dependent on the launch frequency (two orders of magnitude changing from 1 to 5 launches per day), the warning time required is not as high as the one of GT and depends on the capacity of the gun, so on the mass ejected, the Δv obtained is of the same order of magnitude ($10^{-3}\ m/s$) of the one obtained with Kinetic Impactor.

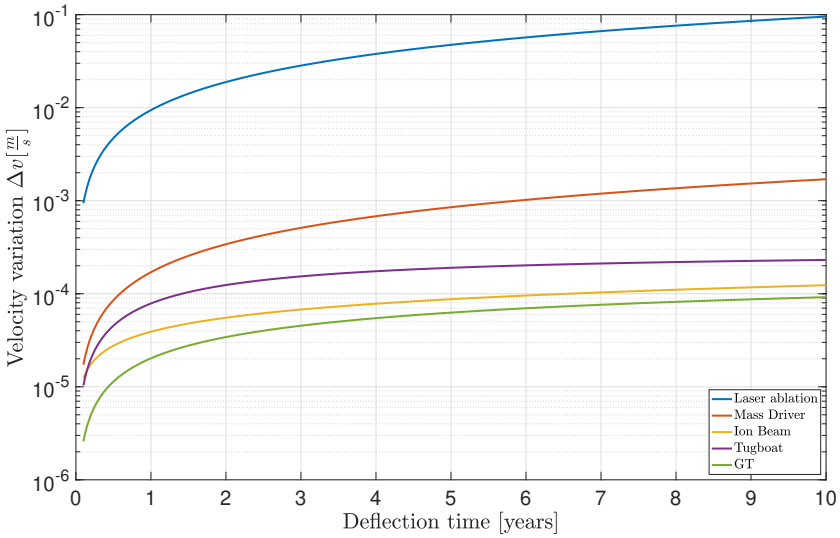

Figure 2.28: Comparison between strategies, $M_{ast} = 2.5 \cdot 10^{11}\ kg$, $d_{ast} = 620\ m$

With the Ion Beam Shepherd strategy the deflection is performed in a precise manner and can be accurately predicted [10]. With respect to mass driver it is a contactless deflection and this reduces the complexity of the mission. In addition the force generated depends on the power and propulsion subsystems not on the mass (like GT) [10] and the deflection system is part of the spacecraft system, so the ionic propulsion can be used both as a propulsion system and for the deflection action. In fig. A.9 it can be noted the order of magnitude of the force generated by the ion thruster and the comparison with the gravity tractor technique. The force generated, and so also the Δv, is higher in the case of the IBS strategy, so it is more efficient than the Gravity Tractor.
The main parameters that affect the performances are the mass of the IBS system and the inverse specific power α, as can be noted from the graphs in fig. A.9. Anyway the efficiency depends on the ion beam divergence angle and distance from the asteroid [51] and problems can arise when the spacecraft is too close to the satellite. It has to be considered also that the results shown before has been obtained with a theoretical optimal specific impulse (around 6000 s), so the real values of deflection force will be lower.

As can be noted in fig. A.9, the impulse obtained with the Ion Beam Shepherd technique is more than an order magnitude higher than the one obtained with gravity tractor. But as can be seen in fig. 2.28 the difference in Δv between the ion beam strategy and the GT is not so high for an asteroid with a diametre of 620 m and a mass of $2.5 \cdot 10^{11}$ kg (2023 PDC asteroid). So the results of the two technologies can be superimposed, but the mission complexity is higher if the ion beam is used.

The Asteroid Tugboat (AT) strategy has been developed has an alternative to the Kinetic Impactor, in fact the idea is the same, but in this case the asteroid is not impulsively pushed, but it is slowly accompanied (pushed or pulled) by the spacecraft. In this case the problem of asteroid fragmentation is avoided. Slow deflection in addiction allows for flexible operational concepts [64] and it provides more thrust with respect to Gravity Tractor: as can be seen in fig. 2.28 the Δv obtained with AT is placed between the couple GT-Ion Beam and the Mass Driver.
Asteroid tugboat is a conceptually simple strategy, but there are some problems to be considered. The first one is that the rotation of the asteroid can become a real issue, because the low thrust thruster is no more able to provide a constant pointing if the asteroid rotates and must be continuously switched on and off. A detailed work has been done on this problem by Sanchez, Colombo and Vasile in [84], defining the scattering factor in order to measure the efficiency of the misalignment from the optimal direction of thrusting. They proposed also the scheduled low thrust model: two spacecrafts land on the opposite sides of the asteroid (always along the equator) such that the thrusters can be properly scheduled (switched on and off) in order to obtain a quasi-constant thrust and reduce the scattering factor [84]. In addition to the problem of the asteroid rotation, a second issue is the need of a strong attachment system between spacecraft and asteroid. Moreover during the operation of the thruster a transient atmosphere made of dust is created around the spacecraft and this could affect the performances. In order to reduce the problem of the transient atmosphere the asteroid can be pulled instead of pushed, but in this case the role of the attachment system becomes even more critical. Lastly, it has to be considered also the high power needed to feed the thruster. Using the results obtained for asteroid 2023 PDC [68], the electric power needed to sustain the maximum value of thrust (3.3 N), considering an efficiency $\eta = 0.15$ [48], is:

$$P_e = \frac{T I_s g_0}{2\eta} = 0.32 \ MW \tag{2.82}$$

The maximum specific power of a solar panel can be 300 W/kg [46], so the mass needed is more than 1000 kg, occupying an area of 119 m^2 (considering an average density of

9 kg/m^2 [46]). So probably solar panels are not the best solution and an other kind of energy sources (like solar concentrators or a small nuclear power plant) have to be considered,reducing the TRL of the mission.

The Solar Collector strategy is strictly connected to the Laser Ablation strategy, both of them exploit the sublimation of the asteroid surface. The first method proposed in literature involves the use of a collector to concentrate solar light and sublimate the material. With this technology the energy is theoretically unlimited, but the lifetime of the collector is very short because of plume influence and degradation of solar cells, radiators and insulation.
This technology nowadays has been substituted by the Laser ablation one, which consists in the use of a laser beam to sublimate the material. The advantages of this technique are that there is no need of phisycally land or the attachment of a system to the surface of the NEA, the required spacecraft mass is low with respect to other strategies (like GT or mass driver) [29] and this is due to the fact that it requires no extra propellant dedicated to the asteroid deflection phase [97]. In addition it provides a higher and more controllable rate of deflection, as can be seen also in fig. 2.28, the Δv obtained with a power of 1000 W is higher than all the other strategies.

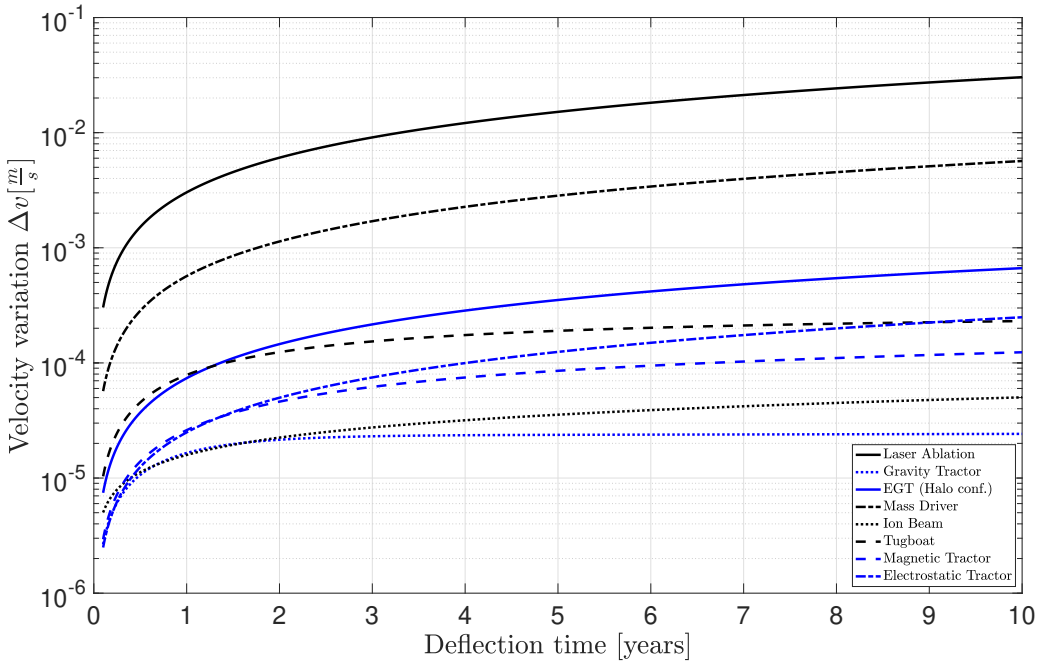

Figure 2.29: Comparison between all the strategies, $M_{ast} = 2.5 \cdot 10^{11}\ kg$, $d_{ast} = 620\ m$

Anyway also in this case there are some disadvantages to be considered, as the optical

degradation, so the laser beam power decreases in time. The working principle of a laser is the excitation of electrons which temporarily jump in an higher energy state. When there are more electrons in the higher energy state than in the lower one, for the minimum energy principle, the electrons fall back to the original state releasing energy, so photons (quantum energy), at a certain wavelength. When a photon has the correct energy it interacts with an excited electron starting the electron avalanche process which leads to the emission of a large number of photons with the same wavelength (from which it results the color of the laser beam) and energy. But this high quantity of energy is not totally released in the laser beam, part of it is released as heat. That's why a laser needs to be continuously cooled down, which means the need of large radiators. Also these radiators are affected by degradation due to plasma interactions.
If the deflection is achievable in a given limit time, laser ablation technique requires a lower mass into space than all the other methods and the use of laser, compared to solar collector, brings to higher conversion losses and provides high light intensity at lower power and longer distance from the target [93].

In section 2.3.9 it has already been explained that the deflection using Yarkovsky effect is unfeasible, in particular for very large asteroids.
The tether-ballast system for asteroid deflection is a useful technique for small asteroids, because for bigger ones the mass of the ballast would be too high, increasing a lot the complexity of the mission. In addition it has to be considered the dynamic problem of the slack tether phenomenon.

2.4.1. Brief comparison

The comparison between all the strategies is summed up in the tables 2.4 and 2.5. The format has been taken from the report of NASA of 2006 [64].

Strategy	TRL	Effectiveness	Warning Time	Complexity
Kinetic Impactor	Very High	High	Long	Very Low
Multiple KI	High	High	Long	Low
Nuclear standoff	Medium	Very High	Short	Low
Nuclear subsurface	Medium	High	Very Short	Medium
Gravity Tractor	Medium	Low	Very Long	Low
Enhanced GT	Medium	Medium	Long	High
Electrostatic Tractor	Very Low	Medium	Long	High
Magnetic Tractor	Very Low	Medium	Long	High
Mass driver	Low	High	Medium	High
Tugboat	Medium	Medium	Long	Medium
Ion beam Shepherd	Medium	Low	Long	Medium
Laser Ablation	Low	High	Medium	Medium
Yarkovsky Effect	Low	Very Low	Very Long	Very High
Tether-Ballast System	Low	Medium	Medium	High

Table 2.4: Comparison between strategy

The TRL is the Technology Readiness Level and it is measured in a scale from 1 (basic technology research) to 9 (highest level of TRL, the system is flight proven successfully). In particular it is considered here:

- Very Low TRL: Technology concept has been formulated, without any test (level 1-2).
- Low TRL: Technologies are evolved to the point where experiments have been performed (level 3-4).
- Medium TRL: Technologies have been validated in a laboratory or in a correct environment (level 5-6).
- High TRL: System prototype has been demonstrated in space environment (level 7-8)
- Very High TRL: the concept is actually flight proven (level 9)

The values of TRL in table 2.4 are taken from [64] [70] and [84]. The only technology with Very High TRL is the Kinetic Impactor strategy, proved by the DART mission. While MKI is not really proven, but the concept of multi-satellite launches is well known. For the Nuclear Explosion mission there are no prototypes available (for safety reasons it can't be proven) so the TRL can't be higher than 6. Considering AT strategy, the problem, which lowers the TRL, is how to generate the high power needed and how to build a

strong attachment system, as explained in the previous section and also underlined by Sanchez, Colombo and Vasile in [84], so the TRL is quite low, from 4 to 6. It can be noted that the TRL level is strictly related to the warning time, because the lower is the TRL the higher would be the time necessary to build the mission. Concerning Laser Ablation strategy the TRL is quite low because the laser is not proved in space, but only on ground. In particular Gibbings explained in [30] that the TRL of laser and laser optics cannot be higher than 3/4, so Low TRL. [29]

The overall effectiveness is defined (by [64]) as the ability to apply the concept to the range of dangerous asteroids, so it is not an absolute measure, but is relative to other alternatives. In this case the most effective technology is the nuclear standoff explosion, which is indeed indicated with 'Very high' in table 2.4. Also Mass Driver and Laser Ablation stand out because of the higher deviation obtained with respect to other slow push strategies, while a technology which exploits the Yarkovsky effect is the less effective.

The warning time required indicates the time needed from the discovery of the potentially hazardous asteroid and the moment when the asteroid is correctly deviated. Generally it can be noted that the slow-push technologies require an higher warning time, even if Laser Ablation and Mass Driver are able to provide good performances even with small warning time.

The complexity of the mission is also analysed in the table, because it is an important factor to be taken into account in a comparison. Higher complexity means higher time to build up the mission and so also higher costs. The simplest strategy, as underlined also in the previous section, is the Kinetic Impactor, while the worst ones are the strategies which require to land (EGT and Mass Driver) or to attach the spacecraft or an object to the asteroid (AT and Magnetic Tractor) together with the the Electrostatic Tractor (which requires to charge the asteroid) and the exploitation of the Yarkovsky Effect.

Strategy	Mass	Spin	Density	Material	Size-Shape	Surface properties
Kinetic Impactor	Yes	Helpful	Helpful	Yes	Helpful	No
Multiple KI	Yes	Helpful	Helpful	Yes	Helpful	No
Nuclear standoff	Yes	No	Helpful	No	No	No
Nuclear subsurface	Yes	No	Yes	Helpful	No	Yes
Gravity Tractor	Yes	Yes	No	No	Yes	No
Enhanced GT	Yes	Yes	Yes	Yes	Yes	No
Electrostatic Tractor	Yes	Yes	Yes	No	Yes	Yes
Magnetic Tractor	Yes	Yes	Yes	Yes	Yes	No
Mass driver	Yes	Yes	Yes	Yes	Helpful	Helpful
Tugboat	Yes	Yes	Yes	No	Yes	Yes
Ion beam Shepherd	Yes	Yes	No	No	Yes	No
Laser Ablation	Yes	Helpful	No	No	No	Yes
Yarkovsky Effect	Yes	Yes	No	No	Yes	Yes
Tether-Ballast System	Yes	Yes	No	Yes	Yes	No

Table 2.5: Dependence of the different strategies on the asteroid properties

While in table 2.5 it is reported if the strategy is dependent on the chemical and physical properties of the asteroid.
The dependence on the material means that the strategy depends on the composition of the asteroid (so S-type, M-type,...) and this is in particular important for strategies that include attaching the spacecraft (AT, Mass Driver, EGT, KI and MKI) or a system (tether or a magnet) to the surface.
Surface properties are referred to all the coefficients and constants that have been listed in the previous sections, so i.e. thermal conductivity, albedo, heat capacity, sublimation enthalpy and temperature.
The format of the table and most of the information are taken from NASA multicriteria comparison [64].
It can be immediately noted that all the strategies are influenced by the mass of the asteroid, because the higher is the mass the more difficult is to achieve the correct deviation.
In conclusion all the strategies need some information on the asteroid properties in order to improve the likehood of success.

2.4.2. Strategies selection for optimisation

The strategies chosen for the optimisation technique are four: Kinetic Impactor, Nuclear Standoff explosion, Gravity Tractor and Laser Ablation.

The kinetic impactor strategy has been selected because of its high TRL level, it has been successfully flight proven by DART mission, and in addition it is conceptually very simple, there's no need of landing and attaching to the asteroid. The only problem is the uncertainties in the composition and the physical properties of the asteroid which can affect a lot the results of the deflection action. But this problem can be partially overcome through an early reconnaissance mission (fly-by or rendezvous to the asteroid).
The nuclear standoff explosion has been chosen mainly because it is the most effective technique, so considering the same mass, it produces the highest values of deflection with respect to all the other strategies. Also in this case the mission complexity is low because the main requirements of the mission are two: rendezvous with the asteroid and detonate the nuclear device at the correct optimal distance. The main problem is in terms of safety, as explained in the previous section, but this strategy in some particular case, when the asteroid has a very high mass and dimensions and the warning time is very small, could be the only one able to deflect the asteroid.
Both the technologies are considered by NASA for the deflection of asteroid 2023 PDC, and so as a consequence are also evaluated in this thesis.
The Gravity Tractor strategy is considered because of its relatively simple mission design and high TRL level. The technology has never really be flight proven, but the whole mission consists only in maintaining the satellite in hovering condition above the asteroid. Another big advantage of this strategy is that there is no dependence on the asteroid composition, so there's no need of an early reconnaissance mission. In addition there is the possibility to use Multiple Gravity Tractor displaced in an artificial Halo orbit, such that the deviation achieved increases a lot.
The laser ablation technology is chosen for the optimisation process because, as can be seen in fig. 2.28 and fig. 2.29, it is able to provide very high Δv with respect to all the other slow push technologies, even if in this case the TRL is very low.

3 | Asteroid Deviation Problem

3.1. Impulsive trajectory to the asteroid

For the impulsive strategies the trajectory chosen to reach the asteroid consists in a Deep Space Manoeuvre (DSM) and a Lambert transfer. So the spacecraft is placed into an orbit around the Sun by the launcher, than at a certain time a DSM is performed, using on board chemical thrusters, in order to reach the correct velocity to place the spacecraft into a Lambert arc and so reach the correct final position (which is the asteroid position).

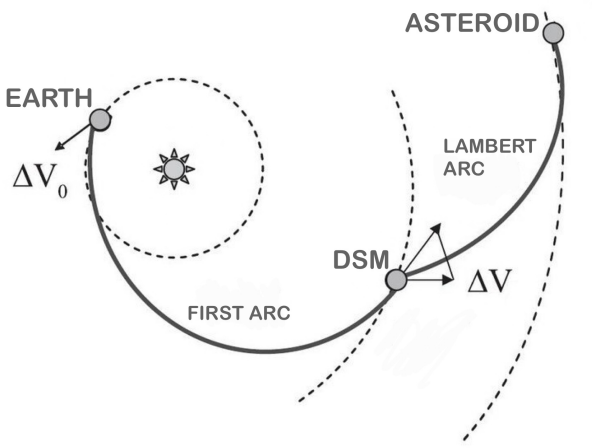

Figure 3.1: Impulsive trajectory

The first Δv, called Δv_0 is given by the launcher and so it is a decision variables which depends on the launcher $c3$. But, as described in [17][7][16][8], also the direction of the spacecraft escape velocity has to be optimised and can be expressed in spherical coordinates. So two angles are defined: $\alpha_{\Delta v_0}$, which can vary from 0 to 2π and represents the in plane component of the velocity, and $\delta_{\Delta v_0}$, which instead varies from $-\pi/2$ to $\pi/2$

and represents the out of plane component:

$$\Delta v_{0,t} = \|\Delta v_0\| \cos \alpha_{\Delta v_0} \cos \delta_{\Delta v_0} \tag{3.1}$$

$$\Delta v_{0,n} = \|\Delta v_0\| \sin \alpha_{\Delta v_0} \cos \delta_{\Delta v_0} \tag{3.2}$$

$$\Delta v_{0,h} = \|\Delta v_0\| \sin \delta_{\Delta v_0} \tag{3.3}$$

Then starting from the initial position, which is the Earth position, and the initial velocity ($\vec{v}_{sc,0}$), which is the velocity of Earth plus the variation of velocity $\Delta\vec{v}_0$, it is possible to compute the orbital parameters of the first arc. Note that the Earth velocity is expressed in the Heliocentric reference frame, while the Δv_0 is in the TNH frame (Transversal-Normal-Out of plane reference frame), so:

$$\vec{v}_{sc,0} = \vec{v}_{Earth,0} + \Delta\vec{v}_0 = \vec{v}_{Earth,0} + \mathbf{R}_{tnh2car}\Delta\vec{v}_{0,tnh} \tag{3.4}$$

For asteroid 2023 PDC NASA (in [68]) defines the time needed before launch (once the asteroid has been identified), because an interplanetary mission requires a certain amount of time for the build-up. So the first day available for launch is the first date possible defined by NASA ($t_{first\ date}$), such that [8]:

$$t_0 = t_{launch} = t_{first\ date} + (t_{MOID} - t_{first\ date} - TOF)\alpha_0 \tag{3.5}$$

Where α_0 can vary from 0 to 1, such that when $\alpha_0 = 0$ the launch happens at the first date possible while when $\alpha_0 = 1$ the launch happens when the asteroid is at the close encounter with Earth (worst choice).
The last decision variable is the time instant at which the DSM takes place. Also in this case the definition given by Bolzoni is taken as a reference:

$$t_{DSM} = t_{launch} + TOF\alpha_1 \tag{3.6}$$

Where TOF is the total time of flight of the mission, so the sum of the first arc and the Lambert arc, and α_1 can vary from 0 to 1, such that the time of flight for the Lambert arc becomes $TOF_{Lambert} = (1 - \alpha_1)TOF$.

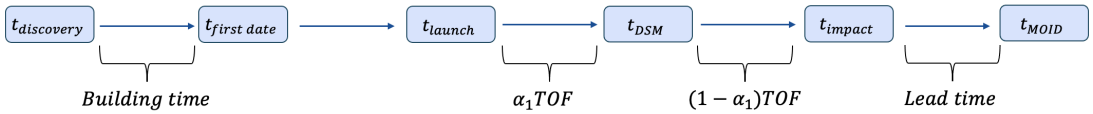

Figure 3.2: Mission timeline

So in the end the set of decision variables for the optimisation process, including the initial mass of the spacecraft is:

$$\mathbf{x}_{impulsive\ traj} = [\alpha_0 \quad \alpha_1 \quad TOF \quad \|\Delta v_0\| \quad \alpha_{\Delta v_0} \quad \delta_{\Delta v_0} \quad m_{sc,0}] \tag{3.7}$$

It can be noted that the arrival final mass of the spacecraft is determined only by the Δv of the DSM manoeuvre, so:

$$m_{sc,f} = m_{sc,0} e^{\frac{-\Delta v_{DSM}}{I_s g_0}} \tag{3.8}$$

3.2. Low thrust trajectory to the asteroid

For the slow-push technologies instead a low thrust trajectory has been implemented. In order to reduce the computational cost the trajectory is shape-based, which means that the position of the satellite is defined as a function of the initial and final orbital elements. In literature a lot of alternatives have been proposed, starting from an exponential sinusoid ([78]) and then to improve the efficiency more complicated shapes were proposed like inverse polynomial and cosine functions([103] [104]) or Fourier series ([91]).
The model used here is one of the most recent, proposed by Zeng, Geng and Wu in 2017 [112]. The main advantage of this model is that it considers trajectory safety constraints, a crucial aspect for the trajectory design problem. In addition the trajectory designed requires less fuel consumption and lower maximum acceleration with respect to the other methods [112].
The shape used for the position vector $\vec{r}$ is:

$$\vec{r} = \phi_1 \vec{r_1} + \phi_2 \vec{r_2} \tag{3.9}$$

Where ϕ_1 and ϕ_2 are the shaping functions, $\vec{r_1}$ and $\vec{r_2}$ are the shaping vectors (which depend on the initial and final orbital elements).

$$\vec{r_k} = \frac{a_k(1-e_k^2)}{1+e_k \cos f_k} \cos f_k \vec{p_k} + \frac{a_k(1-e_k^2)}{1+e_k \cos f_k} \sin f_k \vec{q_k} \tag{3.10}$$

Where $k = 1, 2$ and $\vec{p_k}$, $\vec{q_k}$ are the direction vectors, function of the inclination, the right ascension and the argument of periapsis:

$$\vec{p_k} = \begin{bmatrix} \cos\omega_k \cos\Omega_k - \sin\omega_k \sin\Omega_k \cos i_k \\ \cos\omega_k \cos\Omega_k - \sin\omega_k \sin\Omega_k \cos i_k \\ \sin\omega_k \sin i_k \end{bmatrix} \tag{3.11}$$

$$\vec{q_k} = \begin{bmatrix} -\sin\cos\Omega_k - \cos\omega_k \sin\Omega_k \cos i_k \\ -\sin\omega_k \sin\Omega_k + \cos\omega_k \cos\Omega_k \cos i_k \\ \cos\omega_k \sin i_k \end{bmatrix} \tag{3.12}$$

f is the true anomaly, computed as $f_1 = f_{10} + \theta$ and $f_2 = f_{20} + \theta$. The angle θ is the true anomaly of the transfer orbit but it increases as the number of revolutions increases ($\theta \ \epsilon \ [0 \ \theta_f]$, $\theta_f = f_{end} - f_{20} + 2\pi N_{rev}$). The true anomaly of the spacecraft at departure is f_{10}, while f_{20} is the virtual true anomaly of the target orbit at initial time, f_{end} is the true anomaly of the spacecraft at arrival point.
The shaping functions $\phi_1(\theta)$ and $\phi_2(\theta)$ which are used to compute the position vector $\vec{r}$ are formulated as finite Fourier series:

$$\phi_1(\theta) = \alpha_0 + \alpha_1 \cos\frac{\pi\theta}{2\theta_f} + \alpha_2 \sin\frac{\pi\theta}{2\theta_f} + \alpha_3 \cos\frac{\pi\theta}{\theta_f} + \alpha_4 \sin\frac{\pi\theta}{\theta_f} + \alpha_5 \cos\frac{3\pi\theta}{2\theta_f} \tag{3.13}$$

$$\phi_1(\theta) = \beta_0 + \beta_1 \cos\frac{\pi\theta}{2\theta_f} + \beta_2 \sin\frac{\pi\theta}{2\theta_f} + \beta_3 \cos\frac{\pi\theta}{\theta_f} + \beta_4 \sin\frac{\pi\theta}{\theta_f} + \beta_5 \cos\frac{3\pi\theta}{2\theta_f} \tag{3.14}$$

The coefficients α_i and β_i are determined by the boundary constraints, such that in the end:

$$\phi_1(\theta) = \frac{9}{1} - 3\cos\frac{\pi\theta}{2\theta_f} - 6\sin\frac{\pi\theta}{2\theta_f} - \frac{3}{2}\cos\frac{\pi\theta}{\theta_f} + 3\sin\frac{\pi\theta}{\theta_f} + \cos\frac{3\pi\theta}{2\theta_f} \tag{3.15}$$

$$\phi_1(\theta) = -\frac{7}{2} + 3\cos\frac{\pi\theta}{2\theta_f} + 6\sin\frac{\pi\theta}{2\theta_f} + \frac{3}{2}\cos\frac{\pi\theta}{\theta_f} - 3\sin\frac{\pi\theta}{\theta_f} - \cos\frac{3\pi\theta}{2\theta_f} \tag{3.16}$$

The equation of motion of the spacecraft can be written as:

$$\ddot{\vec{r}} + \frac{\mu}{r^3}\vec{r} = \vec{T_a} \tag{3.17}$$

So the acceleration $\vec{T_a}(\theta)$ can be computed knowing $r(\theta)$ and its derivatives. Once the acceleration is computed than the Δv needed for the low-thrust transfer can be obtained

integrating:

$$\Delta v = \int_0^{\theta_f} \frac{||\vec{T}_a(\theta)||}{\dot{\theta}} \, d\theta \tag{3.18}$$

Considering that the derivative of θ can be computed starting from the orbital angular momentum h_1 and h_2, such that:

$$\dot{\theta} = \frac{\phi_1 h_1 + \phi_2 h_2}{\|\vec{r} \wedge \frac{\partial \vec{r}}{\partial \theta}\|} \tag{3.19}$$

Note that $\dot{\theta} = d\theta/dt$ so, the time of flight (TOF) can be computed as:

$$TOF = \int_0^{\theta_f} \frac{1}{\dot{\theta}} \, d\theta \tag{3.20}$$

In appendix A.9 is shown how to compute in detail the derivatives of the position vector $\vec{r}$, needed to compute the Δv and the TOF. In addition it is reported the validation of the results through a comparison with the ones obtained by the author Zeng in [112].

For the slow push strategies, the decision variables for the optimisation are the number of revolutions N_{rev} of the low thrust trajectory and the spacecraft initial mass, in addition to the departure date t_0. So in the end for slow push strategies the set of decision variables is:

$$x_{low\ thrust\ traj} = [N_{rev} \quad t_0 \quad m_{sc,0}] \tag{3.21}$$

A final remark on the arrival point: this is a rendezvous low thrust trajectory, so the position of the spacecraft at the arrival must be given as an input. But since the TOF is an output the true anomaly of the asteroid is unknown a priori, so inside the optimizer the error between the position of the spacecraft at arrival and the position of the asteroid at that time is minimised.

3.3. Deviation formulas: impulsive deflection

The objective of the asteroid deflection problem is to maximise the MOID (Minimum Orbital Interception Distance) from the Earth to a Near-Earth Asteroid applying to the object a deviating force.
In the case of an impulsive deflection the action is modelled as an impulsive velocity variation Δv. The variation of the orbital elements a,e, i, Ω, ω and the mean anomlay M

after a $\Delta v = [\delta v_t \ \delta v_n \ \delta v_h]$, can be computed through the Gauss' planetary equations:

$$\begin{cases} \delta a &= \dfrac{2a^2 v}{\mu}\delta v_t \\ \delta e &= \dfrac{1}{v}\left(2(e+\cos\theta_0)\delta v_t - \dfrac{r}{a}\sin\theta_0 \delta v_n\right) \\ \delta i &= \dfrac{r\cos\theta_0^*}{h}\delta v_h \\ \delta\Omega &= \dfrac{r\sin\theta_0^*}{h\sin i}\delta v_h \\ \delta\omega &= \dfrac{1}{ev}\left(2\sin\theta_0\delta v_t + \left(2e + \dfrac{r}{a}\cos\theta_0\right)\delta v_n\right) - \dfrac{r\sin\theta_0^* + \cos i}{h\sin i}\delta v_h \\ \delta M &= -\frac{b}{eav}\left(2\left(1+\dfrac{e^2 r}{p}\right)\sin\theta_0\delta v_t + \dfrac{r}{a}\cos\theta_0\delta v_n\right) + \delta n(t_{MOID} - t_0) \end{cases} \tag{3.22}$$

The components of the velocity vector are expressed in the tangential, normal and out of plane reference frame. θ_{MOID} is the true anomaly of the asteroid at MOID (considering the unperturbed orbit), while the argument of latitude θ^* is defined as $\theta+\omega$. The definition of the other parameters are: $r = p/(1 + ecos(\theta))$ is the position vector, $p = a(1-e^2)$, $b = a\sqrt{1-e^2}$, $v = \sqrt{2\mu/r - \mu/a}$ is the orbital velocity, $n = \sqrt{\mu/a^3}$ is the angular velocity and $h = nab$ is the angular momentum. The variation of the mean anomaly takes into account also the variation due to a change in the semi-major axis, represented by the term δn which is the difference between the orbital angular velocity of the old unperturbed orbit and the one of the new orbit.

Once the variation of the orbital elements is computed it is possible to derive the variation in the position vector $\delta r = [\delta s_t \ \delta s_n \ \delta s_h]$ (so in this case radial, transversal and out of plane reference frame) between the perturbed and unperturbed orbit. Since the new orbit can be considered proximal to the old one the proximal motion equation are used:

$$\begin{cases} \delta s_r &= \dfrac{r}{a}\delta a + \dfrac{ae\sin\theta_{MOID}}{\eta}\delta M - a\cos\theta_{MOID}\delta e \\ \delta s_\theta &= \dfrac{r}{\eta^3}(1+e\cos\theta_{MOID})^2\delta M + r\delta\omega + \dfrac{r\sin\theta_{MOID}}{\eta^2}(2+e\cos\theta_{MOID})\delta e + r\cos i\delta\Omega \\ \delta s_h &= r\left(\sin\theta^*_{MOID}\delta i - \cos\theta^*_{MOID}\sin i\delta\Omega\right) \end{cases} \tag{3.23}$$

Where the parameter η is defined as: $\eta = \sqrt{1-e^2}$.
As has been done by Colombo and Vasile in [96] the maximum deviation problem can be defined. The variation of the position at MOID $\delta\vec{r}(t_{MOID})$ is linked to the velocity variation $\delta\vec{v}$ (at the deviation time) through a transition matrix $\mathbf{T}$, considering the vector of the orbital parameter variation $\delta\vec{\alpha}(t_{dev})$.

$$\delta\vec{r}(t_{MOID}) = \mathbf{A}_{MOID}\delta\vec{\alpha}(t_{dev}) = \mathbf{A}_{MOID}\mathbf{G}_{dev}\delta\vec{v}(t_{dev}) = \mathbf{T}\delta\vec{v}(t_{dev}) \tag{3.24}$$

This relation directly links the perturbation applied at the deviation time to the displacement at MOID. The matrix $\mathbf{A}_{MOID}$ and $\mathbf{G}_{dev}$ are 6x3 and can be computed starting from the Gauss' equations and the proximal motion equations ([96]).
The objective is to maximize the deviation at MOID, so the functional to be maximised is:

$$J_{\delta r} = ||\delta\vec{r}(t_{MOID})|| = ||\mathbf{T}\delta\vec{v}(t_{dev})|| = \delta\vec{v}(t_{dev})^T\mathbf{T}^T\mathbf{T}\delta\vec{v}(t_{dev}) \tag{3.25}$$

So since the functional is a quadratic form the maximisation can be done by choosing the vector $\delta\vec{v}(t_{dev})$ parallel to the eigenvector of the quadratic form $\mathbf{T}^T\mathbf{T}$ conjugated to the highest eigenvalue. In this way the optimal direction of the velocity variation is obtained in order to maximise the deviation at MOID.

3.3.1. B-plane representation

Since the hyperbolic trajectory of the asteroid as it encounters Earth will be very close to a straight line it is possible to approximate the pericenter radius of its trajectory with the impact parameter b^* defined in the B-plane (see fig. 3.3), as suggested by C. Colombo in [96].
The B-plane is a plane centered into the focal point of the hyperbola (Earth in this case) and normal to the incoming asymptote, so it is perpendicular to the trajectory plane and it is useful for targeting during fly-bys. The vectors which define the B-plane reference frame are:

$$\hat{\eta} = \frac{\vec{v}_{AST,unperturbed}}{\|\vec{v}_{AST,unperturbed}\|} \tag{3.26}$$

$$\hat{\xi} = \frac{\vec{v}_E \wedge \hat{\eta}}{\|\vec{v}_E \wedge \hat{\eta}\|} \tag{3.27}$$

$$\hat{\zeta} = \hat{\xi} \wedge \hat{\eta} \tag{3.28}$$

Where $\vec{v}_{AST,unperturbed}$ is the unperturbed velocity of the asteroid relative to Earth.

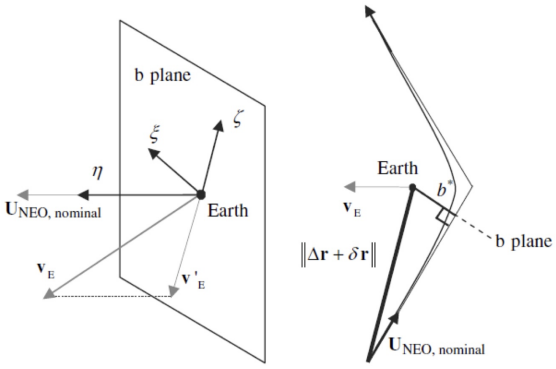

Figure 3.3: B-plane representation [96]

So the displacement δr expressed in eq. (3.24) can be projected into the B-plane, following the method proposed by Petit and Colombo in [77],such that:

$$\delta\vec{b^*} = \mathbf{M}_{\delta\vec{b^*}}\delta\vec{r} \tag{3.29}$$

Where $M_{\delta_b^*}$ is the transformation matrix which depends on the components of the versor $\hat{\eta}$. It is defined as:

$$\mathbf{M}_{\delta\vec{b^*}} = \begin{bmatrix} \hat{\eta}_2^2 + \hat{\eta}_3^2 & -\hat{\eta}_1\hat{\eta}_2 & -\hat{\eta}_1\hat{\eta}_3 \\ \hat{\eta}_1\hat{\eta}_2 & \hat{\eta}_1^2 + \hat{\eta}_3^2 & -\hat{\eta}_2\hat{\eta}_3 \\ \hat{\eta}_1\hat{\eta}_3 & \hat{\eta}_2\hat{\eta}_3 & \hat{\eta}_1^2 + \hat{\eta}_2^2 \end{bmatrix} \tag{3.30}$$

So in the end the displacement in the B-plane can be expressed as $\delta b^* = \mathbf{M}_{\delta b^*}\mathbf{T}\delta\vec{v} = \mathbf{Z}\delta\vec{v}$ and the functional to be optimised becomes:

$$J_{\delta b} = \|\delta\vec{b^*}\| = \delta\vec{v}^T\mathbf{Z}^T\mathbf{Z}\delta\vec{v} \tag{3.31}$$

In the B-plane it is possible to define the capture circle, which traces all the trajectories that will bring to an Earth-grazing close approach. So if the trajectory of the asteroid falls inside this circle it will certainly impact on Earth.

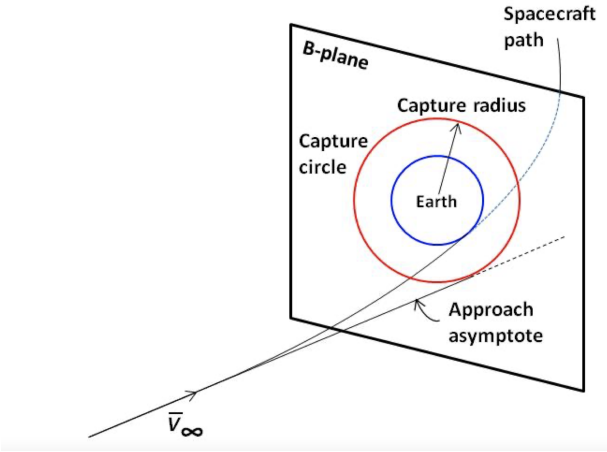

Figure 3.4: Capture circle in the B-plane

The definition is:

$$R_c = R_E\sqrt{\left(\frac{2GM_E}{R_E v_{in}^2}+1\right)} \tag{3.32}$$

Where R_E and M_E are radius and mass of the Earth, while v_{in} is the incoming velocity of the asteroid.

3.4. Deviation formulas: low thrust deflection

In the case of a low thrust deflection the deviation action is continuously applied to the asteroid over a certain time interval.

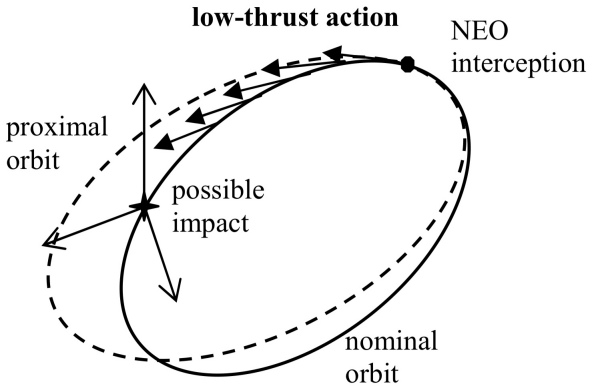

Figure 3.5: Low-thrust deviation [68]

The new orbit is always proximal to the old one, so the equations to compute the displacement in position are the ones in eq. (3.23), expressed in the matrix form as

$\delta\vec{r}(t_{MOID}) = \mathbf{A}_{MOID}\delta\vec{\alpha}$.
The variation of the orbital parameters can be computed by integrating the Gauss' planetary equation over the time interval $[t_i\ t_f]$, where $t_f \leq t_{MOID}$ is the final time of the deviation action:

$$\begin{cases} \dfrac{da}{dt} &= \dfrac{2a^2v}{\mu}a_t \\ \dfrac{de}{dt} &= \dfrac{1}{v}\left(2(e+\cos\theta_0)a_t - \dfrac{r}{a}\sin\theta_0 a_n\right) \\ \dfrac{di}{dt} &= \dfrac{r\cos\theta_0^*}{h}a_h \\ \dfrac{d\Omega}{dt} &= \dfrac{r\sin\theta_0^*}{h\sin i}a_h \\ \dfrac{d\omega}{dt} &= \dfrac{1}{ev}\left(2\sin\theta_0 a_t + \left(2e + \dfrac{r}{a}\cos\theta_0\right)a_n\right) - \dfrac{r\sin\theta_0^* + \cos i}{h\sin i}a_h \\ \dfrac{dM}{dt} &= n - \dfrac{b}{eav}\left(2\left(1+\dfrac{e^2r}{p}\right)\sin\theta_0 a_t + \dfrac{r}{a}\cos\theta_0 a_n\right) \end{cases} \tag{3.33}$$

In this case, since the action is continuous, the velocity variation is substituted by the acceleration $\vec{a}(t) = [a_t\ a_n\ a_h]^T$, expressed in the tangential-normal-out of plane (TNH) reference frame.
It can be noted that instead of integrating the Gauss equations, which is computationally very expensive, it is possible to use semi-analytical formulae, as explained in detail by [18], but in this work of thesis the direct integration is considered.
So in the case of a slow-push strategy the deviation at MOID is:

$$\delta\vec{r}_{MOID} = \vec{r}_{ast,MOID,deviated} - \vec{r}_{ast,MOID,nominal} \tag{3.34}$$

Where $\vec{r}_{ast,MOID,deviated}$ is the position of the asteroid at MOID after the deviation action, so it is computed starting from the orbital elements obtained after the integration of the Gauss' equations. Instead $\vec{r}_{ast,MOID,nominal}$ is the nominal position of the asteroid at MOID, so without deviation, and can be obtained from the data in *NASA JPL Horizons System* [60] for the selected asteroid.
The acceleration $\vec{a}(t)$ is assumed to be aligned with the velocity vector of the asteroid.
Also in this case the vector $\delta\vec{r}_{MOID}$ can be projected into the B-plane and it is possible to compute the impact parameter $\delta\vec{b}$ as in eq. (3.29). So the functional to be maximised is:

$$J_{\delta\vec{b}} = \|\delta\vec{b}\| \tag{3.35}$$

3.5. Hovering control

Most of the slow-push technologies require that the satellite hovers above the asteroid for a determine time interval. A simple model of the in plane hovering dynamics of a spacecraft towing an asteroid is obtained through the Clohessy-Wiltshire-Hill (CWH) equations:

$$\ddot{x_1} = 2n\dot{y_1} + Gm_2\frac{x_2 - x_1}{r^3} \tag{3.36}$$

$$\ddot{y_1} = -2n\dot{x_1} + 3n^2 y_1 + Gm_2\frac{y_2 - y_1}{r^3} \tag{3.37}$$

$$\ddot{x_2} = 2n\dot{y_2} - Gm_2\frac{x_2 - x_1}{r^3} + \frac{1}{m_2}F_x \tag{3.38}$$

$$\ddot{y_2} = -2n\dot{x_2} + 3n^2 y_2 - Gm_2\frac{y_2 - y_1}{r^3} + \frac{1}{m_2}F_y \tag{3.39}$$

Where the index 1 refers to the asteroid and 2 refers to the spacecraft and $r = \sqrt{(x_2 - x_1)^2 + (y_2 - y_1)^2}$ is the distance between them.

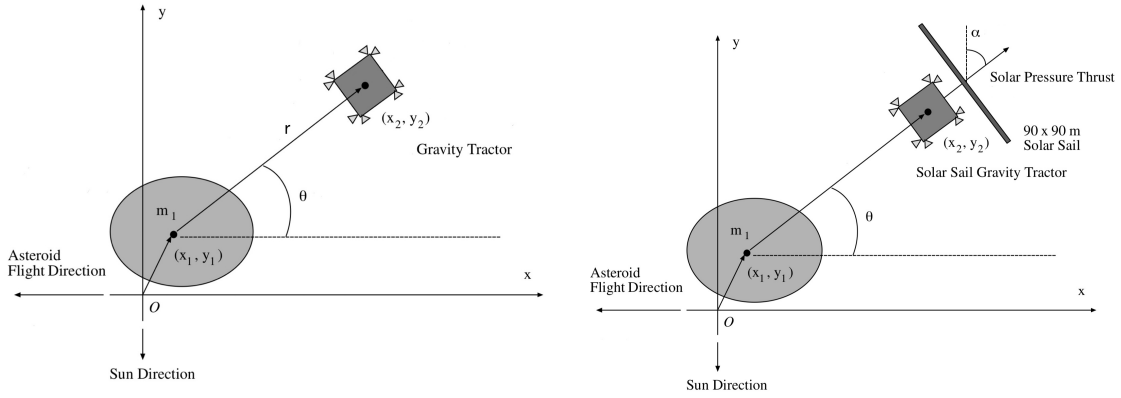

(a) Satellite hovering (b) Satellite with solar sails hovering

Figure 3.6: Geometric diagram of satellite hovering [107]

The control is performed through a PD controller, so the force F_x and F_y are expressed as: $F_x = -K_p(x - x_c) - K_d\dot{x}$ and $F_y = -K_p(y - y_c) - K_d\dot{y}$, where $x = x_2 - x_1$, $y = y_2 - y_1$ and the desired position is (x_c, y_c). The force is limited to a value $F_{max} = 0.01\ N$, typical value obtained with an ion thruster and in addition a tolerance has been set to the vertical and horizontal displacement, such that if the absolute difference between x and x_c and y and y_c is less than 5 m the control force is zero.
The spacecraft is tilted by angle θ in order to avoid the thruster plume impingement.

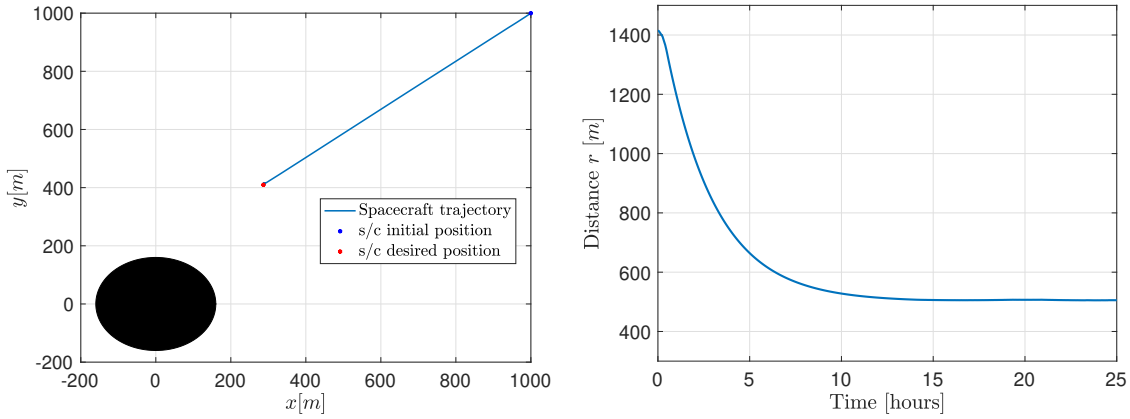

(a) Slew manoeuvre from the initial point to the desired hovering distance

(b) Satellite distance from the asteroid

Figure 3.7: Satellite hovering control

If a solar sail spacecraft is used (fig. 3.6b), in addition to the control force, an additional thrust has to be considered. With a solar sail of dimension 90 x 90 at a distance of 1 AU the thrust produced is $T_0 = 0.045\ N$ [107]. In this case the mass of propellant consumed is lower, in fact without solar sails the mass consumed in 1 year for hovering control, considering an initial spacecraft mass of 1000 kg and a specific impulse of 3000 s, is 3.91 kg, while considering the additional thrust the mass consumed is 3.14 kg.

3.6. Artificial Halo orbit

The CWH equations are always used in order to obtain an halo orbit, but in this case, as suggested by Wie [107], neglecting the effect of a slow orbital motion. So a simple model is obtained:

$$\ddot{x}_{sc} = -\frac{GM_{ast}x_1}{r_1^3} + \frac{T}{m_1} \tag{3.40}$$

$$\ddot{y}_{sc} = -\frac{GM_{ast}y_1}{r_1^3} \tag{3.41}$$

$$\ddot{z} = -\frac{GM_{ast}z_1}{r_1^3} \tag{3.42}$$

Where the distance r is: $\sqrt{x_1^2 + y_1^2 + z_1^2}$. A control force along the x axis is needed to maintain the correct distance with respect to the asteroid, so to counteract the gravity force. The initial conditions are: $x_{sc}(0) = d$ which is the halo orbit distance from the asteroid, $y_{sc}(0) = A$ which is the amplitude, $\dot{z}_{sc} = A\sqrt{GM/r_1^3}$ which is the halo orbit insertion Δv. The other initial conditions are set to 0.

In a more realistic case the thrust vector misalignment (1 degree), halo orbit insertion

errors and a center of gravity offset of the asteroid (10 m) have to be considered. The results can be seen in fig. 3.8, where it can be noted that in reality also a control in y and z axes is needed if the deviations are not acceptable.

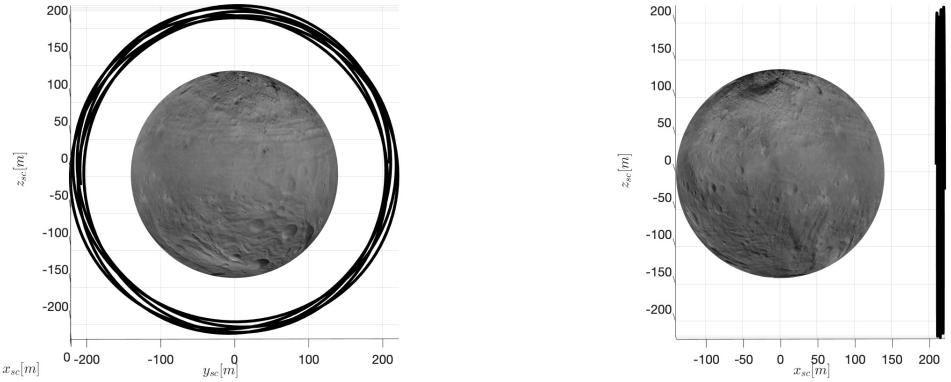

(a) (b)

Figure 3.8: Halo orbit: realistic case

3.7. Target asteroid: NASA 2023 PDC

The objective of the thesis is to find useful strategies for the deflection of the asteroid 2023 PDC, a fictitious asteroid which was developed by NASA as an exercise for the 2023 Planetary Defense Conference [68]. The evolution of the scenario is divided by NASA into epochs, from Epoch 1 to Epoch 4.

During Epoch 1, which lasts 18 months, starting from the day of the discovery, January 10, 2023, the probability of impact increases form 1% to 100% and first information about the asteroid orbit are defined. This is the very first phase of the NEO threat so Earth-based observations take place and the physical characterisation of the asteroid through radar and optical observations is performed [19].

The Epoch 2 starts in November 2023, when it is certain that asteroid 2023 PDC is on a trajectory that will impact Earth on October 22, 2036. The latest orbit estimate indicates that the asteroid will impact somewhere within the continent of Africa.

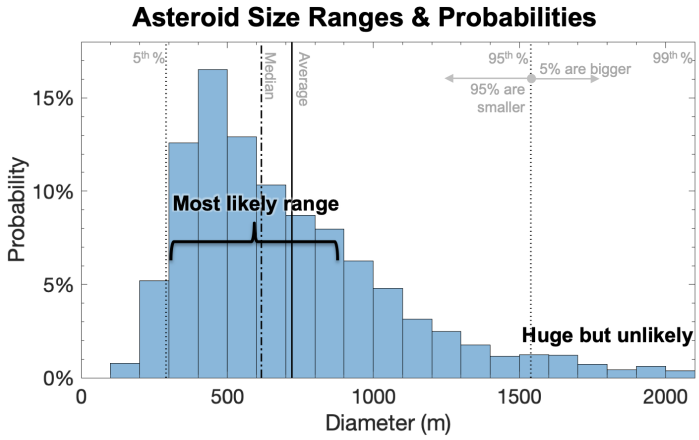

Figure 3.9: Asteroid Size Ranges and Probabilities [68]

During Epoch 2 and 3, thanks to data from ground observations, the first precise information about asteroid orbit and dimensions is available. Since uncertainties are still present a range of value of asteroid mass and size are available, as can be seen in fig. 3.9. The diametre and the mass are summarised at selected percentile levels in table 3.1.

	$5th$ %	$50th$ %	$95th$ %
Diametre $[m]$	290	617	1539
Mass $[kg]$	$2.6 \cdot 10^{10}$	$2.5 \cdot 10^{11}$	$3.8 \cdot 10^{12}$

Table 3.1: Asteroid properties at selected percentile levels

In Epoch 2 the evaluation, planning and implementation of one or more than one reconnaissance missions have to be performed by national space agencies [19]. In this Epoch also first considerations about deflection strategies are considered. NASA selects two strategies: kinetic impactor and nuclear standoff explosion.
When deflected the asteroid moves along the risk chord, so it must be deviated such that the impact point is outside the Earth. The kinetic impactor can decrease or increase the asteroid velocity, but the first option is easier. In the case of 2023 PDC decreasing the velocity means moving the impact point towards west [68], so westward deflection is easier for the kinetic impactor in this case. While for nuclear deflection both directions (eastward and westward) are equally easy.

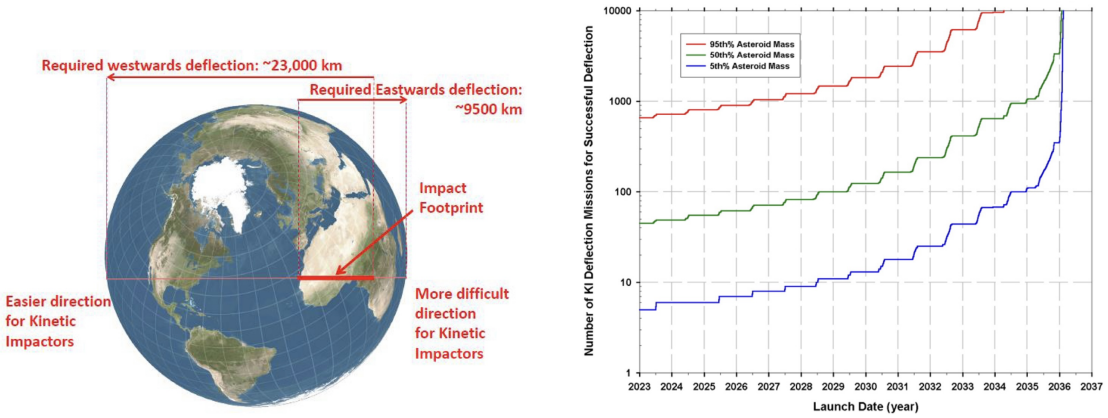

(a) Eastward and westward deflection for KI mission

(b) Number of KI mission required for full deflection

Figure 3.10: KI mission for asteroid 2023 PDC trajectory [68]

The main problem of KI, as underlined by NASA, is that the easiest deflection direction is also the one that requires the highest value of deflection (23000 km against 9500 km). So, always referring to NASA results, a huge number of spacecrafts is needed in order to reach these high values of deflection (fig. 3.11b).
Instead, concerning nuclear deflection, following NASA results, just one Falcon Heavy launch is enough both for the westward and eastward deflection.
Epoch 3 starts thirteen months after Epoch 2, when the fly-by reconnaissance mission reach the asteroid. The information obtained helps to decrease the orbital uncertainties and so leads to a more precise impact location. In addition data on the physical properties and spectral class of the asteroid are obtained: it is a C-type (carbonaceus stony composition).
During Epoch 4 also the rendezvous reconnaissance mission arrives to the asteroid providing more information about deflection requirements.
After Epoch 4 the deflection mission has to be launched and also a backup deflection mission is designed. In fact in case of failure of the baseline mission, which can happen because of launch or system failure or because of effectiveness assessment (too small deflection), another backup mission must be ready [19].
In addition also the re-entry of some asteroid fragments has to be considered, so definition of the possible casualty risk on ground, re-entry corridor and footprint.

3.7.1. Risk assessment

The risk assessment is an important task to be studied when a dangerous asteroid is discovered. Also in the case of asteroid 2023 PDC NASA performs a preliminary work on risk assessment.
In general risk assessment evaluates the severity and likelihood of potential outcomes, considering the level of uncertainty of all the contributing factors. In the case of an asteroid impact the uncertainties are very large: impact probability, asteroid size and properties and orbital and attitude uncertainties which affect the atmospheric entry.
All the uncertainties lead to a very difficult prediction of the impact point and of the impact energy, which is a fundamental parameter to determine the damages on the population.

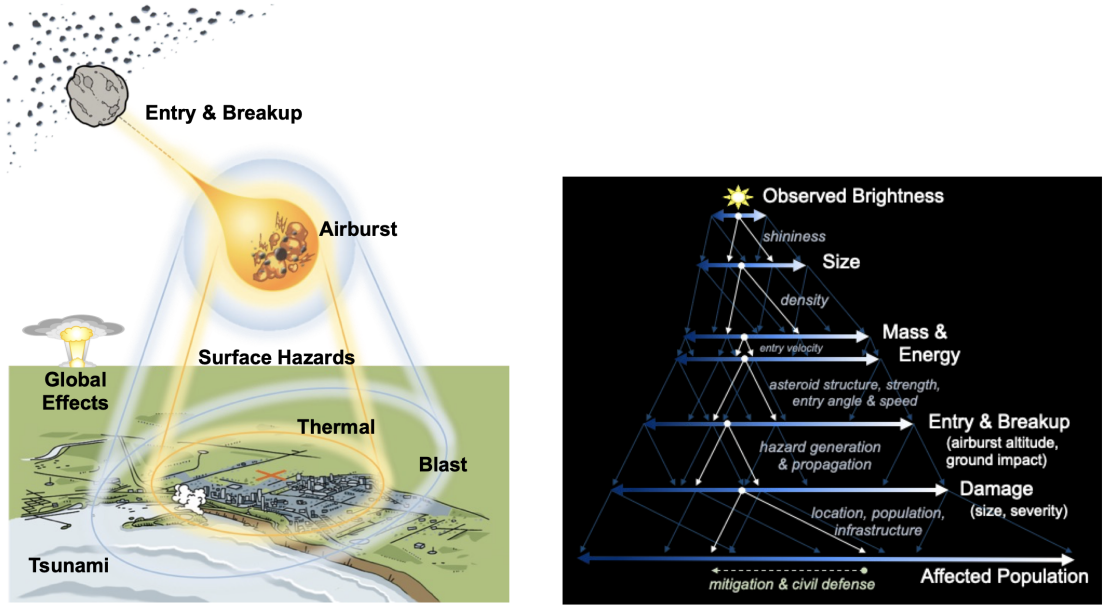

(a) Asteroid impact

(b) Cascade of uncertainties from observation to impact

Figure 3.11: Impact risk assessment [68]

The damages created by asteroid are not only caused by a direct impact, but also an airburst can create strong shockwaves and the disruption in the atmosphere brings to the fall of fireballs. In addition large-scale impacts could produce enough atmospheric ejecta to cause global climatic effects.
An output of the risk assessment analysis (in Epoch 3 in this case) is the Risk Region Swath Map, for asteroid 2023 PDC it is reported in fig. 3.12, which shows the possible locations of impact and underline the areas where the damages would be higher.

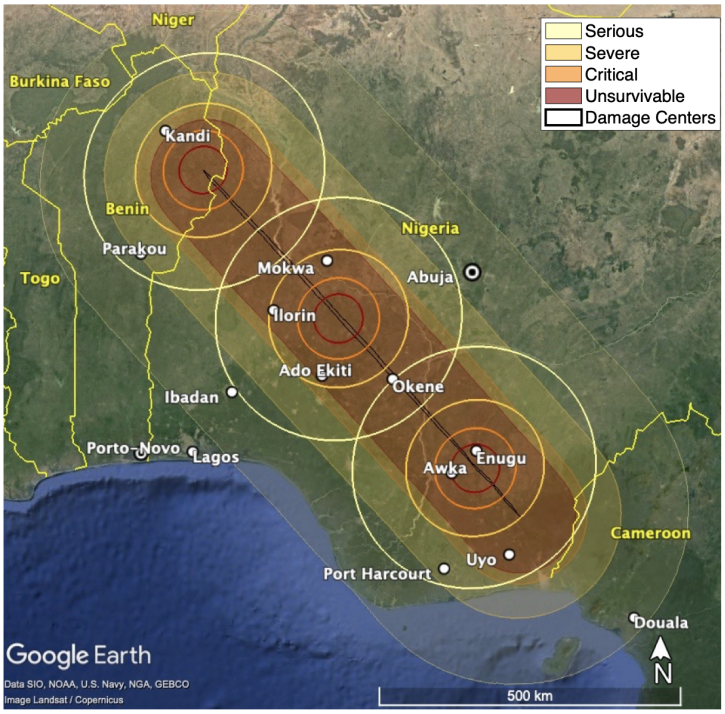

Figure 3.12: Damage risk swath map: shows extent of regions potentially at risk to local ground damage [68]

In particular NASA defines four levels of damage: serious, severe, critical and unsurvivable. In table 3.2 is reported in detail the potential blast damage severities. It can be noted that the more important are the damages the smaller is the damage radius.

Damage level	Potential effects	Damage Radius
Serious	Shattered windows, some structure damage	190 km
Severe	Widespread structure damage	110 km
Critical	Most residential structures collapse	60 km
Unsurvivable	Complete devastation	35 km

Table 3.2: Potential Blast Damage Severities and Sizes [68]

Last but not least, because fundamental in case of asteroid impact, is a study on the affected population ranges along the swath. In fig. 3.13 the affected population along the risk swath (expressed in millions of people) and the impact location probability (for asteroid 2023 PDC) are shown. It can be noted that the area with the highest population density is also the one with the lowest impact probability, even if the population that most probably would be affected by an impact is of around 10 millions people.

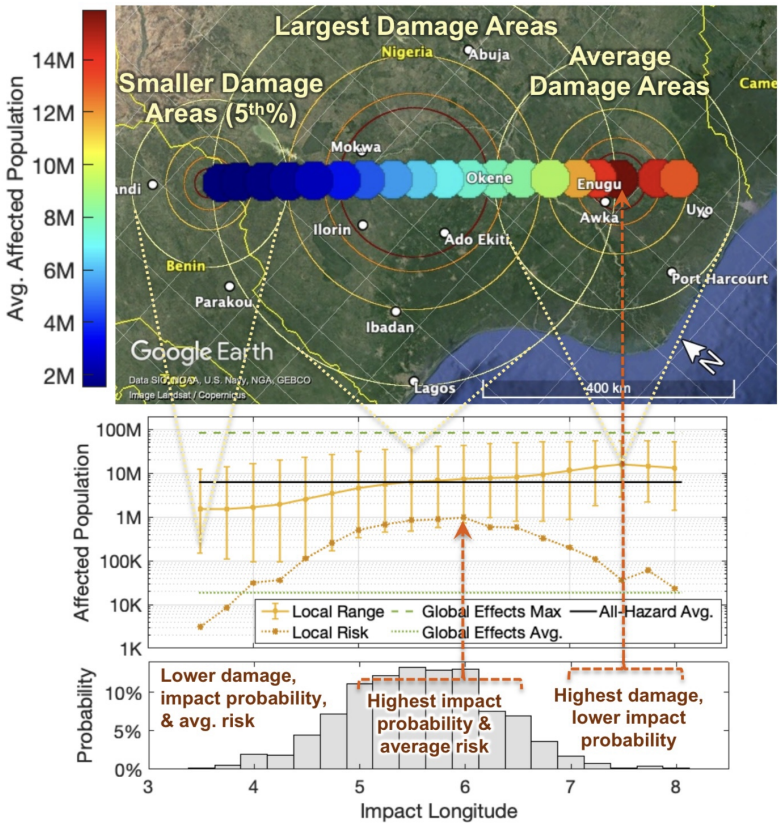

Figure 3.13: Average affected population map and relative impact probability [68]

3.8. Minimisation of the collision probability

Because of the uncertainties in the orbital state of the asteroid a maximum deviation optimisation can bring to different results with respect to a minimum collision probability one.

Following Chan's method, it is possible to derive a solution in a similar way to the one of the maximum deflection [31], such that the functional that has to be maximised is:

$$J_P = \delta\vec{r}^T \mathbf{Q}^* \delta\vec{r} = \delta\vec{b}^T \mathbf{Q}^* \delta\vec{b} \tag{3.43}$$

The matrix $\mathbf{Q}^*$ depends on the covariance of the asteroid position $(\xi\ \zeta)$ in the B-plane at MOID and on the statistical correlation between the two parameters.

$$\mathbf{Q}^* = \begin{bmatrix} 1/\sigma_\xi^2 & 0 & -\rho_{\xi\zeta}/\sigma_\xi\sigma_\zeta \\ 0 & 0 & 0 \\ -\rho_{\xi\zeta}/\sigma_\xi\sigma_\zeta & 0 & 1/\sigma_\zeta^2 \end{bmatrix} \tag{3.44}$$

The uncertainties of the asteroid position at MOID in this work of thesis comes from the initial uncertainties in the asteroid state vector, which are present because observations from Earth are affected by errors.

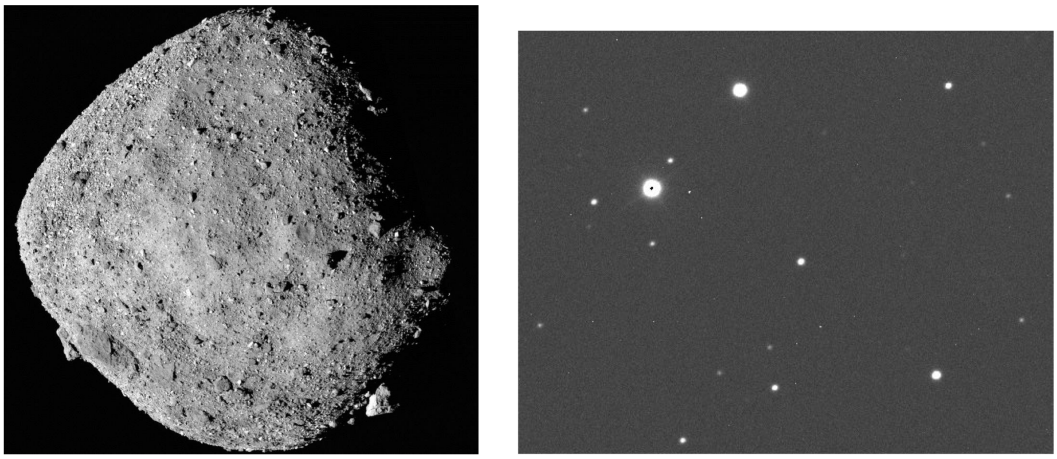

(a) Image from reconnaissance space missions to the asteroid

(b) Remote telescope observations of the asteroid

Figure 3.14: Asteroid observations [68]

The errors are clearly unavoidable because there isn't an available clear image, as in fig. 3.14a, but it can be obtained only through a reconnaissance mission. A tiny point of light is what is actually known from remote telescope observations, thanks to which the brightness and the orbital motion are estimated.
Indeed, as underlined in a work of the Astronomical Observatory of Brera [14], asteroid orbits are computed by fitting astrometric observations and so the result can be expressed through a region of confidence, not through a single solution. For bright, well-observed and Near-Earth objects the uncertainty in position is around 1 arcsecond, while the one in velocity is a fraction of a meter per second (data taken from Minor Planet Center website [41]).
A Monte Carlo analysis has been performed to compute the standard deviation and the statistical correlation of the asteroid position at MOID in the B-plane starting from the uncertainty in the position expressed in Heliocentric reference frame at MOID time.

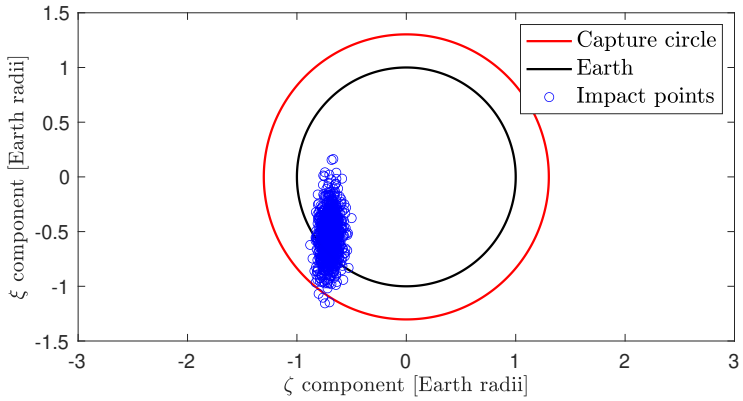

Figure 3.15: Results of the Monte Carlo analysis for the impact points in the B-plane

4 | Results of the optimisation process

The four strategies selected in section 2.4.2 are optimised using the MultiObjective Genetic Algorithm function *gamultiobj* in MATLAB, exploiting Parallel computing to speed up the computation. The population size changes depending on the case and on the complexity of the calculations.
The variables considered to build the Pareto fronts are, in addition to deviation at MOID δr_{MOID}, the warning time $t_w = t_{MOID} - t_0$ (t_0 is the launch date), and the initial spacecraft mass $m_{sc,0}$, as done in 2009 by Colombo, Vasile and Sanchez in [84].
Then the optimal solution, the one that guarantee the highest value of deviation, is selected from the 3D Pareto front which combines the three variables listed before.
Once the best solution is found, a preliminary mission design is performed.
It is also considered another type of mission, which consists in minimizing the collision probability: this concept has been explained in section 3.8.
Since uncertainties are still present at Epoch 3, three different dimensions and masses of the asteroid are considered, as done by NASA in [68]. The values are selected at a determined percentile level, as explained in section 3.7. The first case considers the 5% percentile level, the second one 50% percentile level, the third one the 95% percentile level.
Instead, the orbital parameters of the asteroid are taken from JPL Horizons System [67].
From the 3D Pareto fronts obtained minimizing the functional $J = [-J_{\delta b}\ m_{sc,0}\ t_w]$ it is selected the optimal Pareto solution which guarantees the highest deviation at MOID δr_{MOID}.
Instead from the 3D Pareto fronts obtained minimizing $J = [-J_P\ m_{sc,0}\ t_w]$, where J_P is the probability functional, explained in section 3.8, it is selected the solution which brings to the maximum value of J_P, so to the minimum collision probability.
The minus sign before the functional J_P and $J_{\delta b}$ is necessary because it has to be maximised, not minimised.

4.1. Overview of Pareto optimisation

The generic formulation of a Multi Objective optimisation of N objectives is [71]:

$$Minimize\ \vec{y} = \vec{F}(\vec{x}) = [f_1(\vec{x}),\ f_2(\vec{x}),\ ...\ f_N(\vec{x})]^T \tag{4.1}$$

$$Subject\ to\ g_j(\vec{x}) \leq 0,\ j = 1, 2, ..., M \tag{4.2}$$

Where $\vec{x} = [x_1, x_2, ..., x_P]^T \in \Omega$ is the vector of the decision variables which belongs to a parameter space Ω, $\vec{y}$ is the objective vector and the function $\vec{g}$ represents the constraints. There is a utopian solution, which is optimal for all the objectives, defined as:

$$\vec{x_0^*} \in \Omega :\ \forall \vec{x} \in \Omega,\ f_i(\vec{x_0^*}) \leq f_j(\vec{x}),\quad for\ i = 1, 2, ..., N \tag{4.3}$$

This solution is called *utopian* because in a Multi Objective optimisation it generally doesn't exist since the objectives are in contrast between each other.
Indeed there is a set of solutions which represent different trade-offs between the objectives.
So the concept of Pareto dominance and Pareto optimality can be introduced [71]: a solution belongs to the Pareto front if there isn't another solution which can improve at least one of the objectives without downgrade another one of them. The decision vector $\vec{u}$ is said to *Pareto-dominate* the decision vector $\vec{v}$ in a minimization context if:

$$\forall i \in 1, ..., N,\ f_i(\vec{u}) \leq f_i(\vec{v})\ and\ \exists\ j \in 1, ..., N : f_j(\vec{u}) \leq f_j(\vec{v}) \tag{4.4}$$

So in the end a solution is Pareto optimal if there's not another solution that dominates it and the set of all Pareto optimal solutions is called Pareto front.

4.2. Optimal Kinetic Impactor mission

4.2.1. Pareto fronts

For the Kinetic Impactor mission an impulsive trajectory is exploited, as explained in section 3.1. So the decision variables to be set are:

$$\mathbf{x}_{impulsive\ traj} = [\alpha_0\ \ \alpha_1\ \ TOF\ \ \|\Delta v_0\|\ \ \alpha_{\Delta v_0}\ \ \delta_{\Delta v_0}\ \ m_{sc,0}] \tag{4.5}$$

As explained in the previous chapter the variables α_0 and α_1 vary from 0 to 1, while the angles $\alpha_{\Delta v_0}$ and $\delta_{\Delta v_0}$ vary respectively from 0 to 2π and from $-\pi/2$ to $\pi/2$. The

lower limit to the TOF is set to 100 *days* to guarantee feasibility, lower values will bring to very high Δv so are not considered. While the upper limit is set t0 1000 *days*, to allow for multiple revolution arcs. The calculations performed by NASA in [68], obtained through the NEO Deflection App [63], consider a direct transfer between the Earth and the NEO, so the delivered mass to the object depends only on the c3 of the launcher, defined as the square value of the vectorial difference between heliocentric Earth velocity and the spacecraft velocity required for the heliocentric transfer trajectory (output of the Lambert arc), so it is the initial velocity variation Δv. The results are that the c3 needed is 21 km/s, so the mass available is 6917 kg using a Falcon 9 Heavy launcher.
In order to compare the results a similar mass at launch is considered. The only propellant consumption is the one used for the DSM, which in any case is very low, so the upper bound for the spacecraft mass is set to 7000 kg. As a consequence the value of Δv_0 varies from 0 to $\sqrt{c3_{max}} = 4.2\ km/s$ (see appendix A.11 for the detail). The values of the bounds are summarised in table 4.1.
The momentum enhancement factor β is set equal to 3, as suggested by NASA [68], which refers to the value obtained by the DART mission.
The results obtained using a direct Lambert arc, with no DSM, as done by NASA in [68], are reported in appendix B in order to compare and validate the results.
The first launch date considered is 5 years after the day when impact probability rose above 10% (2023-07-01). In fact, as suggested by NASA in [68], 5 years is a typical time span for an interplanetary mission.

Parameter	**Lower bound**	**Upper bound**
α_1	0	1
α_2	0	1
$\alpha_{\Delta v_0}$	0	2π
$\delta_{\Delta v_0}$	$-\pi/2$	$\pi/2$
$TOF\ [days]$	100	1000
$\|\Delta v_0\|\ [km/s]$	0	4.2
$m_{sc,0}\ [kg]$	100	7000

Table 4.1: Kinetic Impactor mission: optimisation variables

The Pareto front in fig. 4.1a is obtained by minimising the functional:

$$J = [-J_{\delta b}\ t_w] \tag{4.6}$$

Where $J_{\delta b} = \vec{\delta b}^T \vec{\delta b}$ is the norm of the deviation at MOID expressed in the B-plane. While in fig. 4.1b the functional used is:

$$J = [-J_{\delta b}\ m_{sc,0}] \tag{4.7}$$

It can be noted that the higher is the initial mass and the warning time the higher are the final deviation at MOID. In the following figure are reported the Pareto fronts considering asteroid mass at the 5% percentile level (so first case), in appendix C.1.1 are reported all the Pareto fronts for the other two cases.

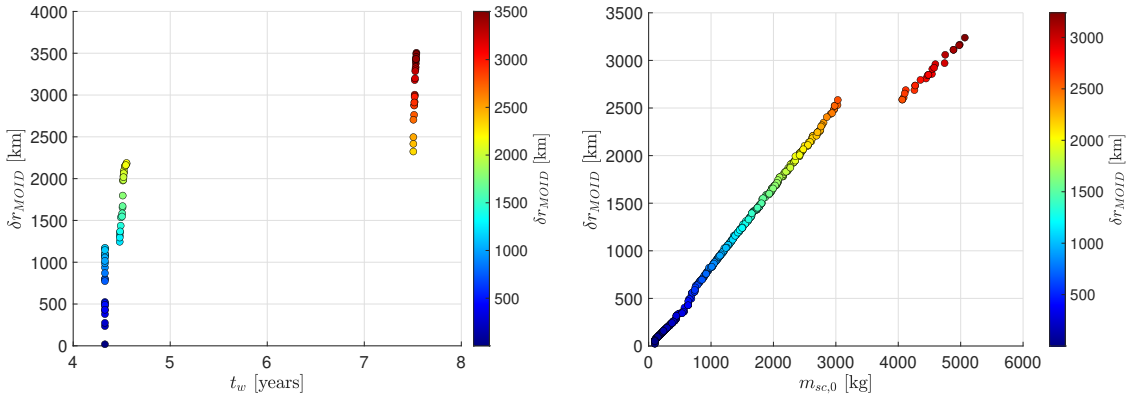

(a) First case Pareto front: deviation at MOID vs warning time

(b) First case Pareto front: deviation at MOID vs initial mass

Figure 4.1: Kinetic Impactor: First case Pareto fronts

The 3D Pareto front in fig. 4.5 is instead obtained by minimising the functional:

$$J = [-J_{\delta b}\ m_{sc,0}\ t_w] \tag{4.8}$$

All the Pareto fronts are obtained considering a population size $N = 50000$.

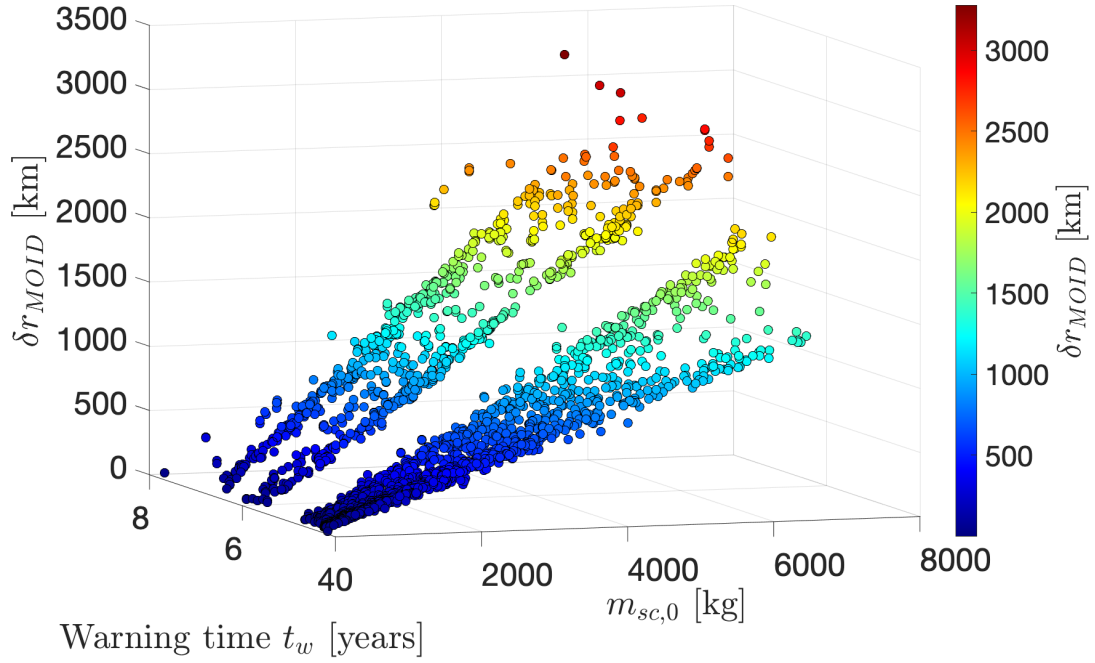

Figure 4.2: Kinetic Impactor First case Pareto front: deviation at MOID vs initial mass vs warning time

It is fundamental to underline that all the solutions obtained are feasible, because a constraint on the spacecraft mass has been considered. The mass of the propellant used cannot be higher than $0.7m_{sc,0}$ [105], in order to leave space for the instruments and the mass of the spacecraft subsystems.

It is important to check also that the impact kinetic energy (SKE), computed through eq. (2.2), is lower than the fragmentation limit Q, which for asteroid 2023 PDC can be set, in the worst case condition, equal to 10 J/kg (see fig. 2.1). In fig. 4.3 the SKE for the first case deflection mission can be seen .
Even if the limit value of Q is not reached, the event of asteroid disruption cannot be excluded a priori and further studies on asteroid surface and composition are needed, so the flyby reconnaissance mission is fundamental to determine precisely the fragmentation limit.

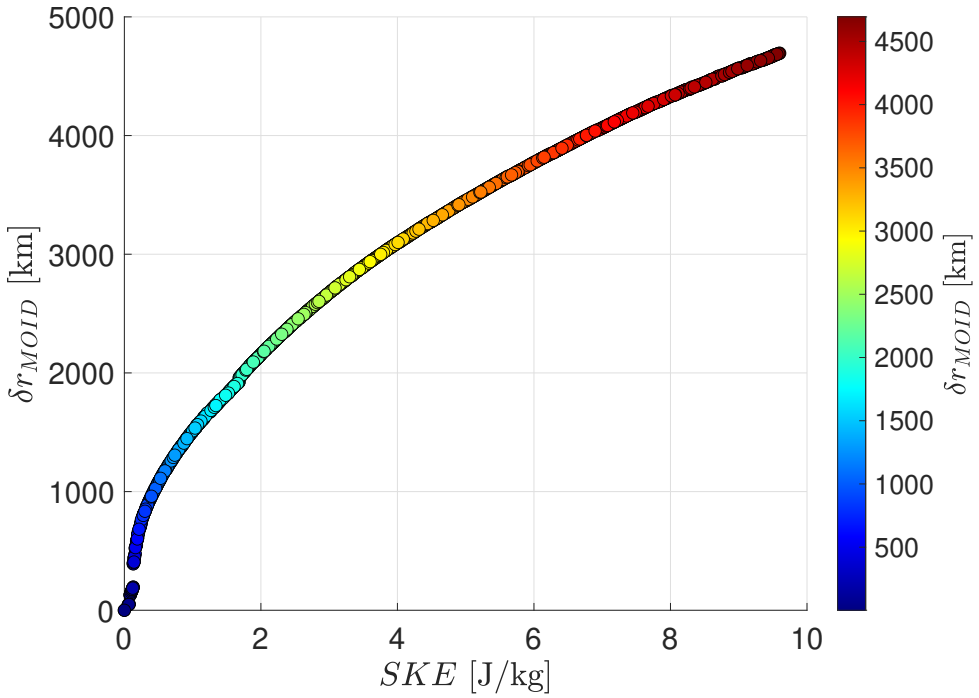

Figure 4.3: Kinetic Impactor First case Pareto front: deviation at MOID vs SKE

4.2.2. Maximum Deflection Mission

In fig. 4.4 the impulsive trajectory with the Deep Space Manoeuvre of the Kinetic Impactor mission is represented. It is obtained by choosing the optimal Pareto solution which guarantees the highest deflection at MOID (δr_{MOID}). In appendix C.1.1 the two graphs of the trajectories, for the second and third cases, are reported.

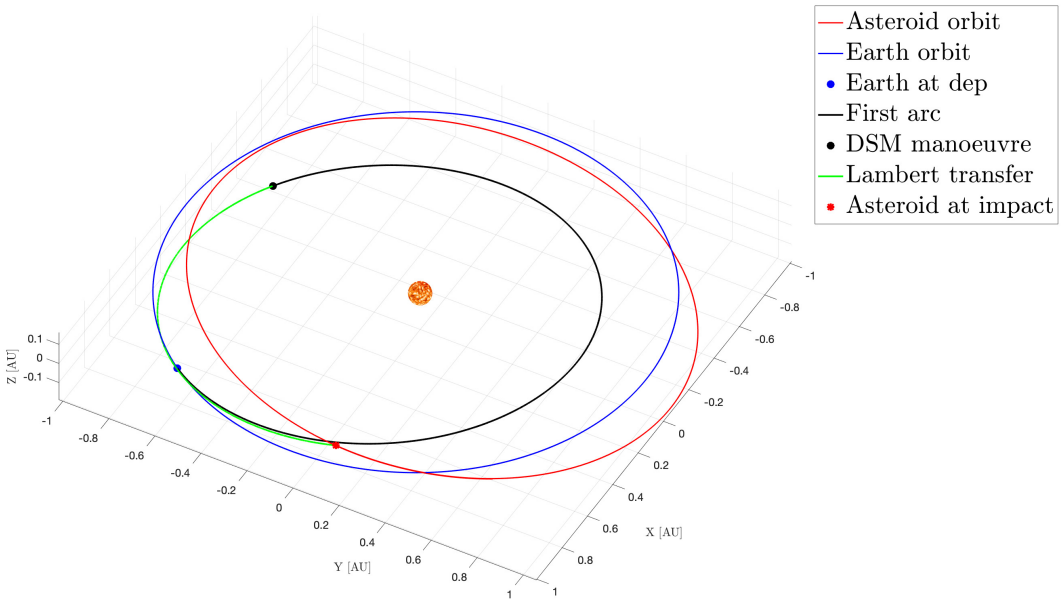

Figure 4.4: Trajectory of the Kinetic Impactor mission (First case)

The results in table 4.2 corresponds to the maximum deflection mission, so they bring to the solution in the 3D Pareto front (fig. 4.5) with the highest deviation at MOID.
The lead time is defined as $t_{lead} = t_{MOID} - t_0$, so the time interval between the launch date and the time instant when Earth and asteroid are at the minimum orbital distance.

Parameter	**First case** 5%	**Second case** 50%	**Third case** 95%
Launch date t_0	2029-08-13	2029-08-15	2030-01-19
DSM date	2030-03-16	2030-03-11	2030-07-02
Impact date	2030-07-13	2030-07-19	2030-11-04
TOF $[days]$	333.7	336.2	288.8
Lead time $[years]$	6.26	6.25	5.95
$\|\Delta v_0\|$ $[km/s]$	3.79	3.52	3.37
$\|\Delta v_{DSM}\|$ $[km/s]$	0.654	0.5325	1.094
$m_{sc,0}$ $[kg]$	5154.6	5841.9	6232.1
$m_{sc,f}$	4363.5	5100.5	4716.1
$\|\Delta v_{KI}\|$ $[m/s]$	$5.05 \cdot 10^{-3}$	$5.76 \cdot 10^{-4}$	$4.72 \cdot 10^{-5}$
$\|\delta r_{MOID}\|$ $[km]$	3304.3	370.9	19.6

Table 4.2: KI: Results of the optimisation

From the values of the deviation at MOID in table 4.2 it can be noted that one single kinetic impactor is not enough to avoid the collision with Earth.
The same result has been obtained by NASA in [68], even if the trajectory considered in that case is a bit different from the one considered in this thesis. A comparison with the same direct transfer trajectory can be seen in appendix B.
Anyway for NASA 9 Falcon Heavy launches are necessary to deviate the asteroid of 23000 km (westward deflection) in the first case. So a total mass into space of 62300 kg is needed. The results obtained in this thesis lead to a deviation of 3304 km with one launch, so just 7 launches are needed and a Multiple Kinetic Impactor (MKI) mission can be performed.
This difference is probably due to the fact that, even if part of the spacecraft mass is consumed, with the DSM manoeuvre the final relative velocity between satellite and asteroid is higher, and so as a consequence also the deviation obtained is higher.

4.2.3. Multiple Kinetic Impactor

The Multiple Kinetic Impactor strategies, explained in section 2.2.1, can be used in order to augment the deviation obtained with a single KI spacecraft and in order to avoid the disruption of the asteroid, since if the spacecraft mass is too high the SKE increases and can overcome the value of the asteroid fragmentation energy Q.
This strategy can be considered feasible if the asteroid dimension falls in the first percentile level. In this case 7 satellites are enough to completely deflect the asteroid.
In the other cases the MKI is not considered since a very high number of launches are needed (for the second case 63), so other strategies are more convenient.
The assumption considered in this analysis is that the launches are simultaneous, so they take place in the same day. In reality the highest launch frequency currently available is the one of Falcon 9 vehicle, which can guarantee a launch every 15 days, thanks to the recovery of the boosters [8].

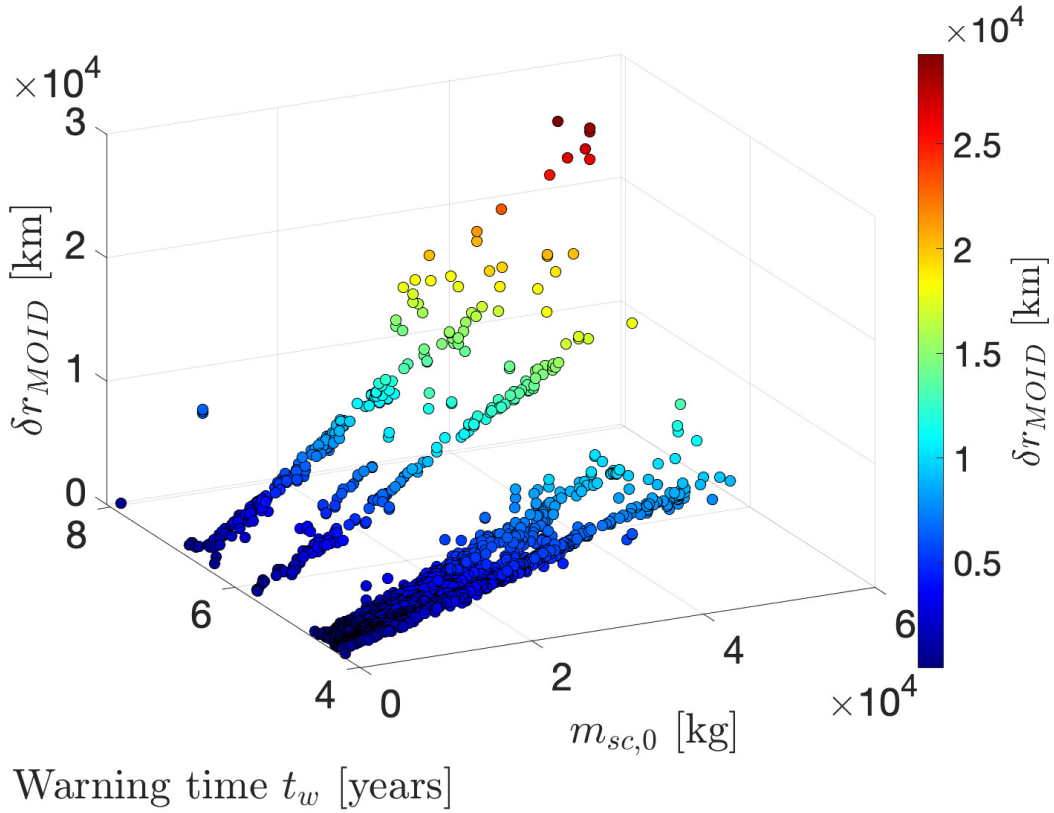

Figure 4.5: Multiple Kinetic Impactor First case Pareto front: deviation at MOID vs initial mass vs warning time

The maximum deviation obtained is $\delta r_{MOID} = 29301\ km$, so higher than the one required for a westward deflection.
The work developed by Gargioli [25] studies in details the uncertainties correlated with the Multiple Kinetic Impactor Strategy.

4.2.4. Mission Design

The kinetic impactor requires no payload for the deflection, the total spacecraft mass at arrival is the deflection system mass, that's why it is important to optimise this value.
In order to perform the DSM manoeuvre chemical propulsion is considered. In particular a liquid bipropellant thruster is needed to reduce the mass of propellant consumed. In fact bipropellant thrusters can guarantee the highest specific impulse between all the chemical propellant, from $300s$ to $500s$.

Oxidizer	Fuel	Specific Impulse (vacuum) I_s [s]	Storage Temperature [K]
LOX	LH2	460	3.2
LOX	RP1 (kerosene)	360	3.7
N_2O_4	MMH (N_2H_4)	336	Ambient temperature

Table 4.3: Liquid bipropellant performances [49]

In table 4.3 the performances of three mixtures fuel/oxidizer are reported. An important property to be considered for the choice is the storage temperature. If the storage temperature is below ambient temperature the propellant is cryogenic, otherwise it is storable. In the case of a kinetic impactor mission the propellant has to be stored for a long time until the DSM takes place, so a cryogenic solution (LOX/LH2 or LOX/RP1), even if it brings to higher specific impulse, is not the best solution because it is difficult to maintain such low temperatures for a long period of time. This is the reason why a good solution is the couple N_2O_4-MonoMetilHydrazine (MMH), also because it is hypergolic, so no ignition system is needed. So the specific impulse provided is 336 s.

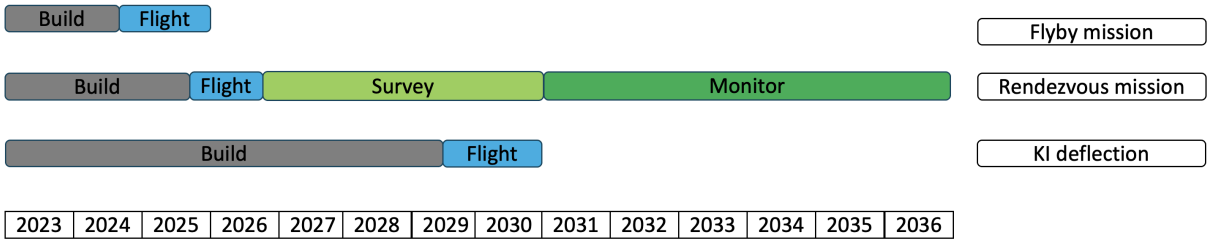

Figure 4.6: Timeline of the missions

In the case of the Kinetic Impactor strategy an early reconnaissance mission is fundamental to determine the composition of the asteroid and its physical properties. As suggested by NASA [68], two missions are considered, the first one is a fly-by mission, which is able to reach the asteroid very soon, but the information collected are not enough to precisely characterize the asteroid, so a rendezvous mission is needed.
The flyby mission has to be launched as soon as possible. So the launch window opens when Epoch 2 starts (so when the probability of impact is 100 %, 18 months after the discovery). The trajectory is obtained through an optimisation process (with a Genetic Algorithm) using a direct Lambert transfer. The decision variables are described in table 4.4, considering that the initial launch date is determined by the building time of the mission [68].

Parameter	Lower bound	Upper bound
Launch date t_0	2024-10-01	2025-10-01
Number of revolution	0	3
TOF	100 *days*	600 *days*

Table 4.4: Flyby reconnaissance mission: optimisation variables

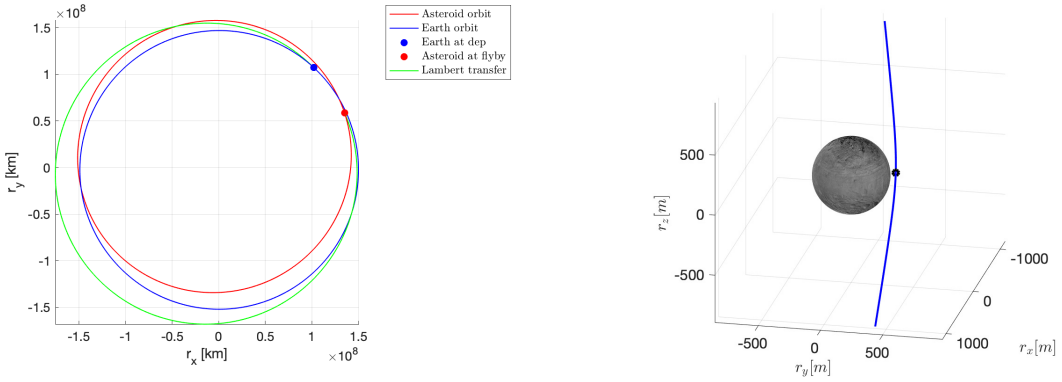

(a) Trajectory of the fly-by reconnaissance mission

(b) Fly-by in asteroid reference frame

Figure 4.7: Fly-by reconnaissance mission

Since the mass of the asteroid is very low (with respect to the mass of a planet) the trajectory after the flyby doesn't change a lot (low Δv obtained), but this is not the aim of the mission.
The flyby mission parameters are summed up in table 4.7.
The aiming radius (or impact parameter Δ) is set equal to 100 m, but its value depends on the characteristics of on board instruments and cameras for the correct observation of the asteroid.

Launch date	2024-11-08
Launcher c3	69.1 km^2/s^2
Flyby date	2025-12-04
TOF	390.6 *days*
Spacecraft mass	1420 kg (Vulcan VC4 launcher)

Table 4.5: Flyby reconnaissance mission

The mass of the spacecraft is obtained through the Launch Vehicle Performance Website

[69], and can be even higher if other launchers are used, see appendix fig. A.12, but, following NASA instructions, the minimum mass needed (for instruments and camera) is 500 kg, so VC4 launcher is enough.
The problem of the flyby is that a very small time is spent in proximity of the asteroid and so only few information can be collected.
Considering the rendezvous mission an electric thruster is used, for the reasons explained before.
The mass at arrival in this case must be sufficiently high to allow the storage of the propellant needed to maintain a stable orbit around the asteroid until the MOID time, in order to monitor the trajectory.
The decision variables are shown in table 4.6 and the quantities that are minimised are the Time of Flight (TOF) and the Δv.

Parameter	**Lower bound**	**Upper bound**
Launch date t_0	2025-06-01	2026-06-01
Spacecraft initial mass $m_{sc,0}$	500 kg	7000 kg
Number of revolution	0	5

Table 4.6: Rendezvous reconnaissance mission: optimisation variables

The trajectory in fig. 4.8 is obtained trough an optimisation process using the the genetic algorithm.

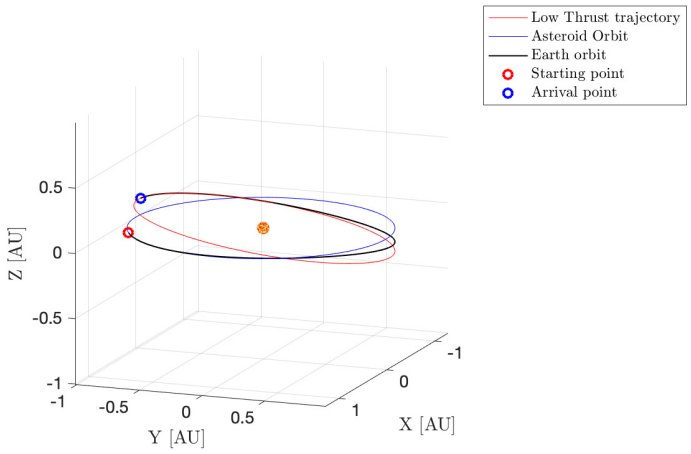

Figure 4.8: Trajectory of the rendezvous LT mission

Launch date	2025-07-21
$m_{sc,0}$	2955 kg
Rendezvous date	2026-06-21
TOF	334.7 $days$
Δv_{LT}	9.56 km/s
$m_{sc,f}$	2332.6 kg (NEXT-C thruster)

Table 4.7: Rendezvous LT reconnaissance mission

4.2.5. Minimum Collision Probability

The minimum collision probability is a completely different mission with respect to the maximum deflection mission, which has been described in the previous section. In fig. 4.9 the Pareto front obtained minimising the functional J is represented, where J is:

$$J = [-J_P \; m_{sc,0} \; t_{warning}] \tag{4.9}$$

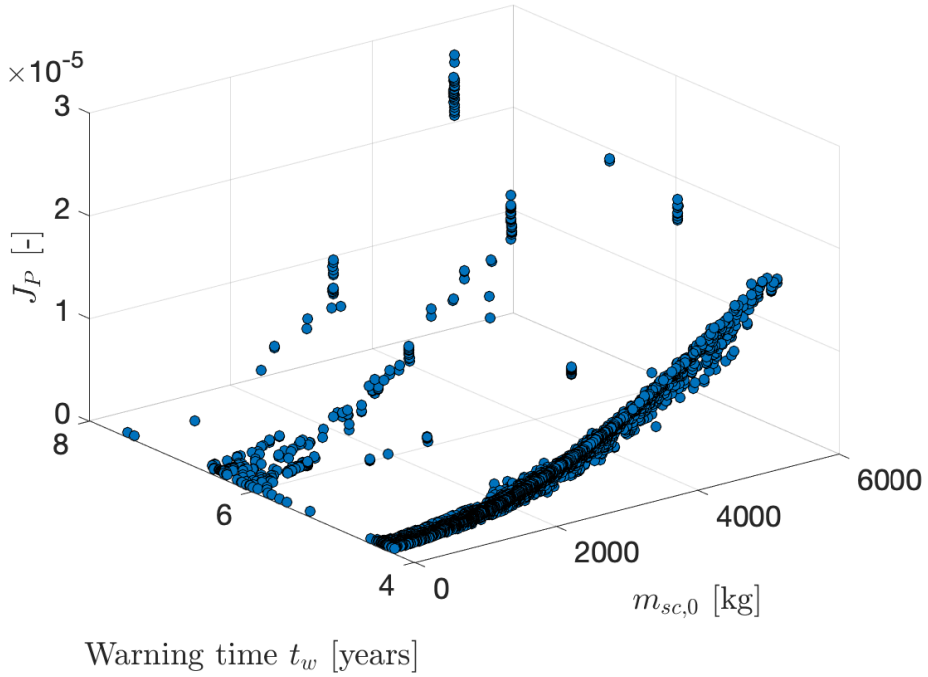

Figure 4.9: Kinetic Impactor: J_P vs spacecraft initial mass vs warning time

In table 4.8 the optimal parameters corresponding to the solution which guarantees the highest value of J_P are reported.

Launch date	2029-09-05
Initial spacecraft mass $m_{sc,0}$ $[kg]$	5151.9
Warning time $[years]$	7.9
Probability functional J_P	$2.7 \cdot 10^{-5}$

Table 4.8: Kinetic Impactor second case: Minimum collision probability

4.3. Optimal Nuclear Standoff Explosion mission

4.3.1. Pareto fronts

The trajectory of the the Nuclear Standoff Explosion Mission is a direct transfer from Earth to the asteroid. In this case it is not considered a DSM manoeuvre basically for two reasons: the first one is that there is the need to maximise the payload mass, which is the mass of the nuclear warhead (the higher is the mass the higher is the energy delivered to the asteroid) and the second one is that in this case, with respect to the Kinetic Impactor mission, there is no reason to maximise the relative velocity between spacecraft and asteroid at arrival, so a direct launch is a better solution.
The upper and lower bounds of the decision variables are expressed in table 4.9.

Parameter	**Lower bound**	**Upper bound**
α_0	0	1
Number of revolution	0	3
TOF	100 $days$	800 $days$

Table 4.9: Nuclear Explosion mission: optimisation variables

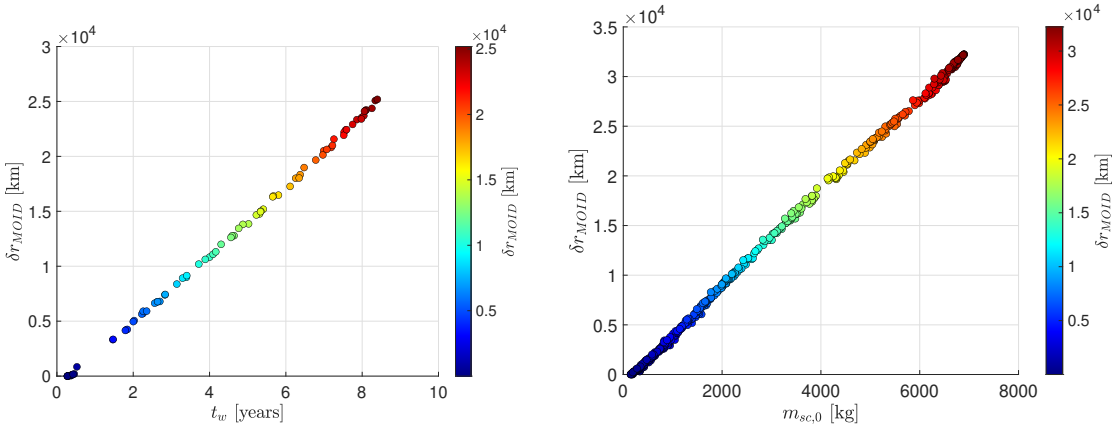

(a) Nuclear Standoff Explosion Pareto front, third case: δr_{MOID} vs t_w

(b) Nuclear Standoff Explosion Pareto front, third case: δr_{MOID} vs $m_{sc,0}$

Figure 4.10: Nuclear Standoff Explosion: third case Pareto fronts

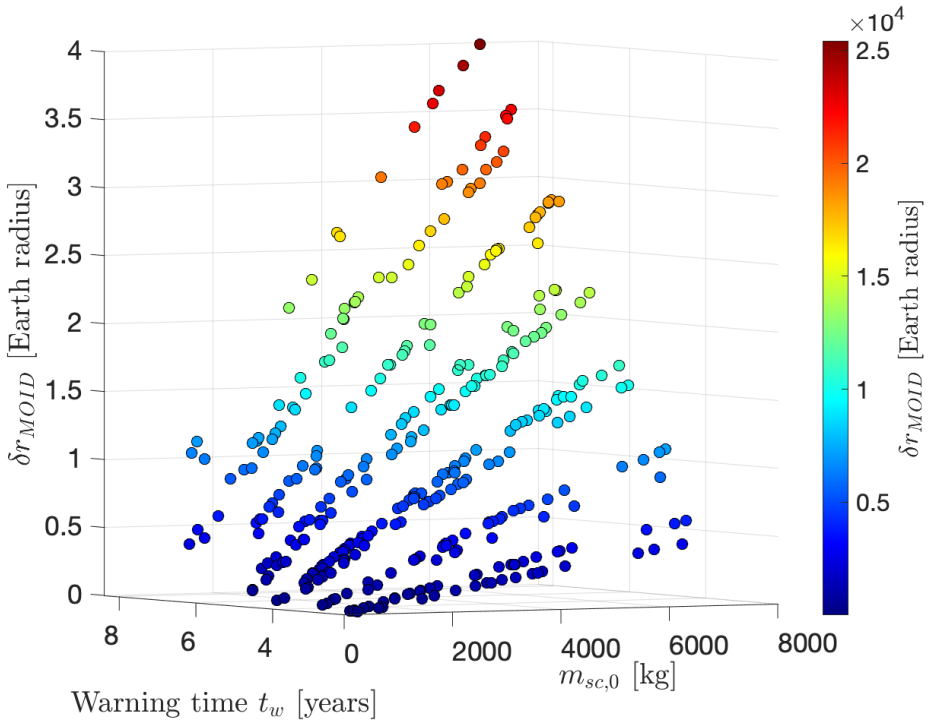

Figure 4.11: Nuclear Standoff Explosion third case: 3D Pareto front

In fig. 4.10 and fig. 4.11 the Pareto fronts of the Nuclear Standoff explosion mission are reported for the third case, which the worst case with mass of the asteroid equal to $M_{ast} = 3.8 \cdot 10^{12}\ kg$ and diametre $d_{ast} = 1539\ m$.
All the Pareto fronts are obtained considering a population size $N = 10000$.

4.3.2. Maximum deflection mission

The maximum deflection mission is the one which maximises δr_{MOID}.
The parameters of the mission are reported in table 4.10.
For the first ($5th$ % percentile: $M_{ast} = 2.6 \cdot 10^{10}\ kg$, $d_{ast} = 290\ m$) and second case ($50th$ % percentile: $M_{ast} = 2.5 \cdot 10^{11}\ kg$, $d_{ast} = 617\ m$) the 3D Pareto fronts can be seen in appendix C.2.

Parameter	**First case** 5%	**Second case** 50%	**Third case** 95%
Launch date	2029-07-05	2028-08-06	2028-08-17
Arrival date	2030-10-22	2029-12-31	2030-01-02
TOF $[days]$	474.7	512.7	502.73
N_{rev}	1	1	1
Lead time $[years]$	6.01	6.81	6.81
$c3$ $[km^2/s^2]$	11.5	18.7	16.3
$m_{sc,0}$ $[kg]$	6729.5	6287.4	6465.9
$\|\Delta v_{nuc}\|$ $[m/s]$	1.754	0.1872	0.03575
$\|\delta r_{MOID}\|$ $[km]$	1074158	129340	24639

Table 4.10: Nuclear standoff mission: Results of the optimisation

In all the three cases the deviation achieved is enough to avoid collision with the Earth. In particular for the third case, the worst one, the deflection at MOID obtained is 24639 km, while the required one for a westward deflection is 23000 km, so there is a very small margin which can be problematic because the mission is full of uncertainties, in particular concerning the asteroid composition and surface materials.
Also NASA in [68] obtained the same results, for all the cases, and for the third one they suggested to build and launch a second back-up mission. The data from the rendezvous low thrust reconnaissance mission will give a feedback on the effective deviation obtained and so if it is necessary the second nuclear warhead will be used.

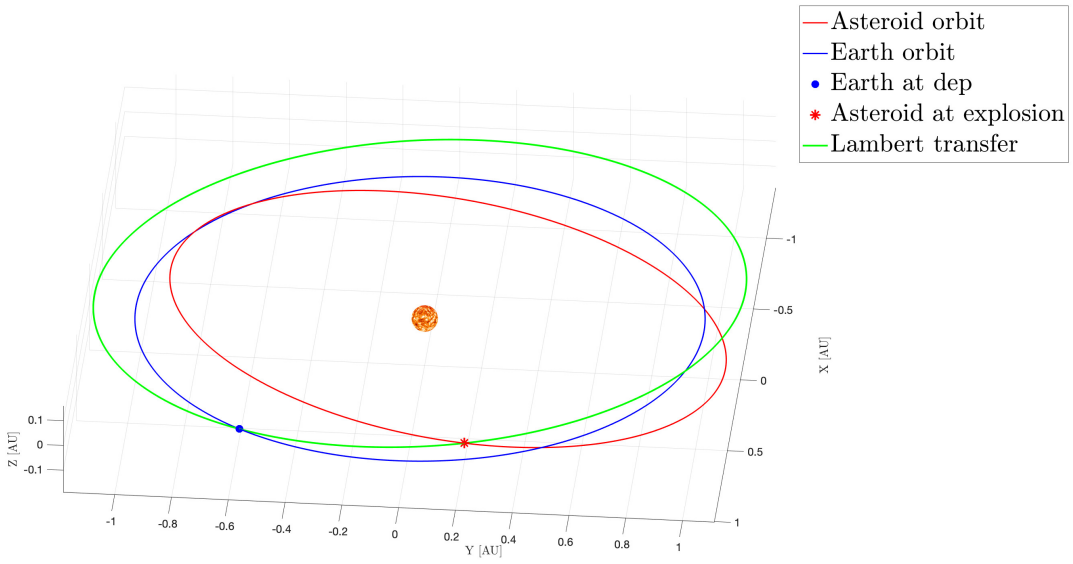

Figure 4.12: Trajectory of the Nuclear Standoff Explosion mission (third case)

4.3.3. Mission Design

The energy released by the nuclear explosion depends on the mass of the nuclear device that can be launched. This can be computed from the initial mass of the spacecraft considering that:

$$m_{sc,0} = m_{nuc} + m_{structure} \tag{4.10}$$

The limit imposed during the optimisation is that the mass of the structure is considered equal to 0.7 $m_{sc,0}$ [84] [105].
So the mass of the nuclear warhead is:

$$m_{nuc} = 0.3 m_{sc,0} \tag{4.11}$$

Not all of this mass is the one of the bomb itself because auxiliary systems are needed, as well as structural components or the explosive which is necessary for the detonation. It is assumed that 10% of the payload mass has to be dedicated to these systems, so:

$$m_{wh} = \frac{0.3 m_{sc,0}}{1.1} \tag{4.12}$$

The energy delivered by the explosion is:

$$E_t = m_{wh} YTW \tag{4.13}$$

Where YTW is the yield to weight ratio. For every kilogram of Uranium-235 that completely fissions, it releases about 17 $ktons/kg$. While Lithium-deuteride (LiD), the most common fusion fuel, yields 50 $ktons/kg$ that undergoes fusion. So fusion is nearly 3 times more energetic per weight than fission. So the more fusion is added to a weapon the better the yield-to-weight ratio is, except for the fact that all fusion weapons require a fission primary small weapon that creates enough energy to start the fusion process.

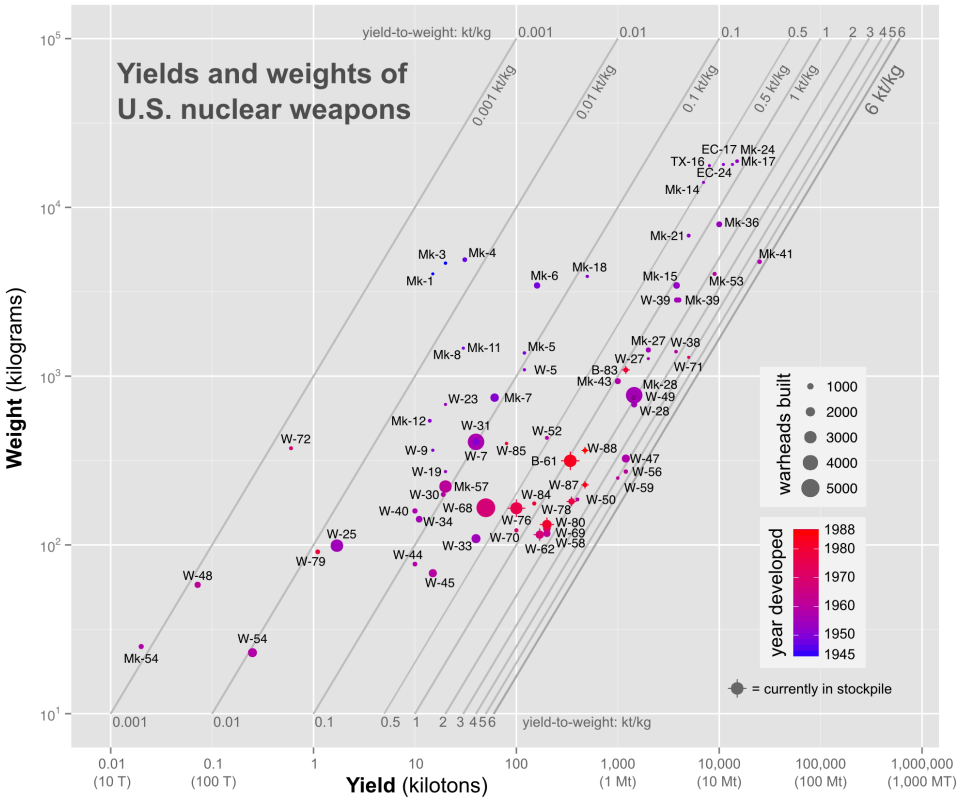

Figure 4.13: YTW of US nuclear weapons

From fig. 4.13 it can be noted that the YTW varies from 0.001 $ktons/kg$ to around 6 $ktons/kg$. A value of 1 $ktons/kg$ has been chosen for the optimisation process, since, as can be seen in table 4.11, the mass of the nuclear warhead is in the order of 10^3 kg, so the weapon Mk-43 or B-83 can be used. Note that choosing an already developed bomb helps to reduce the TRL of the mission.

Asteroid dimensions and mass	Mass available for the Nuclear warhead
First case	1835 kg
Second case	1714 kg
Third case	1763 kg

Table 4.11: Mass of the nuclear warhead

4.3.4. Minimum Collision Probability

Even if conceptually the two types of mission are completely different, the maximisation of the probability functional, which means minimizing the collision probability, is strictly related to the Δv that the strategy is able to provide, as in the case of the Maximum Deflection mission.
The first case is considered in order to have a comparison with the Kinetic Impactor strategy. With the Nuclear Explosion the maximum value of J_P is four orders of magnitude higher then the one obtained with KI strategy, so the probability of collision is significantly reduced.

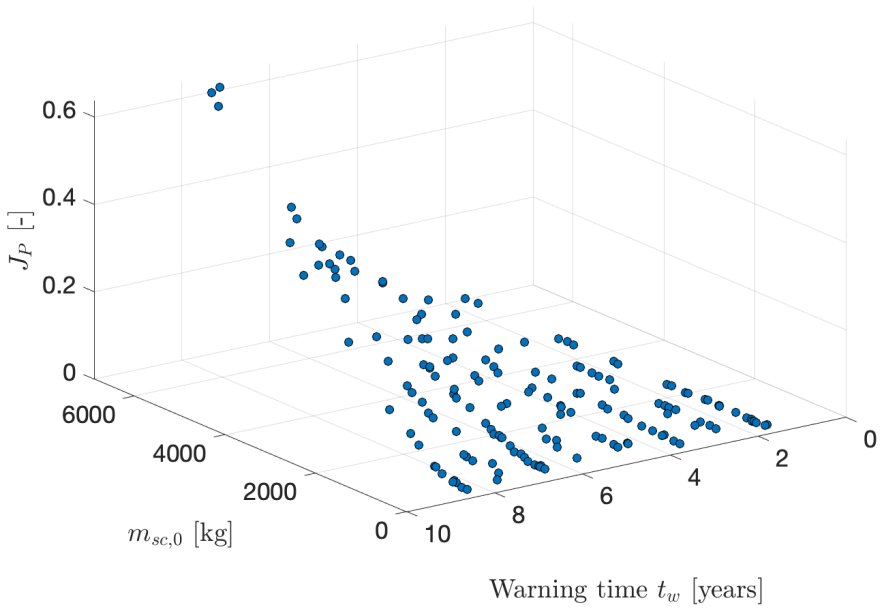

Figure 4.14: Nuclear Standoff Explosion mission: minimum collision probability Pareto front (first case)

Launch date	2028-06-11
Initial spacecraft mass $m_{sc,0}$ $[kg]$	5772.3
Warning time $[years]$	8.31
Probability functional J_P	0.6368

Table 4.12: Nuclear Standoff Explosion second case: Minimum collision probability

4.4. Optimal Gravity Tractor mission

4.4.1. Pareto fronts

The gravity tractor strategy is a slow-push deflection strategy. The trajectory considered in this case is low thrust. As explained in section 3.2, the decision variables for the optimisation in this case are:

$$x_{low\ thrust\ traj} = [N_{rev} \quad t_0 \quad m_{sc,0}] \tag{4.14}$$

The lower and upper bounds are reported in table 4.13.
The first launch date possible depends on the time necessary to prepare the mission. Also in this case 5 years are considered, because it is the typical time necessary for an interplanetary mission.
The initial mass of the spacecraft in this case is not strongly influenced by the launcher c3 as in the case of the impulsive trajectory because the spacecraft only needs to escape from Earth gravitational field, then the on board gridded ion thrusters will bring it to the asteroid. So, since the Earth escape velocity has to be reached, the c3 needed is 0. Always referring to the Falcon 9 Heavy launcher (see fig. A.13), the maximum mass that can be launched in this case is 10985 kg.

Parameter	**Lower bound**	**Upper bound**
N_{rev}	0	5
Launch date t_0	2027-04-03	2036-10-22
Spacecraft initial mass $m_{sc,0}$ $[kg]$	100	10985

Table 4.13: GT mission: optimisation variables

In the following plots the Pareto fronts obtained by minimising the functional $J = [-J_{\delta b}\ m_{sc,0}]$ for fig. 4.15b, $J = [-J_{\delta b}\ t_{warning}]$ for fig. 4.15a, $J = [-J_{\delta b}\ m_{sc,0}\ t_{warning}]$ for fig. 4.16 are reported.

Since the Gravity Tractor strategy is generally useful for small asteroids, the first case is initially considered.

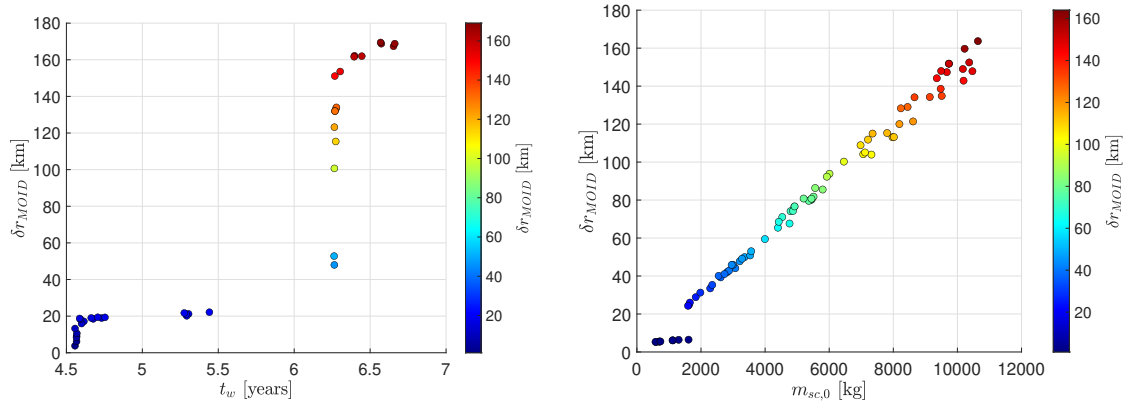

(a) Gravity Tractor Pareto front, first case: δr_{MOID} vs t_w

(b) Gravity Tractor Pareto front, first case: δr_{MOID} vs $m_{sc,0}$

Figure 4.15: Gravity Tractor: first case Pareto fronts

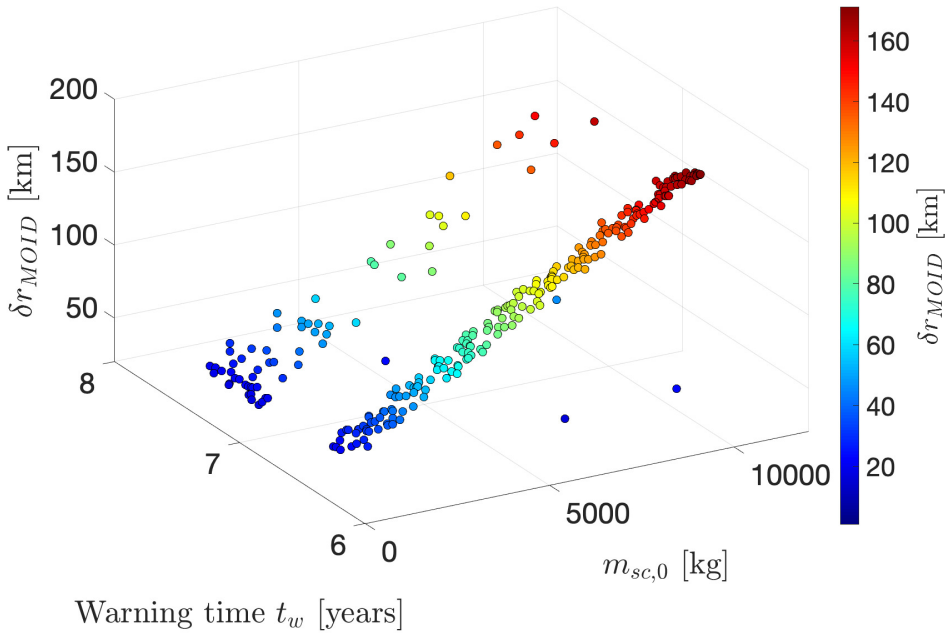

Figure 4.16: Gravity Tractor Pareto front, first case: δr_{MOID} vs $m_{sc,0}$ vs t_w

All the Pareto fronts are obtained with a population size equal to $N = 10000$, lower than KI and Nuclear explosion optimisation. This is because in the case of the slow push strategies (GT and Laser Ablation), with respect to the impulsive ones, the computation

is very expensive since the Gauss' equations have to be integrated in order to determine the orbital elements variation at each time instant.

4.4.2. Maximum Deflection Mission

The low thrust trajectory for the maximum deflection mission is shown in fig. 4.17.

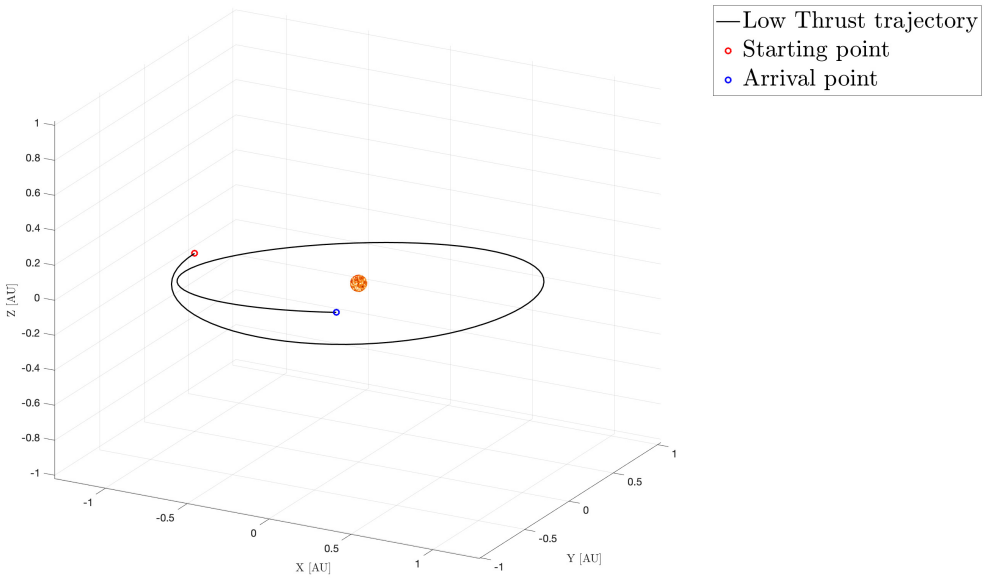

Figure 4.17: Trajectory of the GT mission, first case

The optimal solution which leads to the maximum value of δr_{MOID} is selected from fig. 4.16 as it has been done for the other strategies.

Parameter	First case 5%	Second case 50%
Launch date	2030-03-21	2028-05-11
$m_{sc,0}$ kg	10848.2	10735
Arrival date	2031-07-11	2031-06-30
Number of revolutions	0	2
TOF $years$	1.31	3.13
Δv_{LT} km/s	9.65	8.46
$m_{sc,LT;final}$ kg	8542.8	8706.7
$m_{sc,f}$ kg	8146.5	4493.5
$\|\delta r_{MOID}\|$ $[km]$	169.24	34.1

Table 4.14: Gravity Tractor mission

The Gravity Tractor strategy is not useful for the deflection of asteroid 2023 PDC, since the deviation obtained is much lower than the value needed (9300 km eastward).
The third case is not considered since the deflection would be very low. The problem is the huge quantity of propellant mass needed for the hovering condition, which will reduce significantly the deviation action time.

4.4.3. Mission Design

In this case the initial mass of the spacecraft is:

$$m_{sc,0} = m_{structure} + m_{prop} = m_{structure} + m_{prop,LT} + m_{prop,hovering} \tag{4.15}$$

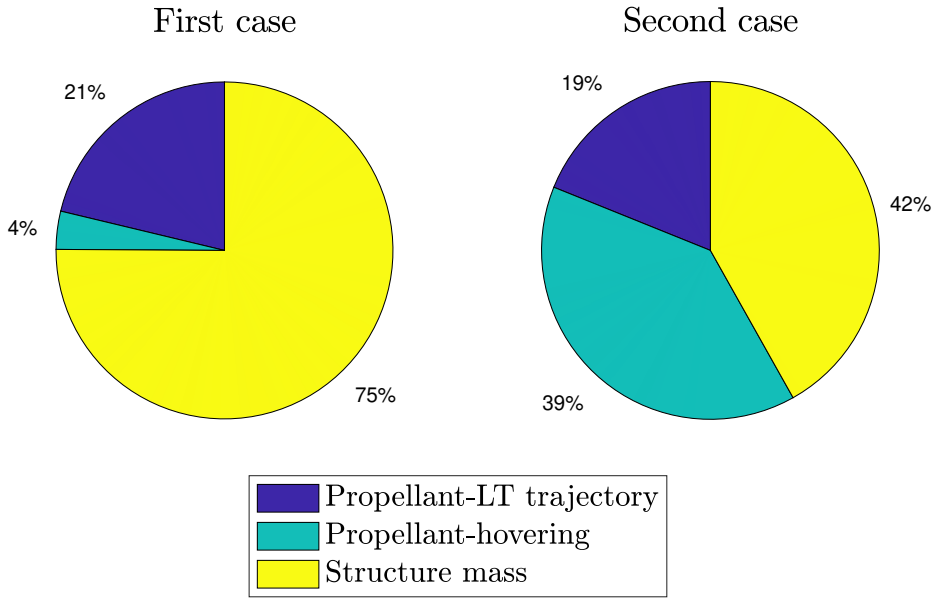

Figure 4.18: Mass distribution for the Gravity Tractor mission

The mass of the structure, which not only includes the structural components, but corresponds to the dry mass of the spacecraft, is considered equal to 0.5 $m_{sc,0}$, so half of the total mass is propellant mass. This value is quite high, but it has to be considered that there is no payload for a GT mission, and in addition it is suggested by the NASA DAWN mission [65], which used an ion thruster, and the propellant mass fraction in that case was 0.4.
In fig. 4.18 it can be noted that the problem is more evident in the second case, when the mass of the asteroid is one order of magnitude higher than the first case and so the propellant mass for the hovering condition is higher.
The mass of propellant needed for the Low Thrust trajectory is computed using the Tsiolkovsky rocket equation, so:

$$m_{prop,LT} = m_{sc,0}(1 - e^{-\frac{\Delta v_{LT}}{I_s g_0}}) \tag{4.16}$$

Concerning the mass needed for the hovering condition, the model described in section 3.5 is used for the computation. The forces F_x and F_y needed for the control along the two

axes are summed up to find the total thrust and then the total impulse is computed through an integration:

$$T(t) = F_x(t) + F_y(t) \tag{4.17}$$

$$I_{TOT} = \int_0^{t_f} T(t)dt \tag{4.18}$$

But the total impulse can be expressed also as: $I_{TOT} = m_{prop} I_s g_0$, so the mass of propellant for the hovering period is:

$$m_{prop,hovering} = \frac{I_{TOT}}{I_s g_0} \tag{4.19}$$

The thruster selected is the gridded ion thruster NEXT-C, which uses Xenon as a propellant and guarantee a specific impulse of 422 s [66]. This engine is flight proven and was already used for the DART mission. Its performances are summerized in table 4.15.

Thrust $[mN]$	$25 - 235$
Maximum Specific Impulse $[s]$	4220
Thruster efficiency	0.7
PPU efficiency	0.94
Thruster mass $[kg]$	14
PPU mass $[kg]$	36

Table 4.15: NEXT thruster parameters

4.4.4. Minimum Collision Probability

In fig. 4.19 the 3D Pareto front is obtained maximising $J = [J_P \; m_{sc,0} \; t_w]$ in the first case.

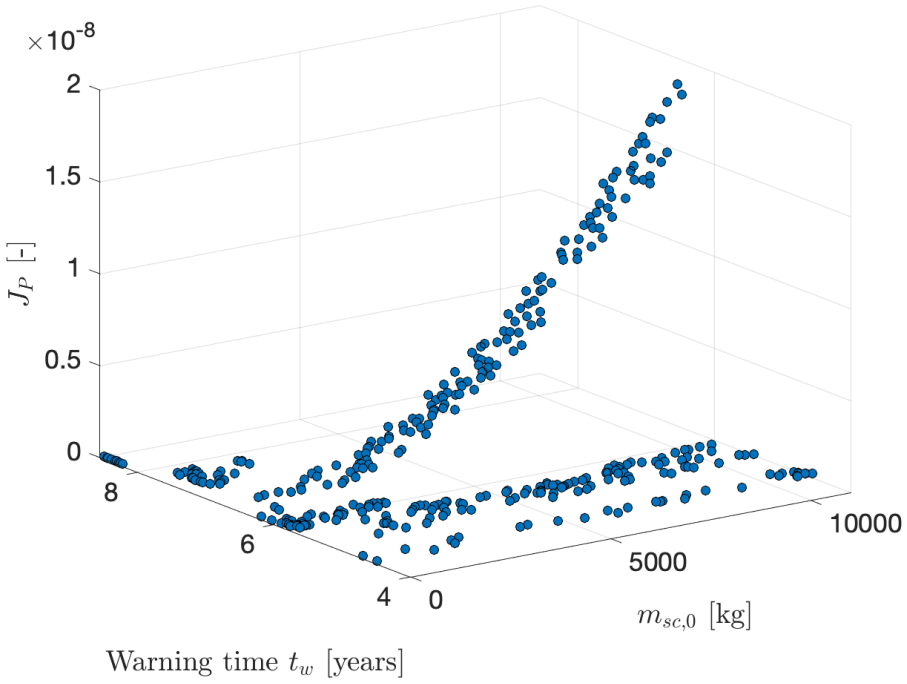

Figure 4.19: Gravity Tractor: J_P vs spacecraft initial mass vs warning time (first case)

The values in table 4.22 are obtained by choosing the optimal Pareto solution which maximises the functional J_P.

Launch date	2030-04-06
Initial spacecraft mass $m_{sc,0}$ $[kg]$	10959
Warning time $[years]$	6.51
Probability functional J_P	$1.8 \cdot 10^{-8}$

Table 4.16: Kinetic Impactor second case: Minimum collision probability

In this case the value of $J_{P,max}$ is even lower than the one obtained with the KI mission, so the probability of collision is higher.
This is strictly related to the fact that the deviation obtained with GT is 1 order of magnitude lower than the one obtained with KI.

4.4.5. Multiple Gravity Tractor - Halo orbit

The Halo orbit configuration can be useful when a Multi-satellite Gravity Tractor configuration is used.
In this case more than one satellite is placed on an Halo orbit, and also more than one

Halo orbit can be used. In particular Wie suggests, in [107], to use two Halo orbits, at a safe distance of 100 m between each other, and to place 4 satellites in each orbit.

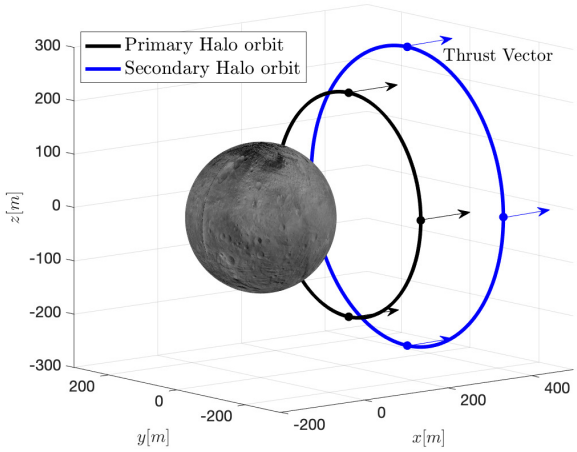

Figure 4.20: Multiple Gravity Tractors in two different Halo orbits

This configuration requires eight Falcon Heavy launches, because eight spacecrafts with a mass of around 11000 kg (or lower, it depends on the optimisation) need to reach the Earth escape velocity.
So an optimisation process with *gamultiobj* function is performed. The Halo orbit mathematical description can be seen in section 3.6.
In addition to the decision variables of the Standard Gravity Tractor strategy (table 4.13) the distance from the first Halo orbit to the asteroid d_1 is considered. The lower bound is set to 10 m, the upper bound is 100 m from the asteroid surface. The acceleration depends on the distance achieved, which increases when the spacecraft is closer to the asteroid, but it has to be considered that the mass of propellant consumed is lower at high distances, so a trade off is necessary.
The distance of the second Halo orbit d_2, as a consequence, is: $d_2 = d_1 + 100$.
In addition in this first analysis all the eight satellites are considered to be launched in the same date, so the results overestimates the deviation achieved, since, as explained for the MKI strategy, the maximum launch frequency is 2 per months.
In the end the decision variables are summarised in table 4.17.

Parameter	Lower bound	Upper bound
N_{rev}	0	5
Launch date t_0	2027-04-03	2036-10-22
Spacecraft initial mass $m_{sc,0}$ $[kg]$	100	10985
Distance d_1 $[m]$	$10 + R_{ast}$	$100 + R_{ast}$

Table 4.17: MGT mission: optimisation variables

The mass of propellant is computed following the procedure explained in section 4.4.3, in particular using eq. (4.19).
In fig. 4.21 it is reported the 3D Pareto front for the first case ($5th\%$ percentile) $M_{ast} = 2.6 \cdot 10^{10}$ kg, $d_{ast} = 290$ m, obtained by minimising the functional:

$$J = [-J_b \; m_{sc0} \; t_w] \tag{4.20}$$

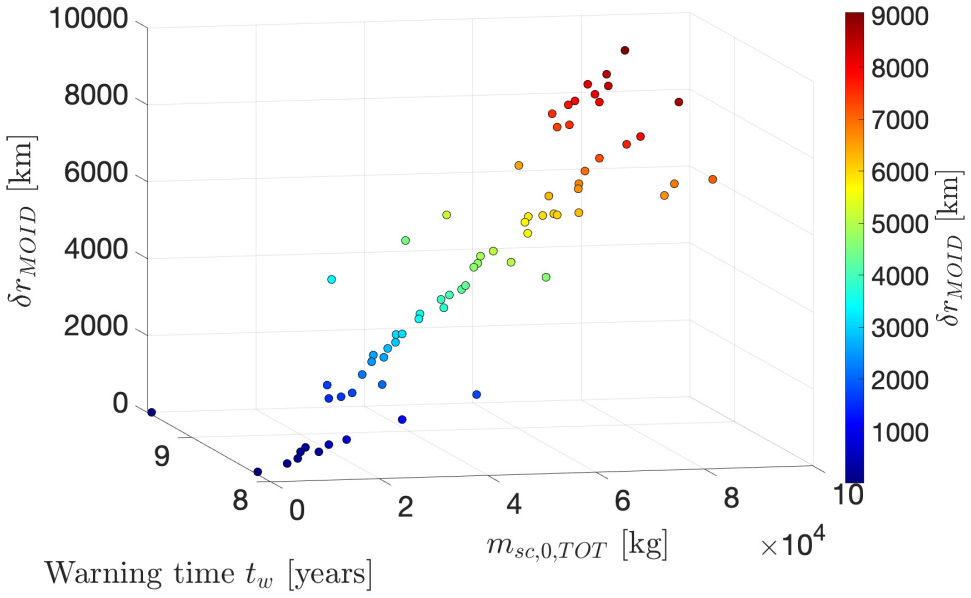

Figure 4.21: Multiple Gravity Tractor Pareto front, first case: δr_{MOID} vs $m_{sc,0}$ vs t_w

In this case the solution which leads to the maximum deflection requires a mass into space of 87995.1 kg, so each of the 8 satellites with a mass of 10999.3 kg. The deviation at MOID obtained is $\delta r_{MOID} = 9652.7$ km. In this case, differently with respect to the KI mission, the deflection is eastward since the semimajor axis is augmented, so the velocity increases. So the required deflection is only 9500 km, as explained in section 3.7. As a

consequence the MGT strategy is a valid option, but only if the real asteroid size and mass is in the first percentile level.
Unfortunately if the second percentile is considered, the deviation is around 1000 km, not enough even for an eastward deflection.

4.5. Optimal Laser Ablation mission

4.5.1. Pareto fronts

Laser Ablation is a slow push strategy, so the trajectory is the same considered for the Gravity Tractor, explained in section 3.2.
The decision variables lower and upper bounds are summarised in table 4.18. In this case the TRL of the mission is not so high as in the case of the KI or the GT, since lasers in space are not currently used. As a consequence the time span for the build up of the satellite is considered equal to 7 years, two years higher than the other missions. So the first date available for launch is in 2030.

Parameter	**Lower bound**	**Upper bound**
N_{rev}	0	5
Launch date t_0	2030-04-03	2036-10-22
Spacecraft initial mass $m_{sc,0}$ $[kg]$	100	10985

Table 4.18: Laser Ablation mission: optimisation variables

As in the previous sections, the three Pareto fronts are reported in the following figures. In fig. 4.22 and fig. 4.23 the Pareto fronts corresponding to the second case of asteroid mass and dimension are reported.

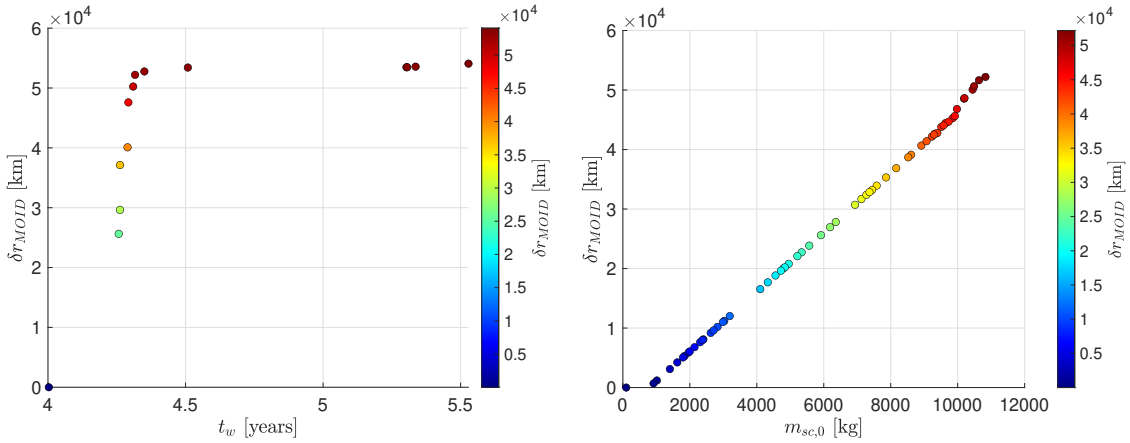

(a) Laser Ablation Pareto front, second case: δr_{MOID} vs t_w

(b) Laser Ablation Pareto front, second case: δr_{MOID} vs $m_{sc,0}$

Figure 4.22: Laser Ablation: second case Pareto fronts

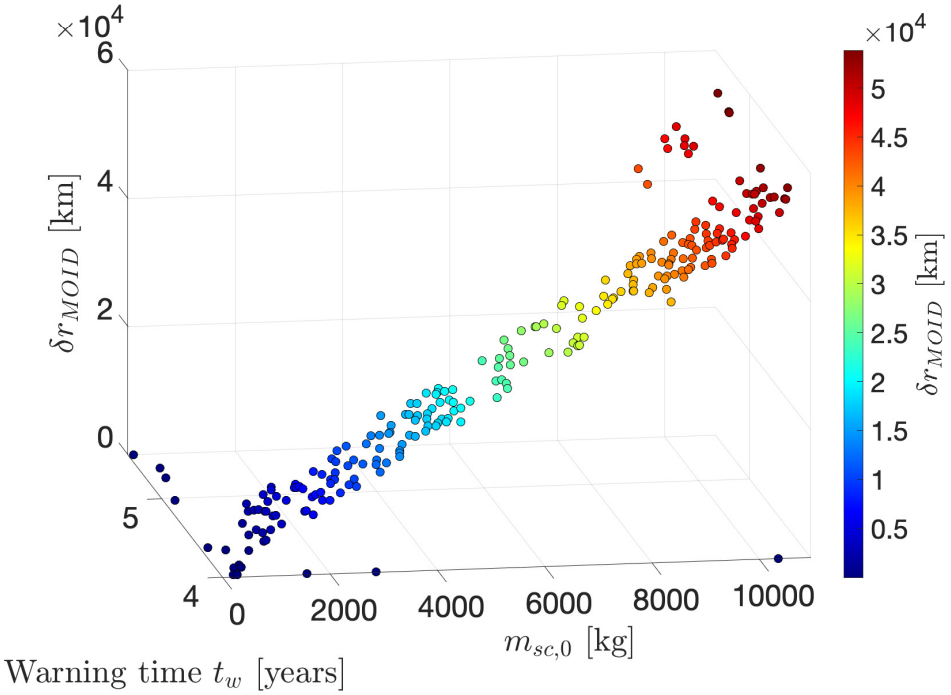

Figure 4.23: Laser Ablation Pareto front, second case: δr_{MOID} vs $m_{sc,0}$ vs t_w

The population size used in this case is 1000, lower with respect to the other cases, but in this case the computational cost is very high since the differential equation (used to integrate the Gauss equations and the mass flow rate) has to be solved for a small time interval, but a lot of times, corresponding to the number of asteroid revolutions along its

rotational axes.

$$N_{rev,ast} = \frac{T_{rev}}{\Delta t_{action}} \tag{4.21}$$

The revolution period of the asteroid depends on its revolution velocity v_{rot}, while Δt_{action} is the deflection action time.
No information is available on the asteroid rotational velocity, so it is assumed to be equal to 1 rev/day.
It is important to underline that solving the differential equation just one time, but for a very long period of time, as in the GT case, requires less computational cost than solve the equation many times, but for a short time interval.

4.5.2. Maximum Deflection Mission

From the 3D Pareto front in fig. 4.23 the optimal solution which guarantees the maximum deflection is selected and the mission parameters are reported in table 4.19. The Pareto fronts for the first and the third case can be seen in appendix C.4.

Parameter	**First case** 5%	**Second case** 50%	**Third case** 95%
Launch date	2032-05-23	2031-04-16	2032-02-28
$m_{sc,0}$ $[kg]$	10888	10947	10957
Arrival date	2035-06-30	2035-06-26	2036-06-25
TOF $[years]$	3.1	4.19	4.32
N_{rev}	3	3	4
Δv_{LT} $[km/s]$	8.53	8.42	8.41
$m_{sc,f}$ $[kg]$	7770.3	7832.0	8639.1
$\|\delta r_{MOID}\|$ $[km]$	1544862	51671	1397.4

Table 4.19: Laser Ablation mission

The deviations, especially in the first and in the second case, are very high with respect to what is required (9300 km eastward deflection). The problem is that the power needed by the laser is very high. So in this two cases a solution with lower power input can be considered, which will lead to much lower deflection at MOID, but always enough to avoid collision.
For the third case the Laser Ablation is not useful, since the deviation obtained is lower than 9300 km.
This can be explained by the fact that the mass of propellant required for the hovering phase is very high because the asteroid is in the order of 10^{12} kg (two orders of magnitude

higher than the one in the first case).
So for both slow push strategies, Laser Ablation and GT, the problem is in the hovering phase when the asteroid mass is high, because the hovering time, which corresponds to the deflection action time, is not enough to deviate completely the asteroid.

In the following chapter the mission design is carried out only for the first two cases, when the Laser Ablation strategy can be used.

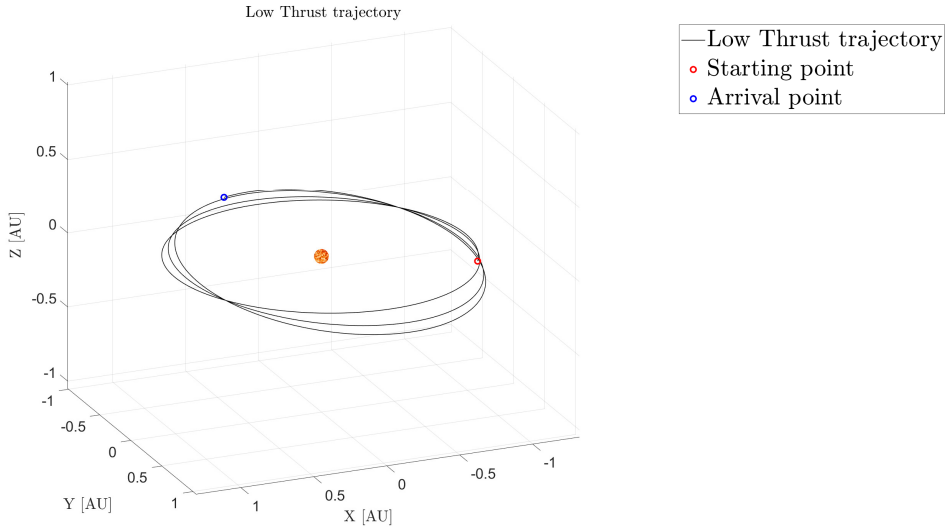

Figure 4.24: Laser Ablation mission: LT trajectory (second case)

4.5.3. Mission Design

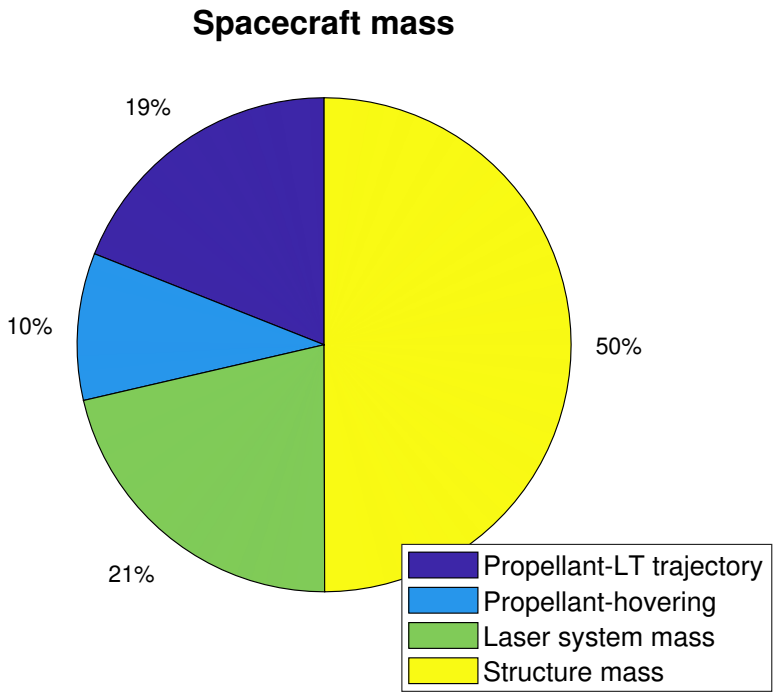

Figure 4.25: Spacecraft mass distribution for laser ablation mission

In the case of a laser ablation mission the total spacecraft mass consists in the sum of the propellant mass, the mass of the structure and the mass of the laser system: $m_{sc,0} = m_{LS} + m_{prop} + m_{structure}$.
The mass of the structure is considered equal to 0.5 m_{dry}, as defined in [84]. This is conceivable because most of the spacecraft mass is occupied by payload, instruments, tanks, mass of all the subsystems, as power subsystem, thermal subsystem and electric subsystem (solar panels, batteries, RTGs).
The propellant mass is given by the mass needed for the low thrust trajectory and the one needed to maintain the hovering condition. So:

$$m_{prop} = m_{hovering} + m_{LT-traj} = \frac{T_{hov}}{I_s g_0} + m_{sc,0}\left(1 - e^{\frac{-\Delta V_{LT}}{I_s g_0}}\right) \tag{4.22}$$

In the first case the mass of propellant is equal to 3115 kg, and as a consequence the mass of the laser system is: $m_{LS} = 2330.4\ kg$.
The mass of the laser system is given by the sum of the power subsystem mass, the radiators mass and the mass of the laser itself plus the optics instruments [99]. The radiators are needed because, as explained in section 2.4 part of the energy generated by

the electron avalanche process is dissipated into heat and so the system has to be cooled down.

$$m_{LS} = \alpha_P P_L + \rho_R (1 - \eta_L) \frac{P_L}{\sigma \epsilon_R T_R^4} + \alpha_L P_L \tag{4.23}$$

Where P_L is the power input to the laser, $\alpha_P = 40\ kg/kW$ is the mass per unit power, $\rho_R = 0.5\ kg/m^2$ is the density of the radiator, ϵ_R their emissivity (considered equal to 0.8), T_R their operating temperature and $\eta_L = 0.55$ is the laser efficiency. The specific mass of the laser α_L is considered equal to 10 kg/kW. The operating temperature of the radiators is the one at which the laser diodes work, so 298 K. All the values are taken from the work of Vasile [99].
So the value of the input power to the laser is:

$$P_L = \frac{m_{LS}}{\alpha_P + \dfrac{\rho_R (1 - \eta_L)}{\sigma \epsilon_R T_R^4} + \alpha_L} \tag{4.24}$$

Using the data reported before, the input power to the laser can reach values up to 50 kW. This is a very high power, but currently produced industrial lasers are able to manage this huge value. The problem is how to generate this amount of power on board of the satellite, considering that also the electric thrusters for hovering need power. The problem of generating the laser input power is considered separately in section 4.5.3.
Two phases of the mission are considered in order to size the power subsystem: the first one is the transfer phase, here the power is needed to feed the electric thrusters during the low thrust trajectory ($P_{e,LT}$) and for other spacecraft systems (communication, instruments and sensors).

$$P_{transfer} = P_{e,LT} + P_{s/s} \tag{4.25}$$

So if T is the electric thrust that has to be generated and η is the efficiency:

$$P_{e,LT} = \frac{T I_s g_0}{2 \eta_{trhuster} \eta_{PPU}} \tag{4.26}$$

The thrust during the LT trajectory is computed through geometrical relations, see appendix A.9 for details. The thruster performance parameters are shown in table 4.15.
The maximum thrust that the electric thrusters have to provide is 0.9 N, so since one NEXT thruster is able to provide maximum 235 mN, four of them are needed. Since the mass of the thruster plus the PPU is 50 kg, the total mass occupied by them is 200 kg.
Then in a second phase of the mission, which is the hovering phase, when the deviation action takes place, the power is always needed to sustain the spacecraft system $P_{s/s}$, then the thruster are switched on to maintain the hovering position and this requires a certain

amount of power ($P_{e,hov}$), which is computed in the same way of $P_{e,LT}$. In the end also the input power to the laser P_L (eq. (4.24)) has to be considered. So:

$$P_{hovering} = P_{s/s} + P_{e,hov} + P_L \tag{4.27}$$

In this section P_L is not considered and will be discussed separately in section 4.5.3.
Note that the maximum thrust in the hovering analysis has been set to 0.5 N, so the power is computed with this value.

	First case	Second case
$P_{transfer}$ $[kW]$	27.7	27.7
$P_{hovering}$ $[kW]$	21.6	21.6
P_L $[kW]$	45.8	46.2

Table 4.20: Power required

In order to generate the power needed for the subsystems and for the electric ion thrusters solar arrays (together with batteries) are considered.
This is currently the best solutions possible, since it is flight proven, high TRL, and also because the use of RTGs is not feasible. The mass of the isotope necessary to provide 20 kW is around 130 kg, which means that more than 30 units are necessary, since each RTGs can contain maximum $3 - 5$ kg of Plutonium [105]. Considering that an RTG weights from 30 to 50 kg [46], the total mass needed would be too high.

Power generated by solar arrays

If solar panels are used, their degradation during years has to be considered in the sizing process. So the power at the beginning of their life is $P_{BOL} = P_0 I_d$, where $P_0 = \epsilon_{BOL} I_0$ and $I_d = 0.8$ [46] is the inherent degradation factor. The power P_0 is given by the solar irradiance at 1 AU (I_0 equal to 1361 W/m^2) and the efficiency at the beginning of life, equal to 0.35, typical value for GaAs (4J) solar arrays ([46]). Then, considering a degradation per year $dpy = 0.03$, the power at the end of life, from which the sizing has to be computed, is $P_{EOL} = P_{BOL}(1 - dpy)^{n_y}$, where n_y is the mission lifetime, expressed in years.
So the dimension and the mass of the solar array can be computed as:

$$A_{SA} = \frac{P}{P_{EOL}} \qquad\qquad m_{SA} = \frac{A_{SA}}{\rho_{SA}} \tag{4.28}$$

Where P is the power that has to be generated and ρ_{SA} is the solar array density and it is considered equal to 8 kg/m^2 [102] which is the one of rigid solar arrays, even if nowadays also thin film solar cells can be used and the density could be lower (0.5 kg/m^2 [102]).

Area of solar arrays	66.2 m^2
Mass of solar arrays	8.2 kg
Mass of batteries	235 kg

Table 4.21: SA and batteries sizing

The mission phase which requires the highest values of SA mass and area is the one considered for sizing. The values for the three cases are reported in table 4.21.
The main problem of solar arrays is the need of a secondary energy source in order to produce energy during eclipse, to perform emergency manoeuvres or to produce energy before the solar arrays deployment. In general batteries are used as a secondary source. Assuming Li-ion batteries the energy density is 130 Wh/kg (as suggested in [102]). The values in table 4.21 are obtained assuming that it is needed to supply full power for 1 hour (specific mass of 8.5 kg/kW).

Laser input power

The main primary energy source used on spacecraft is solar power. The procedure to size solar arrays has been explained before, but the issue is that the area needed if they have to generate also the power for the laser would be too high. For example in the second case the total power in hovering would be:

$$P_{hov} = P_{e,hov} + P_{s/s} + P_L = 67.77\ kW \tag{4.29}$$

This huge power translates into 164 m^2 of solar panels.
Some interplanetary missions used also Radioisotope Thermal Generators (see appendix C.4.3) or fuel cells. In this case, as explained before, the problem is that RTGs produce few power per unit, such that around 100 devices would be necessary to feed also the laser.
For the first case it is instead possible to decrease the power and the correct deviation is always obtained. In fact if the power is set to 10 kW the deviation δr_{MOID} obtained is more than 20000 km, so higher than the one needed for an eastward deflection (9300 km). With such an input power the total request in the hovering phase is 31.6 kW, which means 75 m^2 of solar panel area needed. This value is more feasible, since for example on the *Juno* spacecraft 72 m^2 of solar panels were mounted.

For the second case an option, suggested also by Vasile in [102], is to produce the power needed for the laser using a small nuclear fission reactor. The TRL in this case is very low, but the technology is under development and recent advances, in particular the KRUSTY reactor, reache the TRL 5.

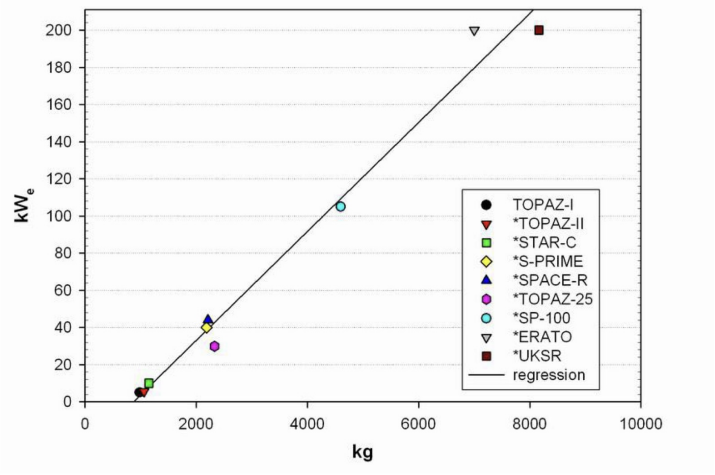

Figure 4.26: Nuclear reactor mass for different electrical power levels [102]

The regression curve that can be extrapolated from fig. 4.26 is:

$$P\ [kW_e] = 0.0293M\ [kg] - 25.63 \tag{4.30}$$

Since the power needed for the laser in the second case is 46.2 kW, the mass of the nuclear reactor is 2451.5 kg.
So in this case the problem is the high mass needed, even if it has been set that the mass of the structures and the subsystems, so excluding the propellant and the payload (the laser in this case), is 0.5 $m_{sc,0}$, so equal to 5473.5 kg.
However using a nuclear electric power system leads to some big advantages: first of all the power is constant, no decay in time and no degradation, and this reduces the operational constraints, then there's no need of secondary energy sources (batteries) because the reactor works both in sunlight and during eclipse.

4.5.4. Minimum Collision Probability

Also for the Laser Ablation another type of mission is considered. This mission consists in the minimization of the collision probability, which means maximising the functional J_P.

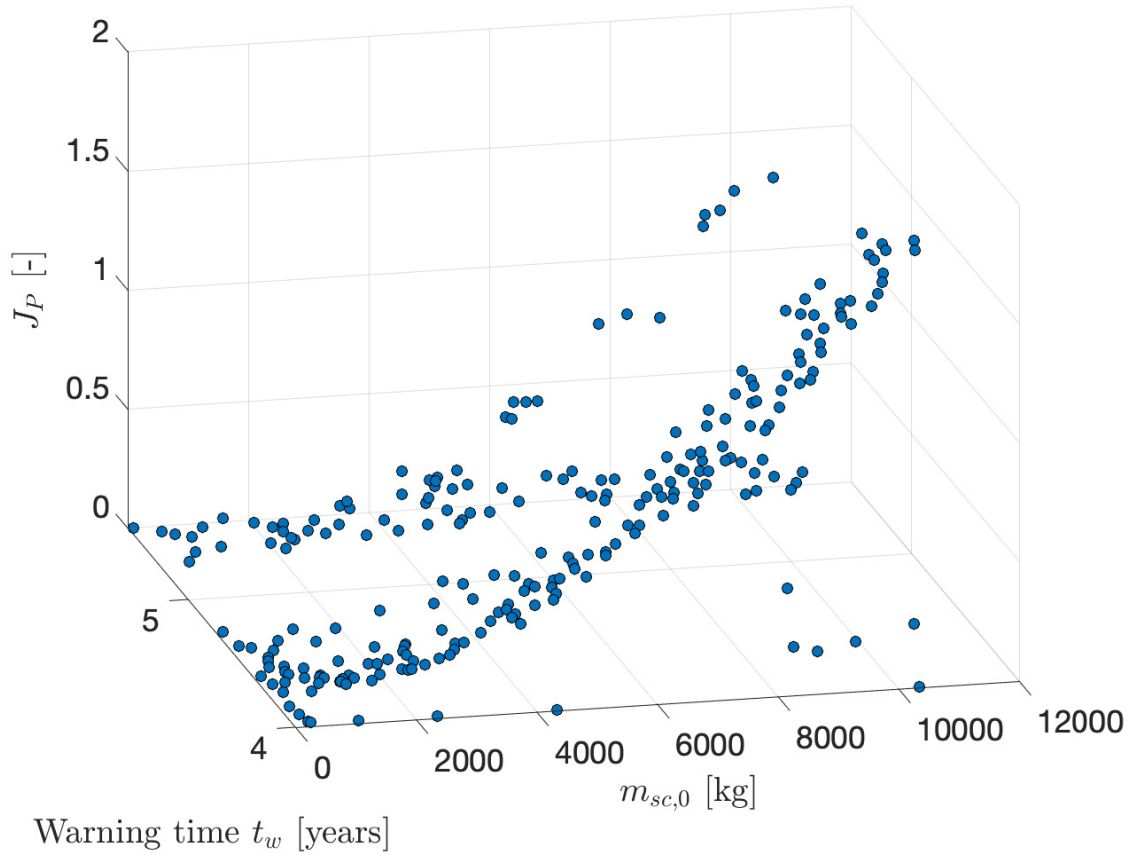

Figure 4.27: Laser Ablation Pareto front: J_P vs t_w vs $m_{sc,0}$ (second case)

In fig. 4.27 the 3D Pareto front obtained through the minimization of $J = [-J_P \; m_{sc,0} \; t_w]$ is reported.

Launch date	2032-06-29
Initial spacecraft mass $m_{sc,0}$ $[kg]$	10830
Warning time $[years]$	4.32
Probability functional J_P	1.7

Table 4.22: Kinetic Impactor second case: Minimum collision probability

In this case the value of J_P obtained is of the same order of magnitude of the nuclear explosion.
Both strategies are able to deflect the asteroid, so as a consequence the probability of collision is very low.

5 | Conclusions

In the second chapter a huge variety of asteroid deflection strategies have been presented. Four of this strategies have been optimised in order to deflect the target asteroid 2023 PDC, proposed by NASA in the Planetary Defence Conference.
Since uncertainties are still present in Epoch 3, three different asteroid masses and dimensions are considered. Unfortunately not all the strategies can be used for all the different cases.
In table 5.1 there is a summary of which strategies can be used for each case. The red cells indicate that the strategy is not able to provide the complete deflection of the asteroid.
In the case of the KI strategy the deflection is westward because the velocity of the asteroid increases, so the required deviation is 23000 km, while for the Gravity Tractor 9500 km are enough since the deflection is eastward.

	Deviation obtained $[km]$		
Strategy	**First case**	**Second case**	**Third case**
Kinetic Impactor	3304.3	370.9	19.6
Multiple Kinetic Impactor (7 s/c)	29301	Not possible	Not possible
Nuclear Standoff Explosion	1074158	129340	24639
Gravity Tractor	169.2	34.1	Not possible
Multiple Gravity Tractor (8 s/c)	9652.7	Not possible	Not possible
Laser Ablation	1544862	51671	1397.4

Table 5.1: Final comparison

The Kinetic Impactor cannot be used, but a MKI configuration with 7 launches is useful for the full dflection in the first case. Instead, Nuclear Standoff Explosion can be used in all the three cases.
The Gravity Tractor strategy, consisting in one single spacecraft hovering above the asteroid, is not useful since the mass is too high.
However a Multiple Gravity Tractor has been proposed. It consists in eight satellites disposed in two Halo orbits. The strategy can be used to deflect the asteroid in the first case.

Anyway further studies have to be performed, in particular on the multiple simultaneous launches.
The Laser Ablation strategy is able to deflect the asteroid in the first two cases, but when the mass of the asteroid is very high (10^{12} kg) the mass of propellant needed for the hovering becomes too high and the technology is no more useful. Also in this case further considerations must be carried on, especially on the generation of the laser input power.

The work is limited by the information available at this Epoch and can be improved once further data are provided by the reconnaissance missions, in particular from the rendezvous mission, on the asteroid size, mass and composition becomes fundamental in order to fully characterise the asteroid properties and then choose the best strategy. In addition the mathematical models of the strategies can be further improved in order to obtain more precise results.

Bibliography

[1] T. J. Ahrens and J. D. O'Keefe. Shock melting and vaporization of lunar rocks and minerals. *Moon*, 4(1-2):214–249, Apr. 1972. doi: 10.1007/BF00562927.

[2] N. Anthony and M. R. Emami. Asteroid engineering: The state-of-the-art of Near-Earth Asteroids science and technology, 6 2018. ISSN 03760421.

[3] B. W. Barbee, P. A. Abell, R. P. Binzel, and D. Mazanek. Future Spacecraft Missions for Planetary Defense Preparation, 2021.

[4] W. Baumjohann and R. A. Treumann. *Basic space plasma physics (revised edition)*. Imperial College Press, 3 2012. ISBN 9781848168961. doi: 10.1142/P850.

[5] M. C. Bazzocchi and M. R. Emami. Comparative analysis of redirection methods for asteroid resource exploitation. *Acta Astronautica*, 120:1–19, 3 2016. ISSN 00945765. doi: 10.1016/j.actaastro.2015.11.021.

[6] R. P. Binzel. Small Main-Belt Asteroid Spectroscopic Survey, 2010. URL `http://smass.mit.edu/smass.html`.

[7] L. Bolsi. Optimal deflection of near-earth objects through a kinetic impactor performing gravity assist. *Master thesis, Politecnico di Milano, Aerospace Engineering Department, Supervisor: C. Colombo*, 2018.

[8] I. Bolzoni. Multiple kinetic impactor for deflection of potentially hazardous asteroids. *Master thesis, Politecnico di Milano, Aerospace Engineering Department, Supervisor: C. Colombo*, 2021.

[9] C. Bombardelli and J. Peláez. Ion beam shepherd for asteroid deflection. *Journal of Guidance, Control, and Dynamics*, 34:1270–1272, 2011. ISSN 15333884. doi: 10.2514/1.51640.

[10] C. Bombardelli, H. Urrutxua, M. Merino, J. Peláez, and E. Ahedo. The ion beam shepherd: A new concept for asteroid deflection. *Acta Astronautica*, 90:98–102, 2013. ISSN 00945765. doi: 10.1016/j.actaastro.2012.10.019.

[11] W. F. Bottke, D. Vokrouhlický, D. P. Rubincam, and D. Nesvorný. THE YARKOVSKY AND YORP EFFECTS: Implications for Asteroid Dynamics. *Annual Review of Earth and Planetary Sciences*, 34(1):157–191, 2006. doi: 10.1146/annurev.earth.34.031405.125154.

[12] W. Brown. A novel push-pull asteroid magnetic Tractor(MT). *Acta Astronautica*, 156:371–374, 3 2019. ISSN 00945765. doi: 10.1016/j.actaastro.2017.12.020.

[13] S. Bus, F. Vilas, and M. Barucci. Visible-Wavelength Spectroscopy of Asteroids. *Asteroids III*, 3, 01 2002.

[14] M. Carpino, A. Milani, and S. Chesley. Error statistics of asteroid optical astrometric observations. *Icarus*, 166:248–270, 12 2003. doi: 10.1016/S0019-1035(03)00051-4.

[15] A. F. Cheng, H. F. Agrusa, B. W. Barbee, A. J. Meyer, T. L. Farnham, S. D. Raducan, D. C. Richardson, E. Dotto, A. Zinzi, V. D. Corte, T. S. Statler, S. Chesley, S. P. Naidu, M. Hirabayashi, J. Y. Li, S. Eggl, O. S. Barnouin, N. L. Chabot, S. Chocron, G. S. Collins, R. T. Daly, T. M. Davison, M. E. DeCoster, C. M. Ernst, F. Ferrari, D. M. Graninger, S. A. Jacobson, M. Jutzi, K. M. Kumamoto, R. Luther, J. R. Lyzhoft, P. Michel, N. Murdoch, R. Nakano, E. Palmer, A. S. Rivkin, D. J. Scheeres, A. M. Stickle, J. M. Sunshine, J. M. Trigo-Rodriguez, J. B. Vincent, J. D. Walker, K. Wünnemann, Y. Zhang, M. Amoroso, I. Bertini, J. R. Brucato, A. Capannolo, G. Cremonese, M. Dall'Ora, P. J. Deshapriya, I. Gai, P. H. Hasselmann, S. Ieva, G. Impresario, S. L. Ivanovski, M. Lavagna, A. Lucchetti, E. M. Epifani, D. Modenini, M. Pajola, P. Palumbo, D. Perna, S. Pirrotta, G. Poggiali, A. Rossi, P. Tortora, M. Zannoni, and G. Zanotti. Momentum transfer from the DART mission kinetic impact on asteroid Dimorphos. *Nature*, 616:457–460, 4 2023. ISSN 14764687. doi: 10.1038/s41586-023-05878-z.

[16] L. Chignoli. Multi-kinetic impactor for asteroid deflection with impact cratering physics uncertainties. *Master thesis, Politecnico di Milano, Aerospace Engineering Department, Supervisor: C. Colombo*, 2019.

[17] C. Colombo. *Optimal trajectory design for interception and deflection of Near Earth Objects*. PhD thesis, University of Glasgow, 2010.

[18] C. Colombo, M. Vasile, and G. Radice. Semi-analytical solution for the optimal low-thrust deflection of near-earth objects. *Journal of Guidance, Control, and Dynamics*, 32:796–809, 2009. ISSN 15333884. doi: 10.2514/1.40363.

[19] C. Colombo, M. Castronuovo, and et al. First SMPAG hypothetical NEO threat exercise Splinter 1. *Space Mission Planning Advisory Group, issue1.0*, 2023.

[20] G. Consolati. The Solar system. *Politecnico di Milano*, 2022.

[21] J. P. S. Cuartielles, C. Colombo, M. Vasile, and G. Radice. A multi-criteria assessment of deflection methods for dangerous NEOs. volume 886, pages 317–336, 2007. ISBN 0735403899. doi: 10.1063/1.2710065.

[22] J. Farquhar and D. Rumble. Comparison of oxygen isotope data obtained by laser fluorination of olivine with KrF excimer laser and CO2 laser, journal = Geochimica et Cosmochimica Acta. 62(18):3141–3149, 1998. ISSN 0016-7037. doi: https://doi.org/10.1016/S0016-7037(98)00219-1. URL `https://www.sciencedirect.com/science/article/pii/S0016703798002191`.

[23] D. B. French and A. P. Mazzoleni. Asteroid diversion using a long tether and ballast. *Journal of Spacecraft and Rockets*, 46:645–661, 2009. ISSN 15336794. doi: 10.2514/1.40828.

[24] D. B. French and A. P. Mazzoleni. Modeling tether-ballast asteroid diversion systems, including tether mass and elasticity. *Acta Astronautica*, 103:282–306, 2014. ISSN 00945765. doi: 10.1016/j.actaastro.2014.04.014.

[25] F. Gargioli. Analysis of uncertainties on multiple kinetic impactor asteroid deflection missions. *Master thesis, Politecnico di Milano, Aerospace Engineering Department, Supervisor: Juan Luis Gonzalo Gomez, Co-supervisor: Camilla Colombo*, 2023.

[26] H. B. Garrett. Design guidelines for assessing and controlling spacecraft charging effects Ultra-reliability View project High energy particle detectors View project, 1985. URL `https://www.researchgate.net/publication/4711584`.

[27] A. Gibbings, J. M. Hopkins, D. Burns, and M. Vasile. On testing laser ablation processes for asteroid deflection. 2011. URL `https://api.semanticscholar.org/CorpusID:56313999`.

[28] A. Gibbings, M. Vasile, I. Watson, J.-M. Hopkins, and D. Burns. Experimental analysis of laser ablated plumes for asteroid deflection and exploitation. *Acta Astronautica*, 90(1):85–97, 2013. ISSN 0094-5765. doi: https://doi.org/10.1016/j.actaastro.2012.07.008. URL `https://www.sciencedirect.com/science/article/pii/S0094576512002718`. NEO Planetary Defense: From Threat to Action - Selected Papers from the 2011 IAA Planetary Defense Conference.

[29] A. Gibbings, M. Vasile, I. Watson, J. M. Hopkins, and D. Burns. Experimental analysis of laser ablated plumes for asteroid deflection and exploitation. *Acta Astronautica*, 90:85–97, 2013. ISSN 00945765. doi: 10.1016/j.actaastro.2012.07.008.

[30] A. L. Gibbings. *LASER ABLATION FOR THE DEFLECTION, EXPLORATION AND EXPLOITATION OF NEAR EARTH ASTEROIDS*. PhD thesis, University of Glasgow, School of Engineering, 2014.

[31] J. L. Gonzalo, C. Colombo, and P. D. Lizia. Analytical framework for space debris collision avoidance maneuver design. *Journal of Guidance, Control, and Dynamics*, 44:469–487, 2021. ISSN 15333884. doi: 10.2514/1.G005398.

[32] C. Gritzner, K. Dürfeld, J. Kasper, and S. Fasoulas. The asteroid and comet impact hazard: Risk assessment and mitigation options, 8 2006. ISSN 00281042.

[33] D. Groath, J. Basart, and B. Wie. Computational Estimation of the Yarkovsky Effect on Asteroid 101955 Bennu. 08 2014. ISBN 978-1-62410-308-7. doi: 10.2514/6.2014-4145.

[34] P. Hammerling and J. L. Remo. Neo interaction with nuclear radiation. *Acta Astronautica*, 36(6):337–346, 1995. ISSN 0094-5765. doi: https://doi.org/10.1016/0094-5765(95)00111-5. URL `https://www.sciencedirect.com/science/article/pii/0094576595001115`.

[35] W. Heard. Dispersion of ensembles of non-interacting particles. *Astrophysics and Space Science*, 43:63–82, 1976. doi: 10.1007/BF00640556.

[36] D. Hestroffer. Small Solar System Bodies as granular media, 12 2019. ISSN 09354956.

[37] T. Hoerth, F. Schäfer, J. Hupfer, O. Millon, and M. Wickert. Momentum transfer in hypervelocity impact experiments on rock targets. volume 103, pages 197–204. Elsevier Ltd, 2015. doi: 10.1016/j.proeng.2015.04.027.

[38] K. A. Holsapple. Catastrophic Disruptions and Cratering of Solar System Bodies: A Review and New Results. *Planetary and Space Science*, 42:1067–1078., May 1994. doi: 10.1016/0032-0633(94)90007-8.

[39] K. R. Housen and K. A. Holsapple. On the Fragmentation of Asteroids and Planetary Satellites. *Icarus*, 84:226–253, 1990. doi: 10.1016/0019-1035(90)90168-9.

[40] J. Hubbell and S. Seltzer. X-Ray Mass Attenuation Coefficients. 2009. doi: https://dx.doi.org/10.18434/T4D01F.

[41] IAU. Minor Planet Center. URL `https://minorplanetcenter.net`.

[42] H. K.A. The Scaling of Impact Processes in Planetary Science. *Annual Review of Earth and Planetary Science*, 21:333–373, May 1993.

[43] R. Kahle, E. Kührt, G. Hahn, and J. Knollenberg. Physical limits of solar collectors in deflecting Earth-threatening asteroids. *Aerospace Science and Technology*, 10(3):256–263, 2006. ISSN 1270-9638. doi: https://doi.org/10.1016/j.ast.2005.12.004. URL `https://www.sciencedirect.com/science/article/pii/S1270963806000125`.

[44] R. Kahle, E. Kührt, G. Hahn, and J. Knollenberg. Physical limits of solar collectors in deflecting Earth-threatening asteroids. *Aerospace Science and Technology*, 10: 256–263, 4 2006. ISSN 12709638. doi: 10.1016/j.ast.2005.12.004.

[45] H. Karttunen and P. Kröger. *Fundamental Astronomy*. Springer Berlin Heidelberg, 2017. doi: 10.1007/978-3-662-53045-0.

[46] M. Lavagna. Electric power subsystem. Politecnico di Milano, Space System Engineering and Operations course, 2022.

[47] E. T. Lu and S. G. Love. Gravitational tractor for towing asteroids. *Nature*, 438, 2005. doi: 10.1038/438177a.

[48] F. Maggi. Electric Propulsion. Politecnico di Milano, Space Propulsion course, 2022.

[49] F. Maggi. LRE-Technology. Politecnico di Milano, Space Propulsion course, 2022.

[50] M. J. Mashayekhi and A. K. Misra. Tether assisted near earth object diversion. *Acta Astronautica*, 75:71–77, 6 2012. ISSN 00945765. doi: 10.1016/j.actaastro.2011.12.018.

[51] D. Mazanek. Near-Earth Asteroid Deflection Strategies Asteroid Grand Challenge: Virtual Seminar Series, 2014.

[52] D. D. Mazanek, D. M. Reeves, J. B. Hopkins, D. W. Wade, M. Tantardini, and H. Shen. Enhanced gravity tractor technique for planetary defense, 2015.

[53] C. R. McInnes. Near Earth object orbit modification using gravitational coupling. *Journal of Guidance, Control, and Dynamics*, 30:870–873, 2007. ISSN 15333884. doi: 10.2514/1.25864.

[54] J. Melosh, I. Nemchinov, and Y. Zetzer. Non-nuclear strategies for deflecting comets and asteroids. -1:1111–1132, 01 1994.

[55] S. Meshcheryakov and Y. M. Lipnitskii. Estimated efficiency of the deflection of a dangerous space object using an explosion or impact. *Technical Physics*, 60(1):26 – 30, 2015. doi: 10.1134/S1063784215010181.

[56] S. A. Meshcheryakov and Y. M. Lipnitskii. Estimated efficiency of the deflection of a dangerous space object using an explosion or impact. *Technical Physics*, 60: 26–30, 2015. ISSN 10637842. doi: 10.1134/S1063784215010181.

[57] H. M. Mott-Smith and I. Langmuir. The Theory of Collectors in Gaseous Discharges. *Phys. Rev.*, 28:727–763, Oct 1926. doi: 10.1103/PhysRev.28.727. URL `https://link.aps.org/doi/10.1103/PhysRev.28.727`.

[58] N. Murdoch, D. Izzo, C. Bombardelli, I. Carnelli, A. Hilgers, and D. Rodgers. Electrostatic tractor for near Earth object deflection, 2008.

[59] H. Nagahara, I. Kushiro, and B. O. Mysen. Evaporation of olivine: Low pressure phase relations of the olivine system and its implication for the origin of chondritic components in the solar nebula. *Geochimica et Cosmochimica Acta*, 58(8):1951–1963, 1994. ISSN 0016-7037. doi: https://doi.org/10.1016/0016-7037(94)90426-X. URL `https://www.sciencedirect.com/science/article/pii/001670379490426X`.

[60] NASA. JPL Horizons System, . URL `https://ssd.jpl.nasa.gov/horizons/app.html#/`.

[61] NASA, . URL `https://www.nasa.gov`.

[62] NASA, . URL `https://solarsystem.nasa.gov`.

[63] NASA. JPL NEO Deflection App, . URL `https://cneos.jpl.nasa.gov/nda/`.

[64] NASA. Near-Earth Object Survey and Deflection Study Final Report, 2006. URL `www.nasa.gov`.

[65] NASA. Dawn Launch Mission to Vesta and Ceres, 2007. URL `https://www.jpl.nasa.gov/news/press_kits/dawn-launch.pdf`.

[66] NASA. NASA's Evolutionary Xenon Thruster-Commercial (NEXT-C), 2017. URL `www.nasa.gov`.

[67] NASA. JPL Horizons System, 2023. URL `https://ssd.jpl.nasa.gov/horizons/app.html#/`.

[68] NASA. Asteroid 2023 PDC Exercise, 2023. URL `https://iaaspace.org/event/8th-iaa-planetary-defense-conference-2023/`.

[69] NASA. NASA Launch Services Program: Launch Vehicle Performance Website, 2023. URL `https://elvperf.ksc.nasa.gov/Pages/Default.aspx`.

[70] NASA. Near-Earth Object Survey and Deflection Analysis of Alternatives Report to Congress, March, 2007.

[71] P. Ngatchou, A. Zarei, and A. El-Sharkawi. Pareto Multi Objective Optimization. pages 84–91, 2005. doi: 10.1109/ISAP.2005.1599245.

[72] J. R. Olds, A. C. Charania, and M. G. Schaffer. Multiple Mass Drivers as an Option for Asteroid Deflection Missions, 2007.

[73] J. R. Olds, A. Charania, M. Graham, and J. G. Wallace. The League of Extraordinary Machines: A Rapid and Scalable Approach to Planetary Defense Against Asteroid Impactors. *Version 1.0, Phase I Final Report, Call for Proposals CP-02-02*, April 30, 2004.

[74] J. Opiela, C. Ostrom, and J. Marichalar. Debris Assessment Software (DAS) Reentry Risk Analysis: Mission Planning for Compliance with NASA Standards. pages 6–9, 08 2017. URL `https://www.researchgate.net/publication/320808841`.

[75] L. W. Parker and J. Lambroise. Theory of cylindrical and spherical Langmuir probes in the limit of vanishing Debye number. *Phys. Fluids.*, 25:2388–2400, 1982.

[76] M. Peck. *Prospects and Challenges for Lorentz-Augmented Orbits*. doi: 10.2514/6.2005-5995. URL `https://arc.aiaa.org/doi/abs/10.2514/6.2005-5995`.

[77] M. Petit and C. Colombo. Optimal deflection of resonant near-earth objects using the b-plane. *Politecnico di Milano*, 2018.

[78] A. E. Petropoulos and J. M. Longuski. Shape-based algorithm for the automated design of low-thrust, gravity assist trajectories. *Journal of Spacecraft and Rockets*, 41(5):787–796, 2004. doi: 10.2514/1.13095. URL `https://doi.org/10.2514/1.13095`.

[79] A. Pitz, B. Kaplinger, B. Wie, and D. Dearborn. Aas 12-225 preliminary design of a hypervelocity nuclear interceptor system (hnis) for optimal disruption of near-earth objects, 2012.

[80] M. E. Ricotti. Reactor phyisics element. *Politecnico di Milano, course of Introduction to Nuclear Engineering*, 2022.

[81] A. S. Rivkin, N. L. Chabot, A. M. Stickle, C. A. Thomas, D. C. Richardson, O. Barnouin, E. G. Fahnestock, C. M. Ernst, A. F. Cheng, S. Chesley, S. Naidu, T. S. Statler, B. Barbee, H. Agrusa, N. Moskovitz, R. T. Daly, P. Pravec, P. Scheirich, E. Dotto, V. D. Corte, P. Michel, M. Küppers, J. Atchison, and M. Hirabayashi.

The double asteroid redirection test (DART): Planetary defense investigations and requirements. *Planetary Science Journal*, 2, 10 2021. ISSN 26323338. doi: 10.3847/PSJ/ac063e.

[82] J. Roa, A. E. Petropoulos, and P. W. Chodas. Characterization and deflection missions of the fictitious asteroid 2019 PDC, 2019. URL `https://cneos.jpl.nasa.gov/pd/cs/pdc19/`.

[83] E. Ryan and H. Melosh. Impact fragmentation: from the laboratory to asteroids. *Icarus*, 133:1–24, April, 1998. ISSN 0019-1035. doi: https://doi.org/10.1006/icar.1998.5915.

[84] J. P. Sanchez, C. Colombo, M. Vasile, and G. Radice. Multicriteria comparison among several mitigation strategies for dangerous near-Earth objects. *Journal of Guidance, Control, and Dynamics*, 32:121–142, 2009. ISSN 15333884. doi: 10.2514/1.36774.

[85] D. J. Scheeres and R. L. Schweickart. The mechanics of moving asteroids. pages 382–390. American Institute of Aeronautics and Astronautics Inc., 2004. ISBN 1563477114. doi: 10.2514/6.2004-1446.

[86] R. Schweickart, E. Lu, P. Hut, and C. Chapman. The Asteroid Tugboat. *Scientific American - SCI AMER*, 289:54–61, 11 2003. doi: 10.1038/scientificamerican1103-54.

[87] J. N. Spitale. Asteroid hazard mitigation using the Yarkovsky effect. *Science*, 296:77, 4 2002. ISSN 00368075. doi: 10.1126/science.1069577.

[88] E. Stuhlinger. *Ion Propulsion for Space Flight*. McGraw–Hill New York, 1964.

[89] F. Stäger, D. Zok, A.-K. Schiller, B. Feng, and G. Steinhauser. Disproportionately High Contributions of 60 Year Old Weapons - Caesium-137 Explain the Persistence of Radioactive Contamination in Bavarian Wild Boars. *Environmental Science Technology*, 8 2023. ISSN 0013-936X. doi: 10.1021/acs.est.3c03565. URL `https://pubs.acs.org/doi/10.1021/acs.est.3c03565`.

[90] J.-P. Sánchez and M. Vasile. On the consequences of a fragmentation due to a NEO mitigation strategy Stardust View project Aerospace Centre of Excellence View project, 2008. URL `http://strathprints.strath.ac.uk/`.

[91] E. Taheri and O. Abdelkhalik. Shape-based approximation of constrained low-thrust space trajectories using fourier series. *Journal of Spacecraft and Rockets*, 49:535–545, 05 2012. doi: 10.2514/1.58789.

[92] N. Thiry and M. Vasile. Statistical multi-criteria evaluation of non-nuclear asteroid deflection methods. *Acta Astronautica*, 140:293–307, 11 2017. ISSN 00945765. doi: 10.1016/j.actaastro.2017.08.021.

[93] N. Thiry, M. Vasile, and E. Monchieri. Mission and system design for the manipulation of phos with space-borne lasers. In *2016 IEEE Aerospace Conference*, pages 1–13, 2016. doi: 10.1109/AERO.2016.7500610.

[94] B. Thiébault, A. Hilgers, E. Sasot, H. Laakso, P. Escoubet, V. Génot, and J. Forest. Potential barrier in the electrostatic sheath around a magnetospheric spacecraft. *Journal of Geophysical Research: Space Physics*, 109, 2004. ISSN 21699402. doi: 10.1029/2004JA010398.

[95] E. A. Thomson. Revised asteroid scale aids understanding of impact risk, 2005. URL `https://news.mit.edu/2005/torino`.

[96] M. Vasile and C. Colombo. Optimal impact strategies for asteroid deflection. *Journal of Guidance, Control, and Dynamics*, 31, 04 2011. doi: 10.2514/1.33432.

[97] M. Vasile and C. Maddock. Design of a Formation of Solar Pumped Lasers for Asteroid Deflection. 6 2012. doi: 10.1016/j.asr.2012.06.001. URL `http://arxiv.org/abs/1206.1336http://dx.doi.org/10.1016/j.asr.2012.06.001`.

[98] M. Vasile and N. Thiry. Nuclear cycler: An incremental approach to the deflection of asteroids. *Advances in Space Research*, 57:1805–1819, 4 2016. ISSN 18791948. doi: 10.1016/j.asr.2015.11.036.

[99] M. Vasile, A. Gibbings, I. Watson, and J. M. Hopkins. Improved laser ablation model for asteroid deflection. *Acta Astronautica*, 103:382–394, 2014. ISSN 00945765. doi: 10.1016/j.actaastro.2014.01.033.

[100] D. Vokrouhlick´yvokrouhlick´y. Diurnal Yarkovsky effect as a source of mobility of meter-sized asteroidal fragments I. Linear theory, 1998.

[101] D. Vokrouhlický, W. F. Bottke, S. R. Chesley, D. J. Scheeres, and T. S. Statler. *The Yarkovsky and YORP effects*, pages 509–531. University of Arizona Press, 1 2015. ISBN 9780816532186. doi: 10.2458/azu_uapress_9780816532131-ch027.

[102] R. Walker, D. Izzo, C. de Negueruela, L. Summerer, M. Ayre, and M. Vasile. Concepts for Near-Earth Asteroid Deflection using Spacecraft with Advanced Nuclear and Solar Electric Propulsion Systems. *Journal of the British Interplanetary Society*, 58:268–278, Jan. 2005.

[103] B. Wall. Shape-based approximation method for low-thrust trajectory optimization. 08 2008. ISBN 978-1-62410-001-7. doi: 10.2514/6.2008-6616.

[104] B. Wall, B. Pols, and B. Lanktree. Shape-based approximation method for lowthrust interception and rendezvous trajectory design. *Advances in the Astronautical Sciences*, 136:1447–1458, 01 2010.

[105] J. R. Wertz, W. J. Larson, D. Kirkpatrick, and D. Klungle. *Space mission analysis and design*. Microcosm, 1999. ISBN 9781881883104.

[106] J. R. Wertz, W. J. Larson, D. Kirkpatrick, and D. Klungle. *Space mission analysis and design*. Microcosm, 1999. ISBN 1881883108.

[107] B. Wie. Dynamics and control of gravity tractor spacecraft for asteroid deflection. *Journal of Guidance Control and Dynamics*, 31:1413–1423, 08 2008. doi: 10.2514/1.32735.

[108] B. Wie. Hypervelocity nuclear interceptors for asteroid disruption. *Acta Astronautica*, 90:146–155, 2013. ISSN 00945765. doi: 10.1016/j.actaastro.2012.04.028.

[109] B. Wie, B. Zimmerman, P. Premaratne, J. Lyzhoft, and G. Vardaxis. Aas 15-567 a new non-nuclear mkiv (multiple kinetic-energy impactor vehicle) mission concept for dispersively pulverizing small asteroids.

[110] K. Yamaguchi and H. Yamakawa. Topics Orbital Deflection of Potentially Hazardous Asteroids Using a Coulomb Force Attractor, 2014.

[111] G. Youtao, F. Yuhai, X. Bo, and W. Ying. Effectiveness analysis of multiple kinetic impacts of near-Earth asteroids. *Advances in Space Research*, 69:2883–2892, 4 2022. ISSN 18791948. doi: 10.1016/j.asr.2022.01.021.

[112] K. Zeng, Y. Geng, and B. Wu. Shape-based analytic safe trajectory design for spacecraft equipped with low-thrust engines. *Aerospace Science and Technology*, 62: 87–97, 2017. ISSN 1270-9638. doi: https://doi.org/10.1016/j.ast.2016.12.006. URL `https://www.sciencedirect.com/science/article/pii/S1270963816308215`.

A | Validation of the results

A.1. Nuclear standoff explosion

The results of the model described in section 2.2.2 are validated through a comparison with the ones obtained by Sanchez in [84]. Here it is considered a fusion device of 600 kg and an initial mass of the spacecraft equal to 2000 kg with the asteroid Apophis as a target.

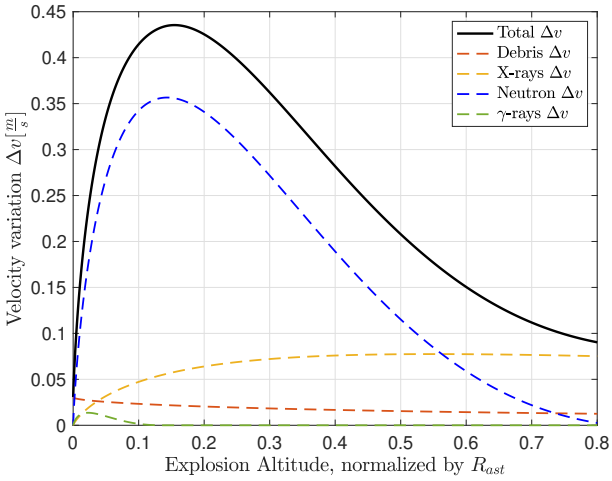

Figure A.1: Deviation obtained with the nuclear standoff explosion varying the altitude of detonation

A.1.1. Opacity and mass-absorption coefficients

The mass attenuation coefficient depends on the total cross section (σ_{TOT}) per atom. The cross section has physically the dimension of an area [m^2], but in reality it represents the probability of having a determined interaction between the atom and another material. In fact it can be computed as the sum of the atomic photoeffect cross section (so the probability that a photoelectric effect can happen) σ_{pe}, the scattering cross section σ_{sc}, and other cross sections relative to electron-positron production and photonuclear effect

[40]. So:

$$\frac{\mu_0}{\rho} = \frac{\sigma_{TOT}}{uA} \tag{A.1}$$

$$\sigma_{TOT} = \sigma_{pe} + \sigma_{scattering} + \sigma_{pair} + \sigma_{pn} \tag{A.2}$$

Where $u = 1.660 \cdot 10^{-24}$ g is the atomic mass unit and A is the atomic mass of the element. The dependence on the cross section explains why the X-rays have an higher opacity than neutrons, because they have an higher cross section with respect to neutrons and γ-rays, and this means an higher probability of interactions, so a lower probability of penetrating inside the matter [34].
In this way the values of μ_0 are computed and tabulated, but for composite material a weighted sum has to be considered according to the atomic percent in the molecule:

$$< \mu_0 >= \sum_i \alpha_i \mu_{0,i} \tag{A.3}$$

This last procedure is valid also for the mass absorption coefficient. This one is computed passing through the energy-transfer coefficient μ_{tr}, which is defined considering, in addition to the cross sections, the average fractions f of the photon energy E that is transferred into kinetic energy of charged particles.

$$\frac{\mu_{tr}}{\rho} = \frac{f_{pe}\sigma_{pe} + f_{inc,scatt}\sigma_{inc,scatt} + f_{pair}\sigma_{pair}}{\mu A} \tag{A.4}$$

As in the previous case if a molecule is considered a weighted sum has to be performed to compute the total energy-transfer coefficients. Then the mass-absorption coefficient is computed as:

$$\frac{\mu_{en}}{\rho_{ast}} = (1 - g)\frac{\mu_{tr}}{\rho_{ast}} \tag{A.5}$$

Where g is is the average fraction of the kinetic energy of secondary charged particles that is lost in radiative energy-loss processes: the computation of g is quite complex and is not reported here for simplicity.

A.2. Gravity Tractor and Tugboat

The validation of the GT and tugboat models proposed in this thesis is done comparing the results with the work of Sanchez, Colombo and Vasile [84]. In fig. A.2 the total impulse obtained with the two strategies varying the deviation action duration is reported, considering the asteroid Apophis as a target and the same initial data of [84].

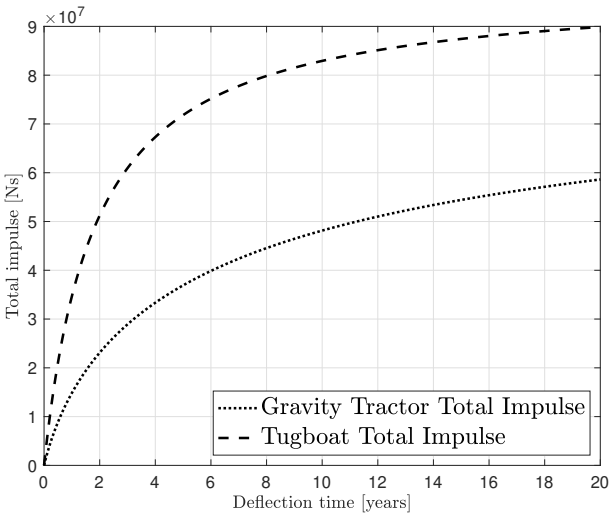

Figure A.2: Total impulse obtained with GT and AT strategies varying the deviation action time

Concerning the halo gravity tractor, in the graph in fig. A.3 the same result explained by Vasile in [98] has been obtained. The standard GT provides higher deviation in a shorter amount of time with respect to the Halo configuration.

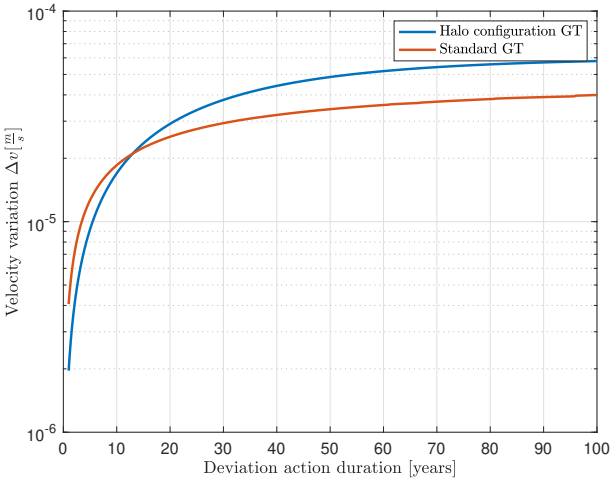

Figure A.3: Δv obtained with Halo configuration and standard GT

A.3. Magnetic Tractor

Using the data in [12] it is possible to compute the magnetic force. So the spacecraft magnet has a radius of 0.5 m with $B = 20\ T$, the magnets on the asteroid have dimensions $R = 1.27\ cm$ and $L = 2.54\ cm$ with $B = 1.4\ T$. The N magnets are distributed uniformly in a square of 3 m. In order to simplify the calculations here it is assumed that all the

magnets are at a distance of half the length of the square (so 1.5 m). With this data the values obtained are shown in fig. A.4a and can be compared with the results of Brown [12].

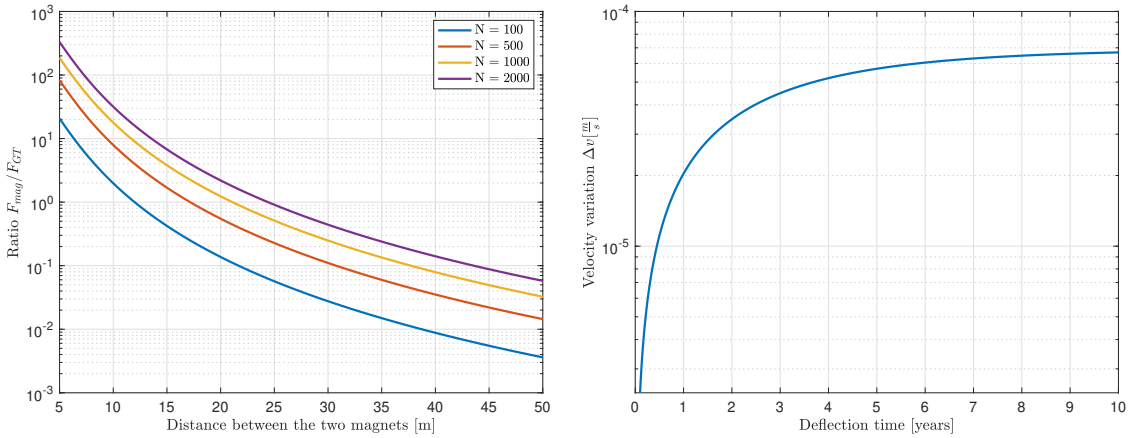

(a) Ratio between magnetic force and gravity force varying the hovering distance and the number of magnets

(b) Δv obtained with the Magnetic Tractor strategy, fixing N = 100, z = 100

Figure A.4: Results of the Magnetic Tractor model

A.4. Electrostatic Tractor

The validation of the model has been done through a comparison with the results obtained by Murdoch et Al. in [58]. Considering $m_{sc} = 500\ kg$, potential of the spacecraft equal to 20 kV and $\lambda = 7.4\ m$. So $q = 12.51\ \mu C$, the results are plotted in fig. A.5. The Δv is obtained multiplying the total force by the time of the deviating action and dividing by the asteroid mass (data taken from [58], $\rho_{ast} = 2000 kg/m^3$ and $r_{ast} = 100\ m$).

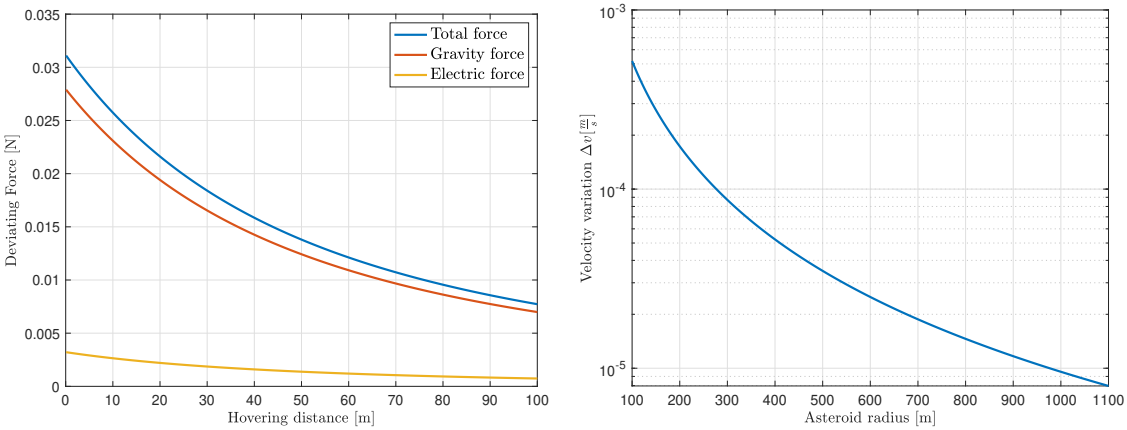

(a) Total, gravitational and electrostatic force varying the hovering distance

(b) Velocity variation obtained varying the asteroid radius (deflection time fixed to 10 years)

Figure A.5: Results of the Electrostatic Tractor model

It can be immediately noted that the electrostatic force is not as high as the gravitational one and this is even more evident as the asteroid diametre increases. In particular the deviation obtained decreases of two order of magnitude (fig. A.5) if the asteroid diametre increases from 100 m to 1100 m.

A.4.1. Details in the design of the electrostatic tractor

The power is $P = VI$, where V is the potential and I is the current, which can be obtained through the process explained in [57]. Considering a Maxwellian distribution of velocities the current density is given by:

$$J_0 = \frac{qn}{2}\left(\frac{2kT}{\pi m}\right)^{1/2} \tag{A.6}$$

Where k is the Boltzmann constant and n is the charge density. So the current produced can be expressed [57] [58] in two limiting cases, the first one happens when the space charge of the plasma (Debye length) is neglected (inferior limit I_{inf}), while the second one, which is the upper limit, takes place if we consider that the current is limited by the charges entering the sheath (I_{up}). So in the end the current is:

$$I_{inf} = 4\pi r^2 J_0\left(1 - \frac{qV}{kT}\right) < I < 4\pi r^2 J_0 = I_{up} \tag{A.7}$$

So the real value of current stays in this interval and can be obtained through the "turning point method" of [75] or using the software developed in [94].

There is the need of defining how to generate the high power needed to charge the asteroid. Three methods are proposed in [58], the first one is revised considering a different radioactive element:

- The use of a radioactive alpha emitter material: in this case the power generated is $P = p_{iso} M_{iso} \eta_{conv} = 2^{-t/t_{1/2}} M_{iso} \eta_{conv}$, where M is the mass of the isotope and $t_{1/2}$ is the half life time. The power decay in time because the number of radioisotopes decreases in time (depending on the half life time of the material). The choice of the radioactive material depends on what is needed, Polonium has low $t_{1/2}$ and so guarantees high specific power and can be used for short missions, while Plutonium has very high $t_{1/2}$ so with just a small mass it can be generated power for a long time.
- Another option is to land on the asteroid and place on the surface an electron or ion gun to directly generate charges. In this way a finer control is obtained.
- It is also possible to shoot charges from the spacecraft, in this case both the asteroid and the spacecraft will be charged.

A.5. Ion beam

The validation of the model proposed has been done comparing the results with the one obtained by Bombardelli et Al. in [10]. Here the density of the asteroid is set to 2000 kg/m^3, the deflection time and the hovering distance in fig. A.9b are set respectively to 2 years and $2R_{ast}$. The efficiency is considered equal to 0.7.

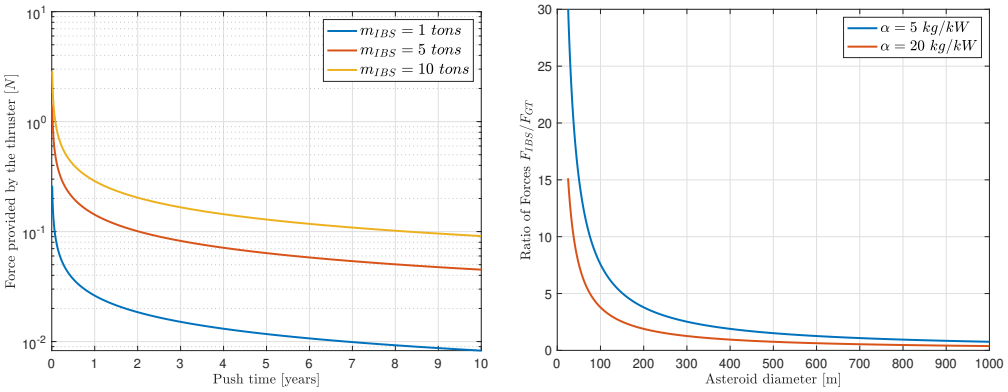

(a) Force provided by the ion thruster

(b) Comparison between IBS strategy and Gravity Tractor strategy

Figure A.6: Results of the Ion Thruster deflection strategy

The results are the same obtained in [10].

A.6. Mass driver

The model explained in this thesis for the mass driver strategy has been validated through a comparison with the results obtained by Olds in [72]. So the asteroid momentum change due to the mass ejection for two types of asteroid is shown in fig. A.7: one is rotating with a duty cycle of 15% and the other one is non rotating.

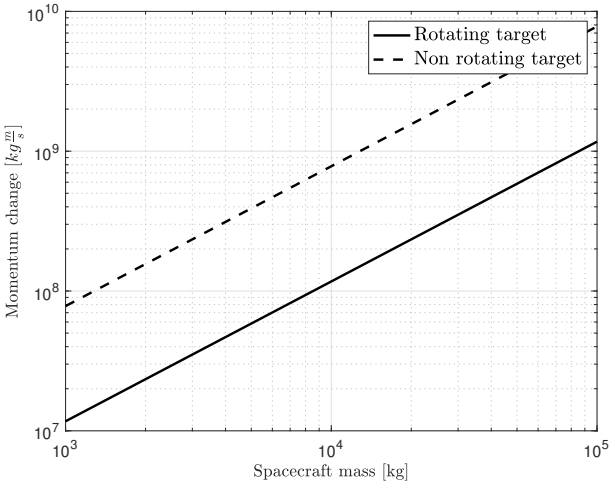

Figure A.7: Effective asteroid momentum change due to mass ejection

The results are the same explained by Olds.

A.7. Solar Collector

The results of the solar collector model presented before are validated with the one obtained by Sanchez, Vasile and Colombo in [84].

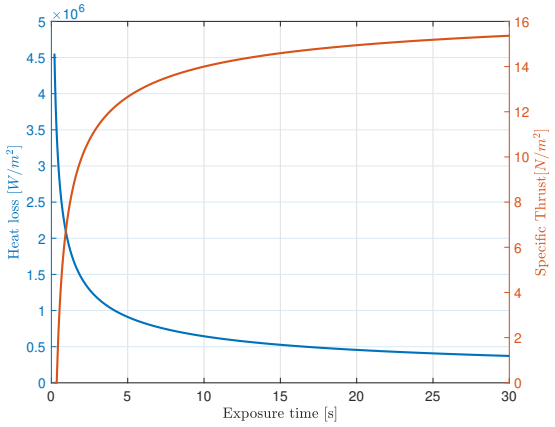

Figure A.8: Conductive heat loss and thrust varying the exposure time

In fig. A.8 the rotational velocity has been neglected in order to vary the exposure time of the illuminated zone. It can be seen that the conductive heat flux decreases in time, while the radiative heat flux is not reported because it is constant and equal to $8.6 \cdot 10^5\ W/m^2$.

A.8. Laser ablation

The Laser Ablation model is validated by comparing it with the results obtained by Gibbings, Vasile, Watson, Hopkins and Burns in [29] and the ones obtained by Vasile, Gibbings, Watson and Hopkins in [99].
Using the same initial data considered in [99], so asteroid mass $M_{ast} = 1.1 \cdot 10^9\ kg$, density $\rho_{ast} = 3500\ kg/m^3$ and one rotation per day, for a laser with power input of 8200 W and spot diametre of 1 mm shooting at a distance of $250m$ from the asteroid surface, the Δv obtained by Vasile is 0.025 m/s, while the results of the model proposed in this thesis is 0.0241 m/s.

The solution of the diffusion equation is validated through the comparison with the results obtained by Gibbings in [29]. The diffusion equation is the one used to compute the thickness of the deposited material, so:

$$\frac{dh}{dt} = \frac{\overline{v}\rho_{plume}(r,\theta)}{\rho_{layer}} cos(\psi_{vf}) \tag{A.8}$$

The results in fig. A.9a are obtained at a distance r equal to 3 *cm* from the spot.

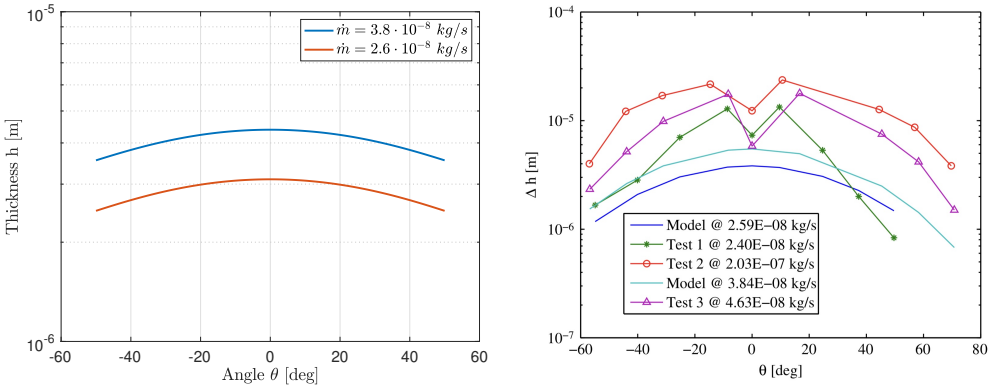

(a) Thickness of the deposited material, solution of the diffusion equation

(b) Thickness of the deposited material obtained by Gibbings [29] and comparison with experimental model

Figure A.9: Solution of the diffusion equation

A.9. Low thrust trajectory

The derivative of the position vector $\vec{r}$ is obtained by the direct integration of equation $\vec{r} = \phi_1\vec{r}_1 + \phi_2\vec{r}_2$, considering that both $\vec{r}_k$ and ϕ_k depends on θ.

$$\dot{\vec{r}} = \frac{d\vec{r}}{dt} = \frac{\partial\vec{r}}{d\theta}\frac{d\theta}{dt} = \left(\frac{\partial\phi_1}{\partial\theta}\vec{r}_1 + \phi_1\frac{\partial\vec{r}_1}{\partial\theta} + \frac{\partial\phi_2}{\partial\theta}\vec{r}_2 + \phi_2\frac{\partial\vec{r}_2}{\partial\theta}\right)\dot{\theta} \tag{A.9}$$

With:

$$\frac{\partial\vec{r_k}}{\partial\theta} = \frac{a_k(1-e_k^2)}{(1+e_k\cos f_k)^2}[-\sin f_k\vec{p}_k + (\cos f_k + e_k)\vec{q}_k] \tag{A.10}$$

While the derivative of eq. (A.9) is:

$$\begin{aligned}\ddot{\vec{r}} = \Bigg(&\frac{\partial^2\phi_1}{\partial\theta^2}\vec{r}_1 + 2\frac{\partial\phi_1}{\partial\theta}\frac{\partial\vec{r}_1}{\partial\theta} + \phi_1\frac{\partial^2\vec{r}_1}{\partial\theta^2} + \frac{\partial^2\phi_2}{\partial\theta^2}\vec{r}_2 + 2\frac{\partial\phi_2}{\partial\theta}\frac{\partial\vec{r}_2}{\partial\theta} + \\ &+\phi_2\frac{\partial^2\vec{r}_2}{\partial\theta^2}\dot{\theta}^2 + (\frac{\partial\phi_1}{\partial\theta}\vec{r}_1 + \phi_1\frac{\partial\vec{r}_1}{\partial\theta} + \frac{\partial\phi_2}{\partial\theta}\vec{r}_2 + \phi_2\frac{\partial\vec{r}_2}{\partial\theta})\ddot{\theta}\end{aligned} \tag{A.11}$$

Where:

$$\frac{\partial^2\vec{r}_k}{\partial\theta^2} = \frac{a_k(1-e_k^2)}{(1+e_k\cos f_k)^3}[-(\cos f_k + e_k + e_k\sin^2 f_k)\vec{p}_k + \sin f_k(2e_k^2 + e_k\cos f_k - 1)\vec{q}_k] \tag{A.12}$$

The second derivative of the true anomaly $\ddot{\theta}$ is instead computed differentiating the equation of $\dot{\theta}$ with respect to time:

$$\ddot{\theta} = \dot{\theta}\left(\frac{\partial\phi_1}{\partial\theta}h_1 + \frac{\partial\phi_2}{\partial\theta}h_2\right)\frac{1}{\|\vec{r}\times\frac{\partial\vec{r}}{\partial\theta}\|} - \frac{\phi_1 h_1 + \phi_2 h_2}{\|\vec{r}\times\frac{\partial\vec{r}}{\partial\theta}\|^2}\|\vec{r}\times\frac{\partial\vec{r}}{\partial\theta}\|^2\dot{\theta} \tag{A.13}$$

With the same initial data used in [112], shown in table A.1 the trajectory is shown in fig. A.10 and the results (with the comparison) can be seen in table A.2. The small discrepancy with the values obtained by Zeng can be due to the different numerical integration method used.

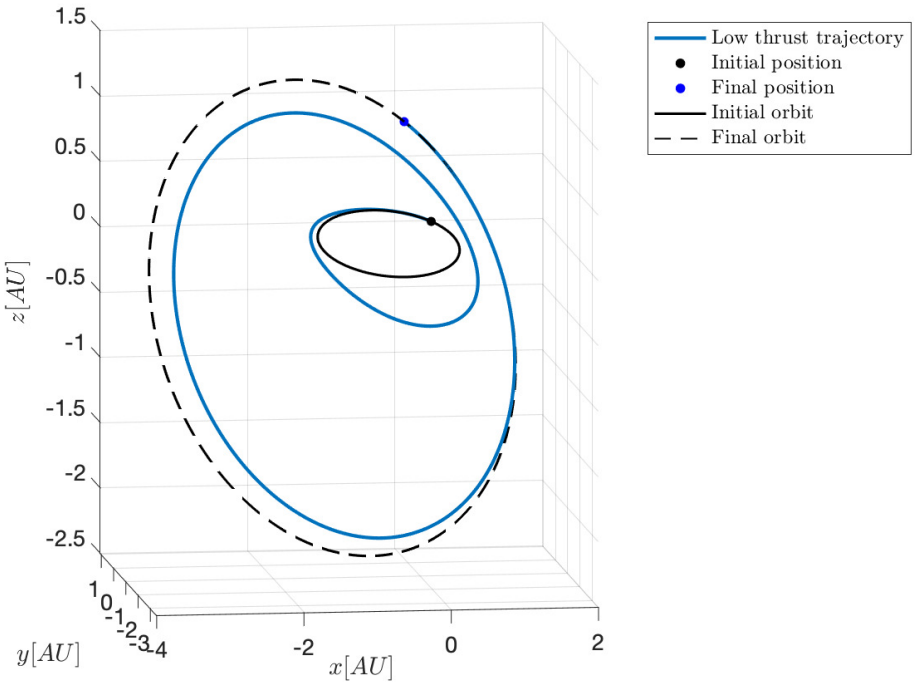

Figure A.10: Low thrust trajectory

Orbital elements	Initial Orbit	Target Orbit
Semi-major axis	1 *AU*	3 *AU*
Eccentricity	0.4	0.6
Inclination	10°	40°
Right ascension	15°	25°
Argument of periapsis	25°	25°
True anomaly	10°	40°

Table A.1: Initial and final data for low thrust trajectory

	Δv $[km/s]$	TOF $[years]$	$T_{a,max}$ $[km/s^2]$
Results	26.1656	6.1139	2.2929e-6
Results by Zeng	26.6130	6.1020	2.6550e-6

Table A.2: Results of low thrust model

A.10. Asteroid deviation problem

To validate the results, the model proposed in section 3.3 is applied to asteroid 2000SG344 and the values obtained are the same presented by Colombo in [96]. The velocity out of plane component is not showed because it is always lower than 10^{-14}.

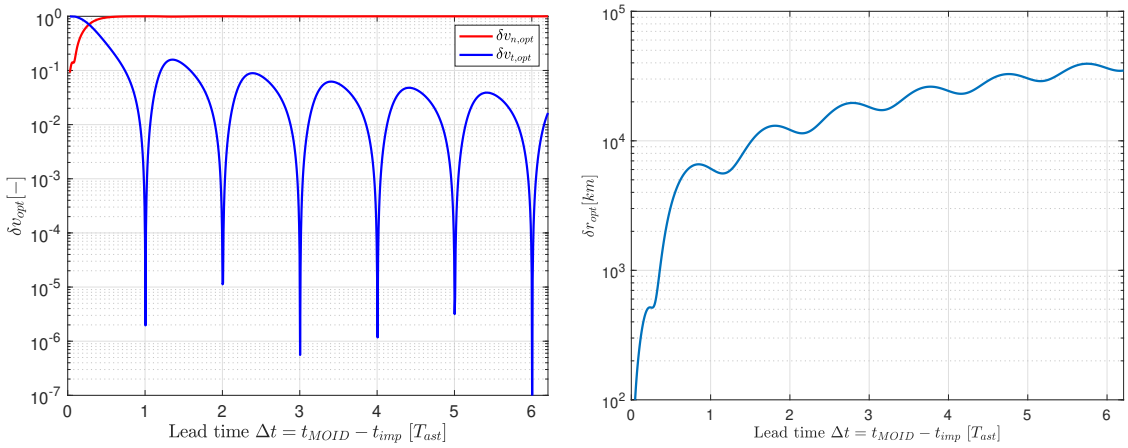

(a) (b)

Figure A.11: Maximum deviation for asteroid 2000SG344

A.11. Launcher c3

In this section the graphs relating the c3 energy with the mass that can be launched are shown. These plots are obtained through the Launch Vehicle Performance Website [69].

For the flyby early reconnaissance mission the c3 needed is 70 km^2/s^3, and the launchers which can guarantee this value are the ones in fig. A.12.

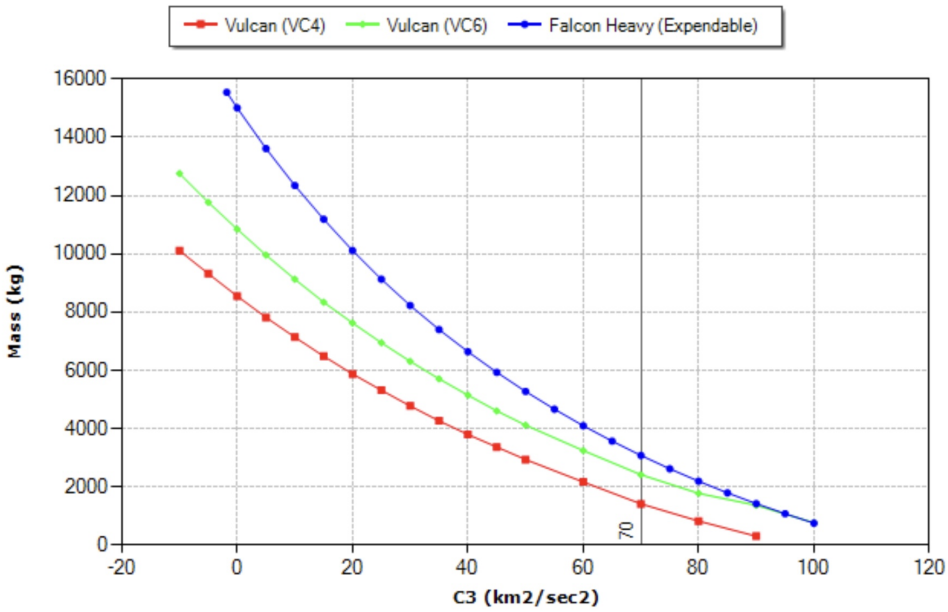

Figure A.12: c3 energy for flyby early reconnaissance mission

Instead for the KI mission the c3 needed is 21 km/s, and the launcher proposed by NASA is the Falcon Heavy, which, as can be seen in fig. A.13, is able to launch about 6900 kg of payload mass.

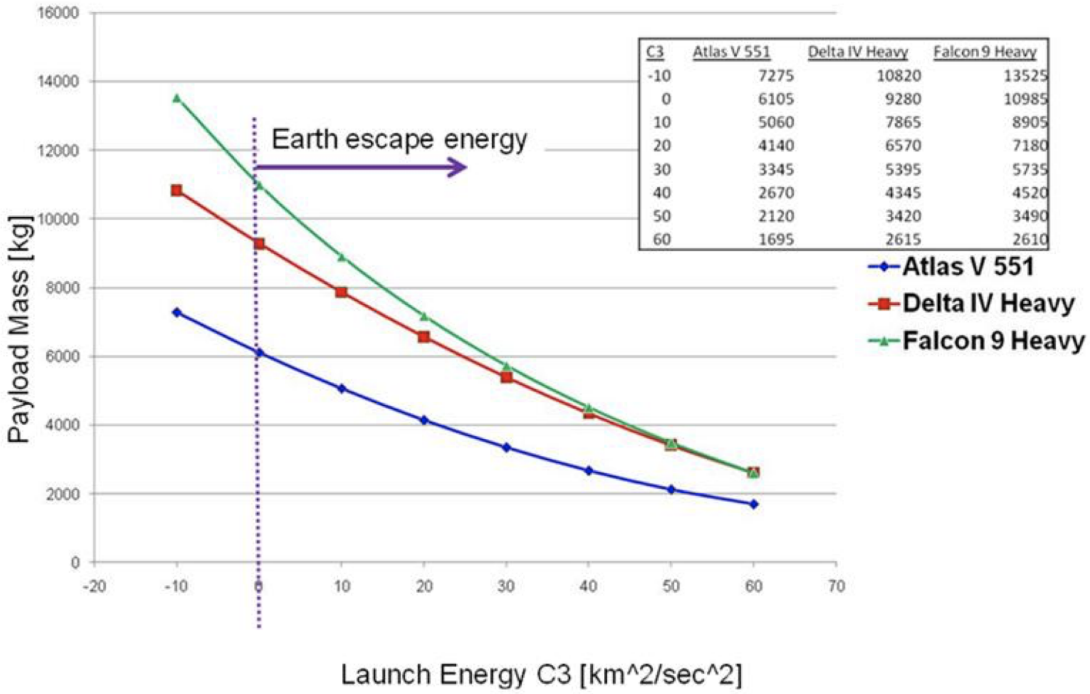

C3	Atlas V 551	Delta IV Heavy	Falcon 9 Heavy
-10	7275	10820	13525
0	6105	9280	10985
10	5060	7865	8905
20	4140	6570	7180
30	3345	5395	5735
40	2670	4345	4520
50	2120	3420	3490
60	1695	2615	2610

Figure A.13: c3 energy for KI mission [69] [68]

B | Direct KI mission

Direct impact means that a direct Lambert transfer from the Earth to the asteroid is considered. In this case the decision variables for the optimisation are the launch date, defined by the variable α_0, the number of revolution of the Lambert arc, the initial mass of the spacecraft and the Time of Flight.

Parameter	Lower bound	Upper bound
α_0	0	1
Number of revolution	0	3
TOF	100 *days*	800 *days*

Table B.1: Direct KI mission: optimisation variables

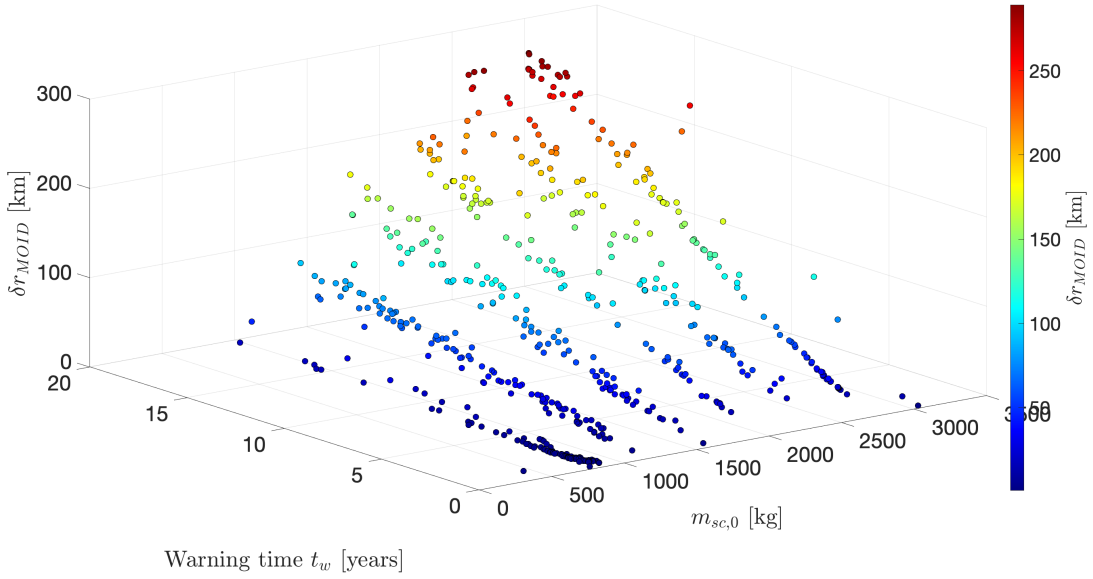

Figure B.1: Kinetic Impactor direct transfer Second case Pareto front: deviation at MOID vs initial mass vs warning time

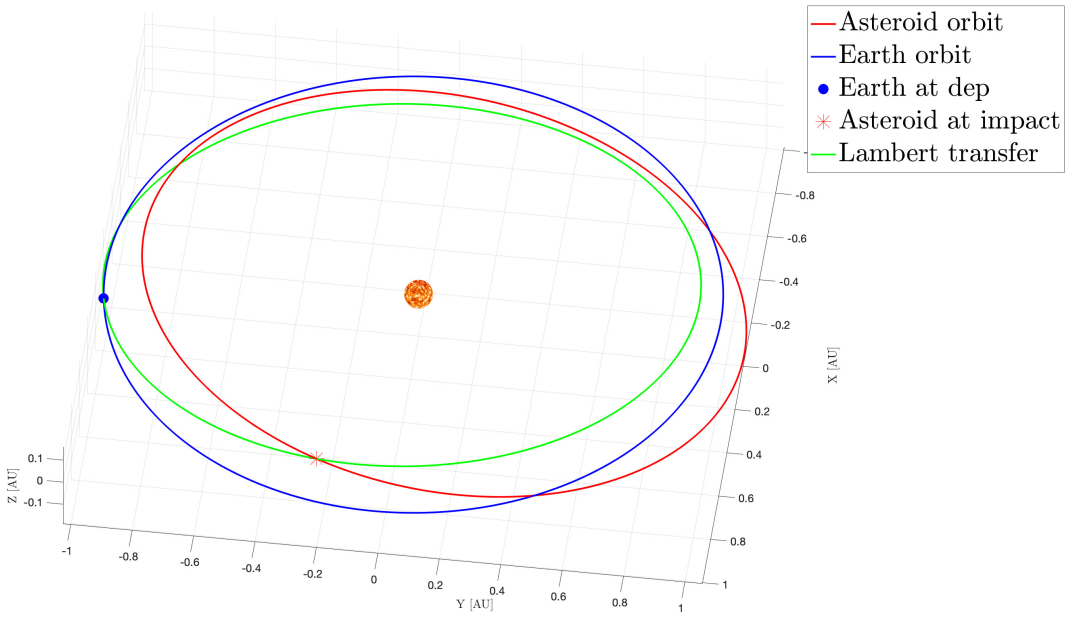

Figure B.2: KI trajectory of direct hit

The Pareto front in fig. B.1 is obtained considering that the mass and diametre of the asteroid falls into 50% percentile level (second case, see table 3.1).
Considering the maximum deviation in the Pareto front, the parameters of the mission are expressed in table B.2.

Parameter	**Optimal value**
Launch date	2029-06-30
Impact date	2031-07-31
Number of revolutions	2
TOF $[days]$	761.8
$c3$ $[km^2/s^2]$	19.2
m_{sc} $[kg]$	6352.2
$\|\|\Delta v_{KI}\|\|$ $[m/s]$	$5.35 \cdot 10^{-4}$
δr_{MOID} $[km]$	289.37

Table B.2: KI direct transfer: Results of the optimisation

NASA indicates that, for the second case, around 85 Falcon Heavy launches are needed in order to reach the correct deviation (23000 km westward), so a total mass of 588000 kg.

The results obtained from fig. B.1, so a total deviation at MOID of 289.37 km, lead to 79 FH launches needed to reach the correct value of deviation.

C | Pareto fronts

C.1. Kinetic Impactor

C.1.1. Second case

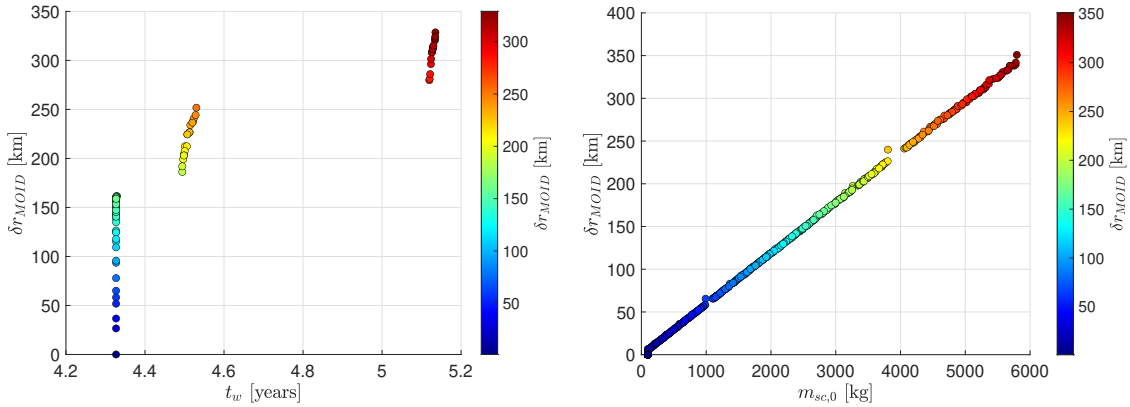

(a) Second case Pareto front: deviation at MOID vs warning time

(b) Second case Pareto front: deviation at MOID vs initial mass

Figure C.1: Kinetic Impactor: Second case Pareto fronts

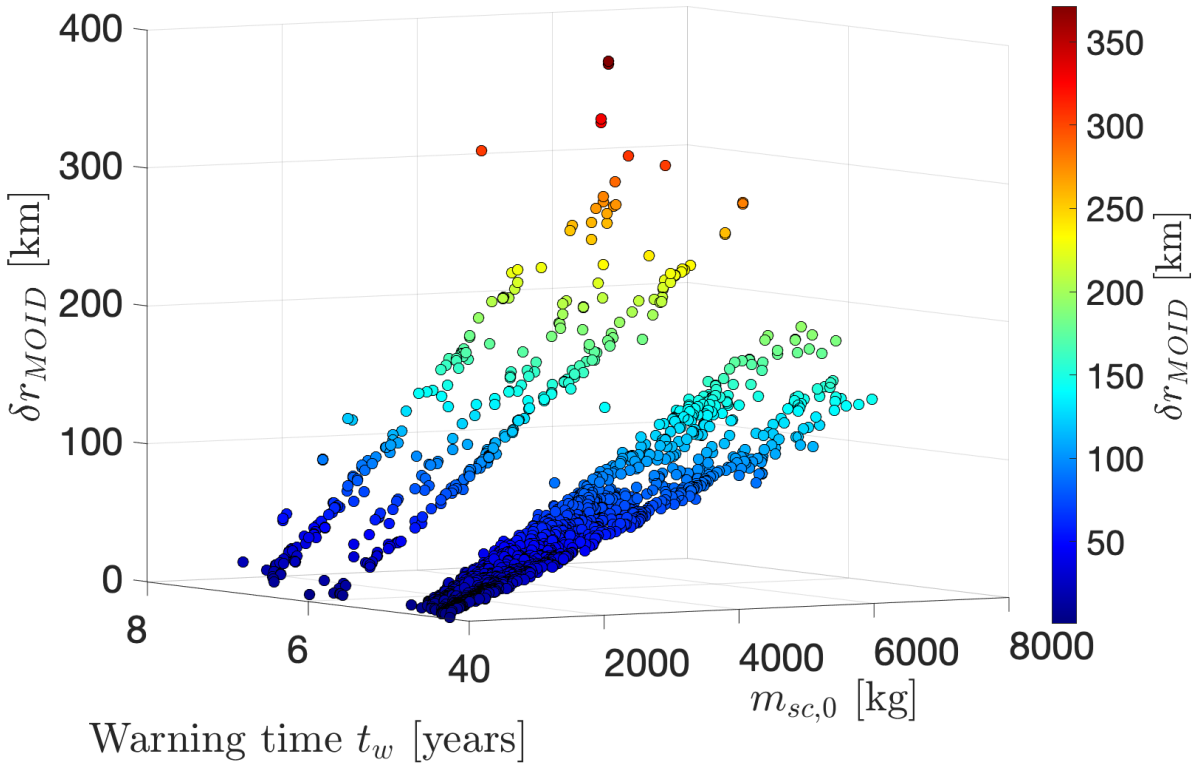

Figure C.2: Kinetic Impactor Second case Pareto front: deviation at MOID vs initial mass vs warning time

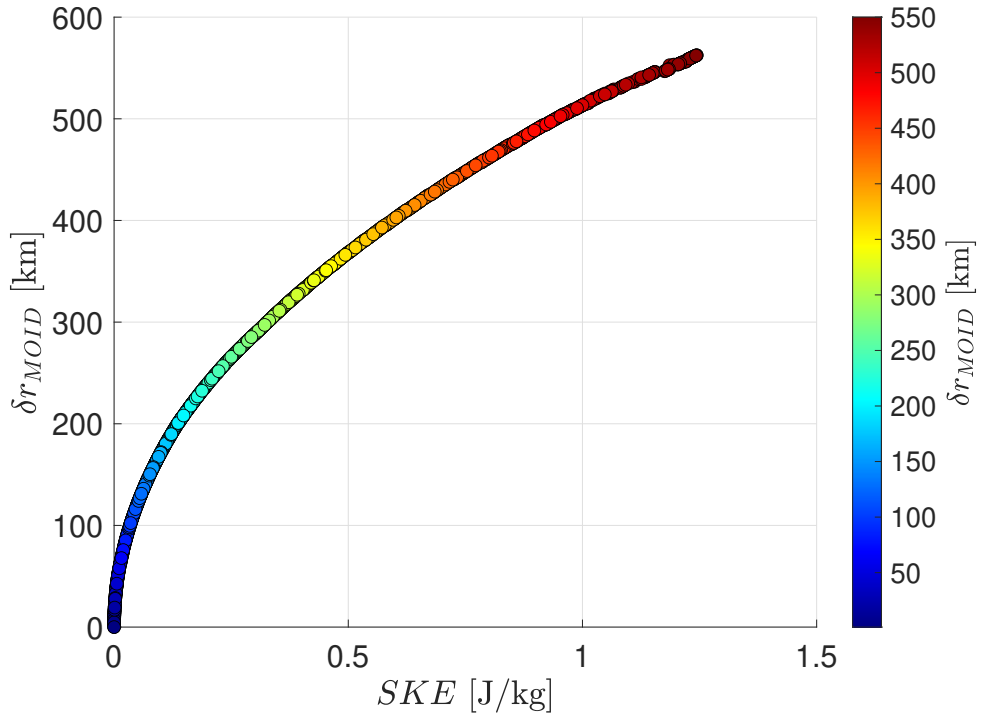

Figure C.3: Kinetic Impactor Second case Pareto front: deviation at MOID vs SKE

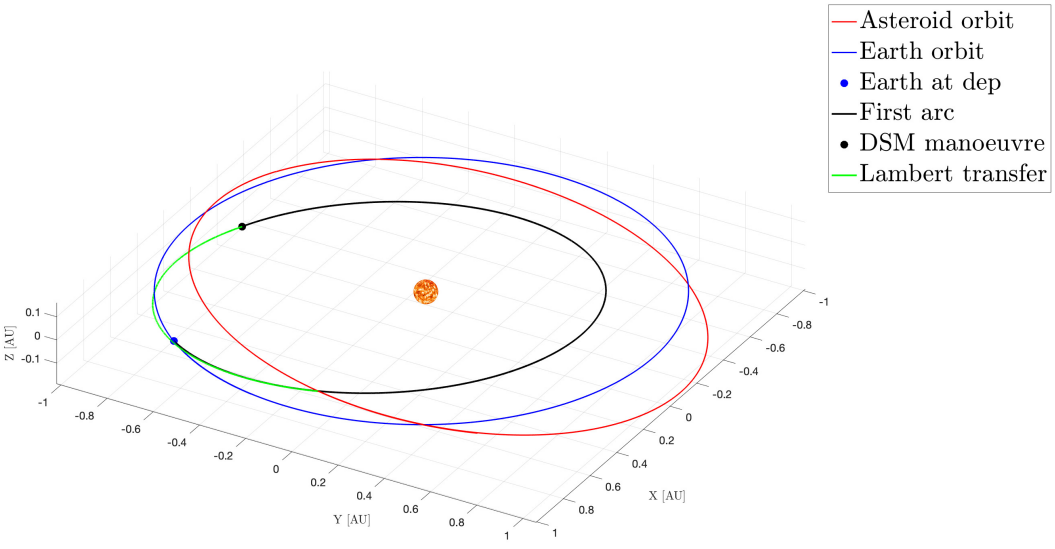

Figure C.4: Trajectory of the Kinetic Impactor mission: Second case

C.1.2. Third case

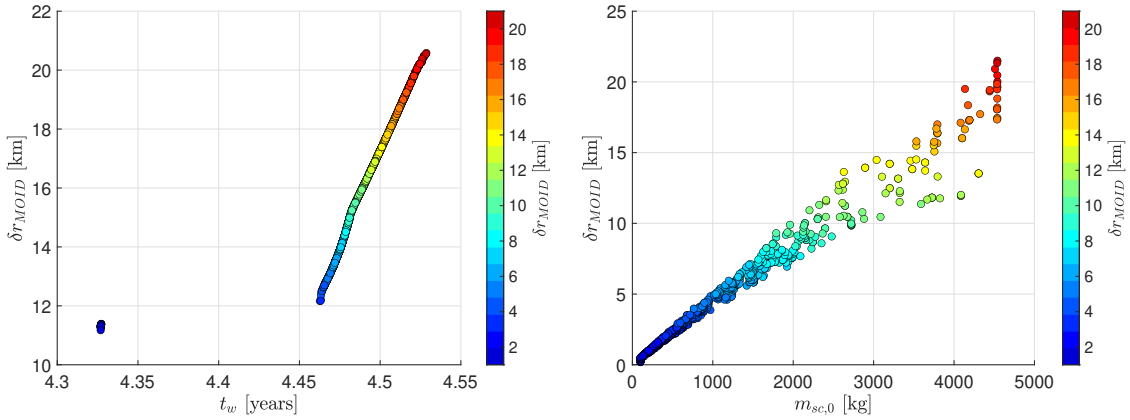

(a) Third case Pareto front: deviation at MOID vs warning time

(b) Third case Pareto front: deviation at MOID vs initial mass

Figure C.5: Kinetic Impactor: Third case Pareto fronts

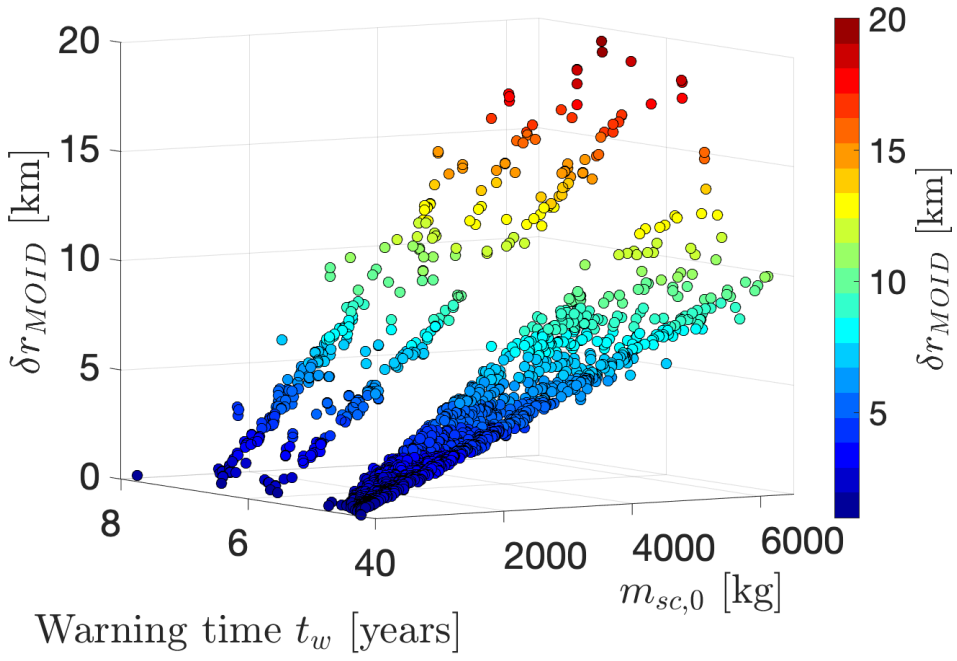

Figure C.6: Kinetic Impactor Third case Pareto front: deviation at MOID vs initial mass vs warning time

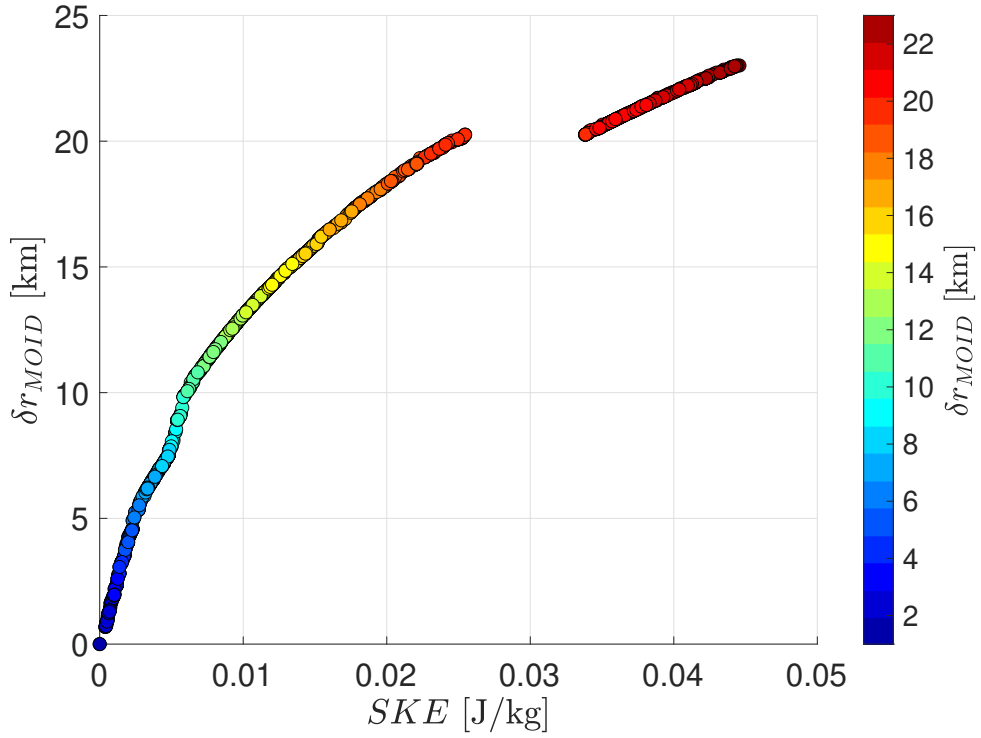

Figure C.7: Kinetic Impactor Third case Pareto front: deviation at MOID vs SKE

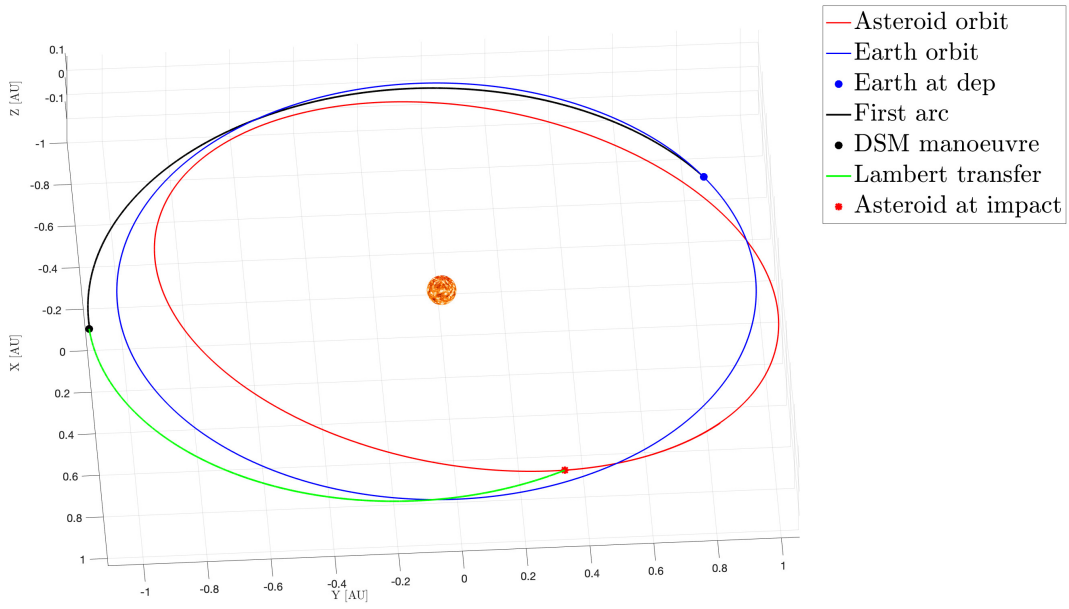

Figure C.8: Trajectory of the Kinetic Impactor mission: Third case

C.2. Nuclear Standoff Explosion

C.2.1. First case

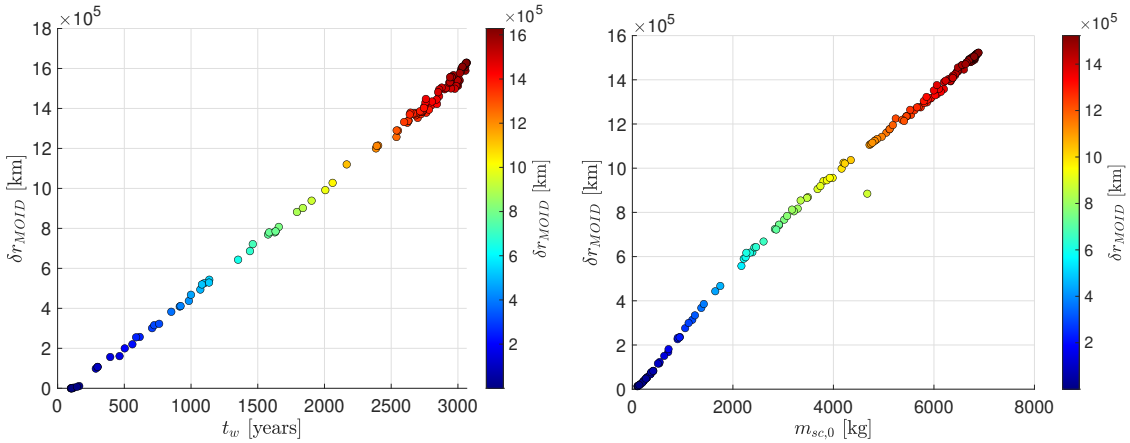

(a) Nuclear Standoff Explosion Pareto front, first case: δr_{MOID} vs t_w

(b) Nuclear Standoff Explosion Pareto front, first case: δr_{MOID} vs $m_{sc,0}$

Figure C.9: Nuclear Standoff Explosion: first case Pareto fronts

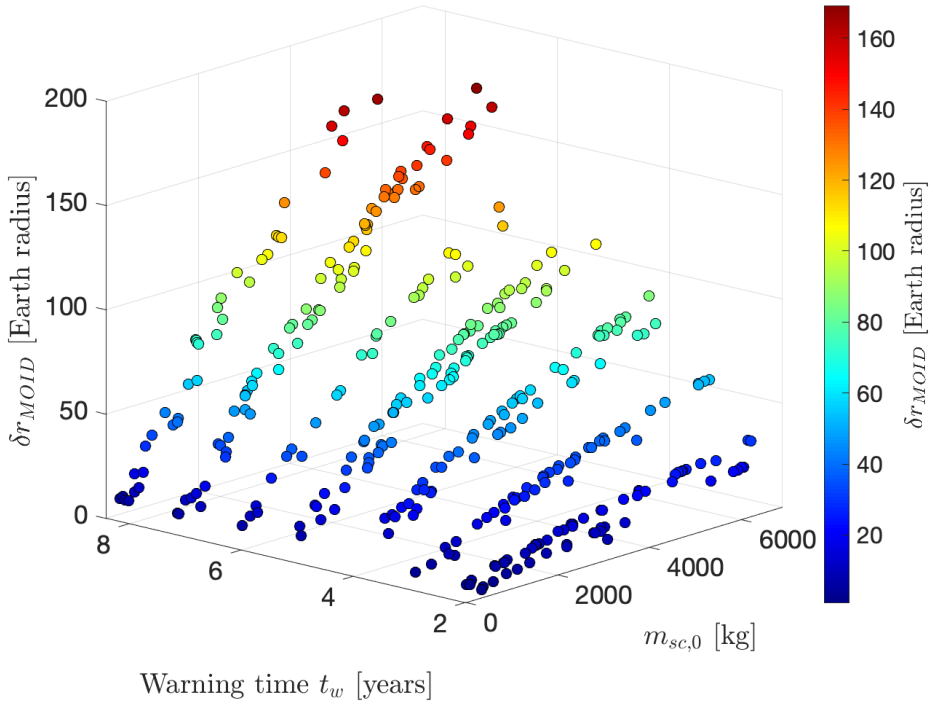

Figure C.10: Nuclear Standoff Explosion first case: 3D Pareto front

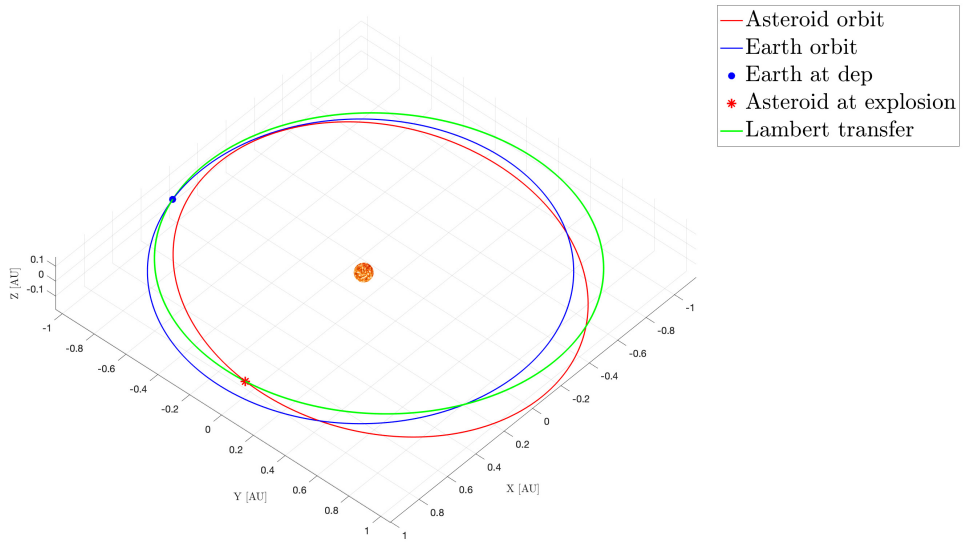

Figure C.11: Trajectory of the Nuclear Standoff Explosion mission, first case

C.2.2. Second case

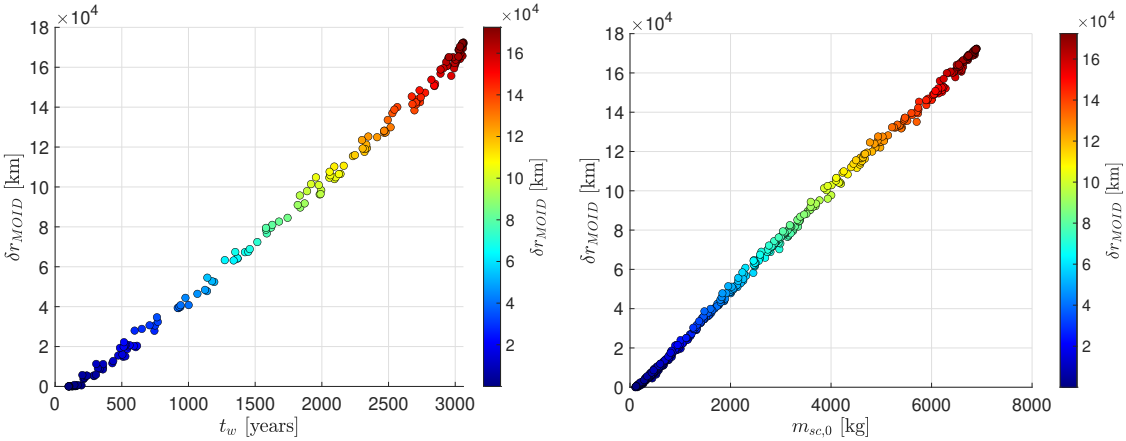

(a) Nuclear Standoff Explosion Pareto front, second case: δr_{MOID} vs t_w

(b) Nuclear Standoff Explosion Pareto front, second case: δr_{MOID} vs $m_{sc,0}$

Figure C.12: Nuclear Standoff Explosion: Second case Pareto fronts

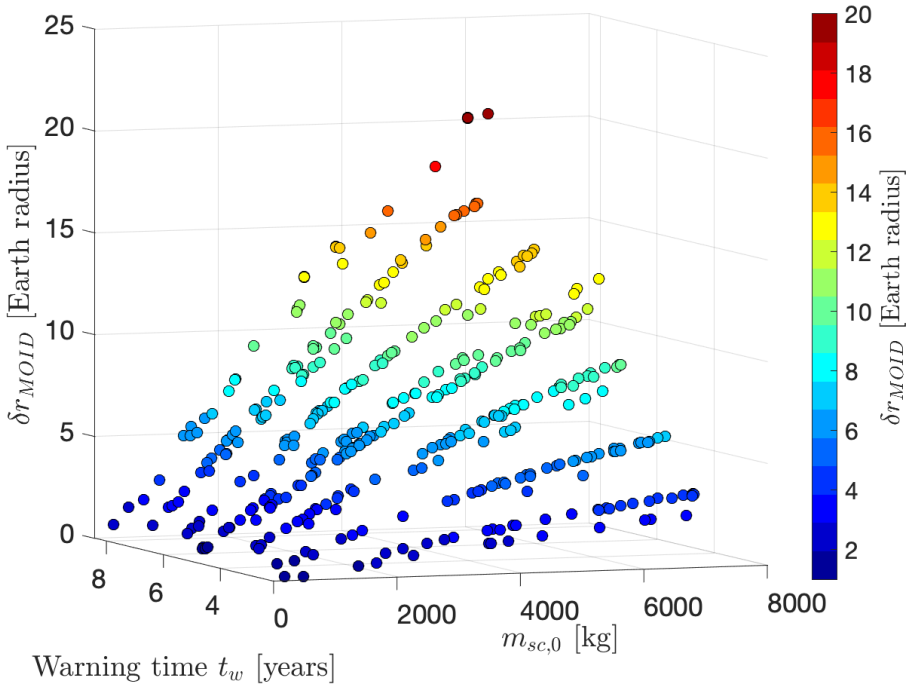

Figure C.13: Nuclear Standoff Explosion: 3D Pareto front

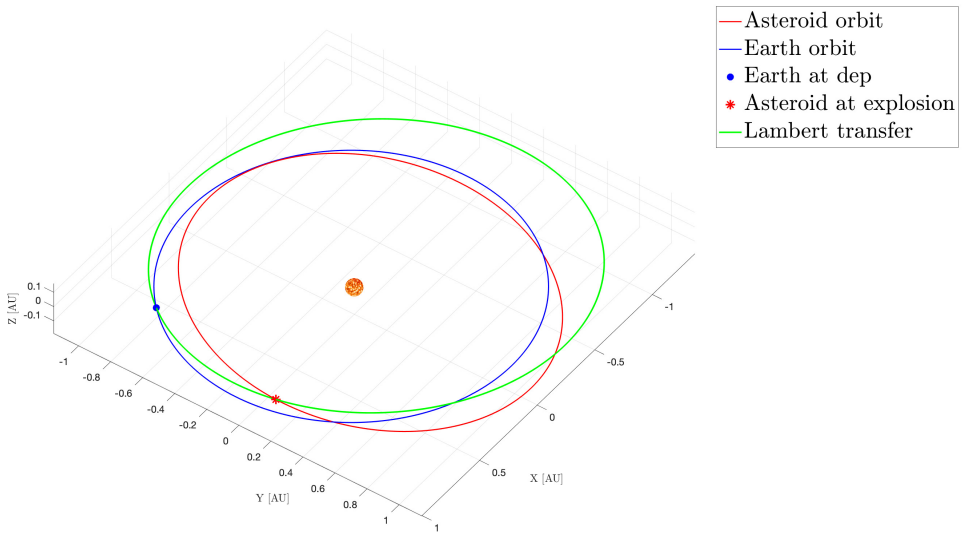

Figure C.14: Trajectory of the Nuclear Standoff Explosion mission (second case)

C.3. Gravity Tractor

C.3.1. Second Case

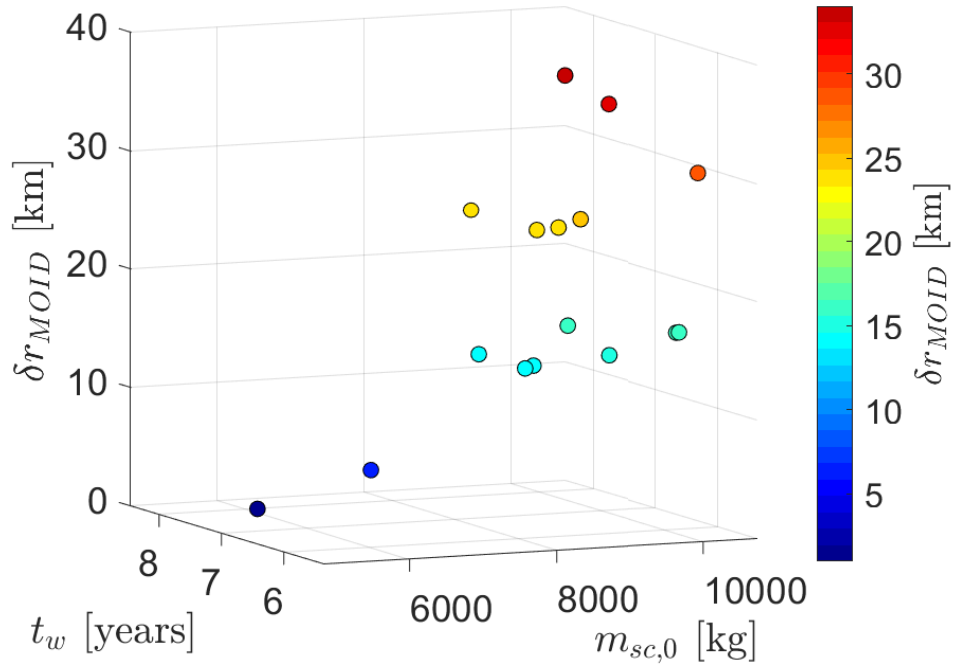

Figure C.15: Gravity Tractor Pareto front, second case: δr_{MOID} vs $m_{sc,0}$ vs t_w

It can be noted that in this case the optimal solutions found by the optimizer are few, since the mass of the propellant must be always higher than 0.5 m_{sc0}. However in this case the mass needed for hovering is high since the mass of the asteroid is one order of magnitude higher than the first case.
For this reason the third case is not even considered, the mass needed for hovering would be too high such that the time spent in that condition wouldn't clearly be enough to deflect the asteroid.

C.4. Laser Ablation

C.4.1. First case

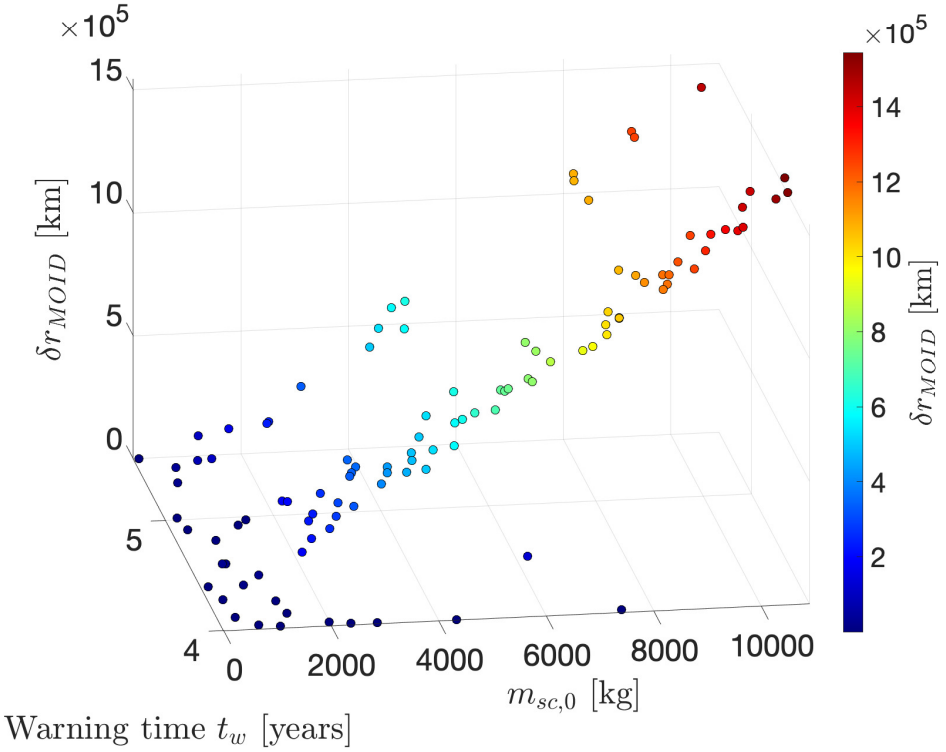

Figure C.16: Laser Ablation Pareto front, second case: δr_{MOID} vs $m_{sc,0}$ vs t_w

C.4.2. Third case

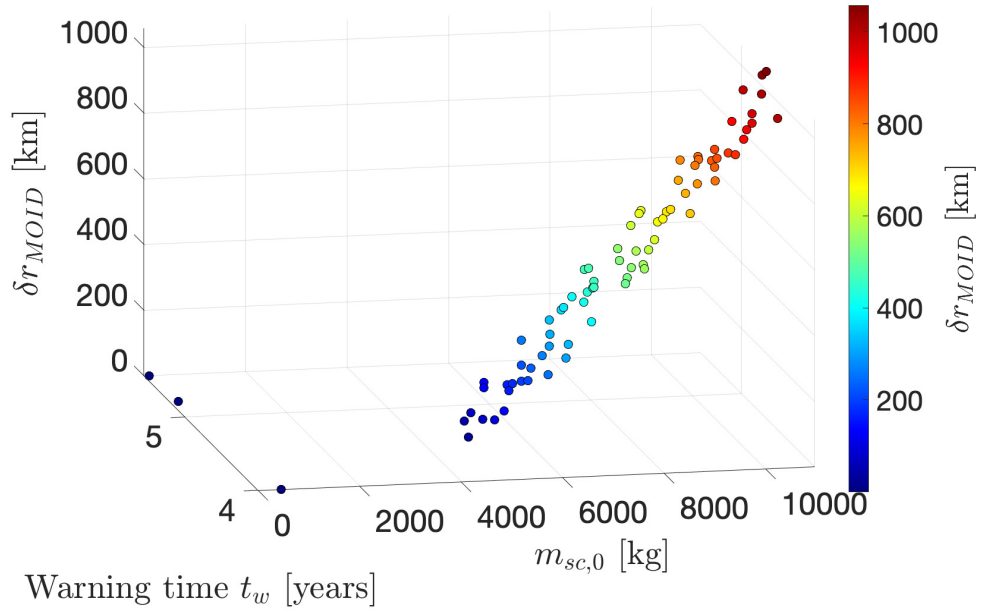

Figure C.17: Laser Ablation Pareto front, second case: δr_{MOID} vs $m_{sc,0}$ vs t_w

C.4.3. RTGs

These devices exploit the energy produced by the natural decay of a radioactive isotope and then transform this thermal energy into electric energy. In this case Stirling RTGs are considered, since their conversion efficiency is much higher than classical RTGs which exploit the Seebeck effect (materials that create an electric potential from a difference in temperature). In this case the efficiency is very low, around 6%, while if the Stirling cycle is used to convert thermal into electric energy the efficiency increases to 30%. Since the mission lifetime is long the isotope chosen is 238-Plutonium (Pu^{228}), which guarantees lower initial specific power with respect to Polonium, but the half-life time is much higher then Po^{210} and this brings to a lower mass needed.

Isotope	Specific power (P_0)	Half-life time ($t_{1/2}$)
Pu-238	0.56 W/g	87.74 years
Po-210	141 W/g	136 days

Table C.1: Isotopes for RTGs

So the power at the end of life is computed considering the half-life time of the radioiso-

tope:

$$P_{EOL} = P_0 \left(\frac{1}{2}\right)^{\frac{t_f}{t_{1/2}}} \tag{C.1}$$

Where t_f is the final time of the mission, so in this case when the deviating action stops. The thermal power generated by the RTGs is the electric power needed divided by the efficiency ($\eta = 0.3$), so:

$$P_{th} = \frac{P_L}{\eta} \tag{C.2}$$

So the isotope mass can be computed as:

$$M_{isotope} = \frac{P_{th}}{P_{EOL}} \tag{C.3}$$